

---

---

# Thermal Conductivity and Thermal Rectification in Carbon Nanotubes

Reverse Non-Equilibrium Molecular Dynamics Simulations

---



TECHNISCHE  
UNIVERSITÄT  
DARMSTADT

Vom Fachbereich Chemie  
der Technischen Universität Darmstadt

zur Erlangung des akademischen Grades eines  
Doktor rerum naturalium (Dr. rer. nat)

genehmigte  
Dissertation

eingereicht von

**M.Sc. Chem. Mohammad Alaghemandi**

aus Golpayegan, Iran

Berichterstatter: **Prof. Dr. Florian Müller-Plathe**

Mitberichterstatter: **Prof. Dr. Nico Van der Vegt**

Eingereicht am: 1 Februar 2010

Mündliche Prüfung am: 22 März 2010

Darmstadt 2010

D17

---

---

## Acknowledgements

I am heartily thankful to my supervisor, Prof. Dr. Florian Müller-Plathe, whose guidance, encouragement, supervision and support from the preliminary to the concluding level enabled me to develop an understanding of the subject. His mentorship was paramount in providing a well rounded experience consistent my long-term career goals. For everything you've done for me, Prof. Müller-Plathe, I thank you.

Special thanks go to my co-advisor, Prof. Dr. Michael C. Böhm, who is most responsible for helping me complete the writing of the papers as well as the challenging research that lies behind them. Michael has been a friend and mentor. He was always there to meet and talk about my ideas, to proofread and mark up my papers, and to ask me good questions to help me think through my problems (whether philosophical, analytical or computational).

Besides my advisors, I would like to thank Prof. Dr. Nico Van der Vegt as well as the rest of my thesis committee for reading my dissertation and for their encouragement.

I would like to gratefully thank Dr. Frédéric Leroy and Dr. Joachim Schulte for their helpful discussion and friendly collaboration during the project.

I also would like to sincerely thank Miss Elena Algaer and Dr. Thomas J. Müller as well as all Müller-Plathe research group members for their friendship, understanding, collaboration and help.

Many friends, especially Mr. Hossein Ali Karimi-Varzaneh, have helped me stay sane through these difficult years. Their support and care helped me overcome setbacks and stay focused on my graduate study. I greatly value their friendship and I deeply appreciate their belief in me.

I gratefully and sincerely thank my parents for their faith in me and allowing me to be as ambitious as I wanted. It was under their watchful eye that I gained so much drive and an ability to tackle challenges head on.

Most importantly, none of this would have been possible without the love and patience of my wife, Leili. I dedicate this thesis with my deepest and sincerest thanks to her.

Financial support of this work by Priority Program 1155 "Molecular Simulation in Chemical Engineering" of the Deutsche Forschungsgemeinschaft is gratefully acknowledged.

Lastly, I offer my regards and blessings to all of those who supported me in any respect during the completion of the project.

---

---

## Contents

Summary .....	1
Zusammenfassung .....	3
1..... INTRODUCTION .....	5
2..... THERMAL CONDUCTIVITY OF CARBON NANOTUBES .....	8
2.1. Introduction	8
2.2. Theoretical background	9
2.3. Computational details	9
2.4. Results and discussion	9
2.4.1. Length dependence of the thermal conductivity	9
2.4.2. Temperature dependence of the thermal conductance	11
2.4.3. Thermal rectification in CNTs	12
2.5. Conclusions	15
2.6. References	15
3..... THERMAL RECTIFICATION IN MASS-GRADED NANOTUBES .....	16
3.1. Introduction	16
3.2. Theoretical background	17
3.3. Computational conditions	18
3.4. Microscopic model for thermal rectification	18
3.5. Conclusions	20
3.6. References	21
4..... THERMAL RECTIFICATION IN NANOSIZED MODEL SYSTEMS .....	22
4.1. Introduction	23
4.2. Theoretical tools	26
4.3. Computational details	29
4.4. Calculated thermal rectification parameters	31
4.4.1. Mass-graded nanotubes	31
4.4.2. Nanotube simulations with a gradient in the bond force constant	34
4.4.3. Mass-graded 2D and 3D models	35
4.4.4. Mass-graded polyacetylene-like models	36
4.4.5. Topological thermal rectification	38
4.5. Analysis of the projected density of vibrational states – the spectral rectification parameter $R_p$	39
4.6. Conclusions	41
4.7. References	43
5..... THERMAL CONDUCTIVITY OF CARBON NANOTUBES WITH BONDLENGTH ALTERNATIONS .....	46
5.1. Introduction	47
5.2. Theoretical tools	51
5.3. Computational conditions	53
5.4. Results and discussion	54
5.4.1. Crystal orbital data	54
5.4.2. Thermal conductivity	58

---

5.4.3.	Correlation between $\lambda$ and the projected phonon DOS	60
5.5.	Conclusions	62
5.6.	References	63
6.....	CONCLUSION AND OUTLOOK.....	67
	Publications .....	69
	Curriculum Vitae.....	70
	Eidesstattliche Erklärungen.....	71

---

## Summary

---

The purpose of this research is an investigation of the thermal conductivity ( $\lambda$ ) and thermal rectification of carbon nanotubes as well as the different factors which have an influence on these quantities. As computational tool we have used reverse non-equilibrium molecular dynamics (RNEMD) simulations.

In chapter 1 we have briefly discussed the importance of research in nanoscale science. Furthermore the motivation for this work has been explained.

In chapter 2 we have investigated the thermal conductivity of single-walled and multi-walled carbon nanotubes by RNEMD as a function of the tube length ( $L$ ), temperature and chiral index. We found that the thermal conductivity in the ballistic-diffusive regime follows a  $L^\alpha$  law. The exponent  $\alpha$  is insensitive to the diameter of the carbon nanotube; at room temperature  $\alpha \approx 0.77$  has been derived for short carbon nanotubes. The temperature dependence of the thermal conductivity shows a peak between 250 and 500 K. We have also defined and shortly discussed the phenomenon of thermal rectification in mass-graded and extra-mass-loaded nanotubes.

In chapter 3 the thermal rectification in nanotubes with a mass gradient has been studied in more detail. We predict a preferred heat flow from light to heavy atoms which differs from the preferential direction in one-dimensional (1D) monoatomic systems. This behavior of nanotubes is explained by anharmonicities caused by transverse motions which are stronger at the low mass end. The present simulations show an enhanced rectification with increasing tube length, diameter and mass gradient. Implications of the present findings for applied topics are mentioned concisely.

In chapter 4 we have extended our work on thermal rectification from mass-graded quasi-one-dimensional nanotubes to the other model systems. Mass-graded polyacetylene-like chains behave like single-file chains as long as the mass gradient is hold by the backbone atoms. The thermal rectification in nanotubes with a gradient in the bond force constant ( $k_r$ ) has been studied, too. They show a preferred heat transfer from the region with large  $k_r$  to the domain with small  $k_r$ . Thermal rectification has been studied also in planar (2D) and 3D mass-graded systems where the heat flow followed a preferred direction similar to that observed in nanotubes. Additionally, a more realistic system has been implemented. Here a different number of carbon nanotubes have been grafted on both sides of a graphene sheet. We have found that the transfer of the vibrational energy as well as the generation of low-energy modes at atoms with large masses is responsible for the sign of the thermal rectification.

In chapter 5 the thermal conductivity of carbon nanotubes (CNTs) with chirality indices (5,0), (10,0), (5,5) and (10,10) has been studied by reverse non-equilibrium molecular dynamics simulations as a function of different bondlength alternation patterns ( $\Delta r$ ). The  $\Delta r$  dependence of the bond force constant ( $k_{rx}$ ) in the MD force field has been determined with the help of an electronic band structure approach. From these calculations it follows that the  $\Delta r$  dependence of  $k_{rx}$  in tubes with not too small diameter can be mapped by a simple linear bondlength–bondorder correlation. A bondlength

---

alternation with an overall reduction in the length of the nanotube causes an enhancement of  $\lambda$  while an alternation scheme leading to an elongation of the tube is coupled to a reduction of the thermal conductivity. This effect is more pronounced in CNTs with larger diameters.

---

## Zusammenfassung

---

In meiner Doktorarbeit habe ich mich mit der Wärmeleitfähigkeit ( $\lambda$ ) und der thermischen Rektifikation in Kohlenstoff-Nanoröhren (CNTs) sowie mit den Faktoren, die diese Größen beeinflussen, beschäftigt. Als theoretisches Werkzeug für diese Analyse verwendete ich Nichtgleichgewichts Molekulardynamik Simulationen (Typ: RNEMD).

In Kapitel 1 meiner Arbeit wird ein kurzer Überblick über wichtige Forschungsergebnisse in der Nanowissenschaft gegeben. In diesem Zusammenhang erkläre ich auch die Motivation der hier vorgelegten Arbeit.

Die Wärmeleitfähigkeit von Monoröhren und Multiröhren als Funktion ihrer Längen ( $L$ ), der Temperatur und des sogenannten Chiralitätsparameters wird in Kapitel 2 behandelt. Im Rahmen meiner Untersuchungen habe ich gefunden, dass  $\lambda$  unter ballistisch-diffusionskontrollierten Bedingungen einem  $L^\alpha$  Gesetz folgt. Der Parameter  $\alpha$  hängt nicht vom Durchmesser des Systems ab. Für kurze Röhren wird bei Raumtemperatur ein Wert von  $\alpha \approx 0.77$  gefunden. Die Wärmeleitfähigkeit zeigt ein Maximum zwischen 250 und 500 K. In Kapitel 2 habe ich mich auch kurz mit dem Phänomen der sogenannten thermischen Rektifikation beschäftigt. Als Modellsysteme wurden hier Nanoröhren mit einem Massengradienten sowie Nanoröhren mit externen Massen gewählt.

Auf die Wärmeleitfähigkeit in Nanoröhren mit einem Massengradienten gehe ich in Kapitel 3 dann näher ein. Unsere Untersuchungen zeigen, dass der Energietransport von leichten zu schweren Teilchen bevorzugt stattfindet. Dies unterscheidet sich von der bevorzugten Transportrichtung von "schwer nach leicht" in einer eindimensionalen (1D) monoatomaren Kette. Wir erklären dieses Verhalten der CNTs mit einer Kopplung zwischen transversalen und longitudinalen Phonon-Moden, die für leichte Atome stärker ist. Unsere Untersuchungen zeigen, dass die thermische Rektifikation mit der Länge der Nanoröhre, dem Durchmesser und dem Massengradienten zunimmt. Mögliche Anwendungen dieser Befunde werden kurz vorgestellt.

Im vierten Kapitel erweitere ich die Analyse der thermischen Rektifikation von quasi-1D-Nanoröhren mit einem Massengradienten auf andere Modellsysteme. 1D Ketten mit einer Polyacetylen-Struktur mit Massengradienten auf dem Hauptstrang verhalten sich wie entsprechende eindimensionale monoatomare Kette. In diesem Kapitel meiner Arbeit habe ich ebenfalls Nanoröhren analysiert, in denen ein Gradient in der Kraftkonstanten ( $k_r$ ) für die C-C Bindungen auftritt. Hier findet der bevorzugte Energietransfer vom Bereich hoher  $k_r$  zum Bereich kleiner  $k_r$  statt. Ein weiteres Thema dieses Kapitels ist die Analyse der thermischen Rektifikation in planaren (2D) und 3D Systemen mit einem Massengradienten. Diese Systeme verhalten sich wie die Nanoröhren mit einem Massengradienten. Schließlich stelle ich in diesem Kapitel auch ein realistisches System vor, i.e. Kohlenstoff-Nanoröhren, die an eine Graphit-Schicht gebunden sind. Hier diskutiere ich die Bedeutung des Transfers von Schwingungsenergie sowie die Erzeugung niederenergetischer Moden an schweren Atomen. Die thermische Rektifikation wird durch diese Größen bestimmt.

---

Thema des fünften Kapitels ist die Wärmeleitfähigkeit in Kohlenstoff-Nanoröhren mit Chiralitätsindizes (5,0), (10,0), (5,5), und (10,10) als Funktion der Anordnung von Einzel- und Doppelbindungen erzeugt durch Variation der Bindungslängen ( $\Delta r$ ). Auch für diese Untersuchungen wurde die RNEMD Methode herangezogen. Die Änderung der Kraftkonstanten  $k_r$  für die C-C Schwingungen wurde mithilfe von elektronischen Bandstruktur-Rechnungen bestimmt. Für CNTs mit grösserem Durchmesser lässt sich diese Bestimmung auf Basis einer linearen Korrelation zwischen Bindungslänge und Bindungsordnung durchführen. Eine Anordnung von Einzel- und Doppelbindungen, die mit einer Reduktion der Länge der Röhre verbunden ist, führt zu einer Vergrößerung der Wärmeleitfähigkeit. Der umgekehrte Effekt tritt ein, wenn die Röhre durch das Bindungsmuster verlängert wird. Generell ist dieser Effekt im Fall von CNTs mit grösserem Durchmesser stärker ausgeprägt.



---

## 1. INTRODUCTION

---

The physics of carbon nanotubes<sup>1-5</sup> is intimately coupled to emerging computational fields in nano-science,<sup>6</sup> nano-technology,<sup>7</sup> materials science and condensed matter physics. These computational fields can be split into two branches, i.e. numerical modeling and computer-based simulation,<sup>8,9</sup> to calculate the mechanical, thermal and electronic properties of nano-scale structures, as well as nano-scale processes that occur in nanoscopic systems. Computational nano-science forms an indispensable pathway in the research concerned with an intelligent manipulation and structural transformation of condensed phases at their most fundamental levels. This new field of research offers a complete control over the structure and functioning of physical matter at the atomistic and molecular scales. This control implies that physical matter can be interrogated atom-by-atom and molecule-by-molecule,<sup>10,11</sup> and new forms of materials can be designed by a precise positioning of individual atoms. In short, computational nano-science has created efficient possibilities for the investigation of existing nano-structures and to operate at highly reduced length, time and energy scales.

The discovery of carbon nanotubes<sup>12</sup> has opened world-wide a new and very active research field in theoretical and experimental condensed matter physics and materials science. They exhibit exceptional electronic, mechanical, thermal, and transport properties.<sup>13-18</sup> Their electronic properties can turn them into metallic or semi-conducting nano-wires, depending on their chirality or helicity.<sup>3</sup> These electronic properties are highly sensitive to local distortions in the nanotube geometry that can arise due to mechanical deformations and the presence of molecular adsorbates. Nanotubes have also unique, and in many ways extraordinary, mechanical properties.<sup>19</sup> With having a Young's modulus estimated to be of the order of several TPa, they are the material with the highest tensile strength known so far.<sup>20-22</sup> They are capable of sustaining high strains without fracture. Among other things they are proposed as the functional units for the construction of the future molecular-scale machines, providing the simplest forms of molecular bearings, shafts and gears in highly complex nano-electromechanical systems.<sup>23</sup>

An important use of carbon nanotubes lies in nanoscopic functional devices. Hence, besides their mechanical stability and performance, their thermal stability plays a crucial role. In contrast to the mechanical and electronic properties for which a significant number of investigations have been carried out, investigations of the thermal properties of nanotubes have not received the same kind of attention, either experimentally or computationally.<sup>24-28</sup>

Measurements of the thermal conductivity of nanotubes, in analogy to measurements of other properties, are influenced by some degree of uncertainty. This is caused by impurities or defects that could be present.<sup>29</sup> Numerical simulations such as MD have been playing an increasingly important role in this field. Both equilibrium and non-equilibrium types of MD simulations have been applied to model the transport properties of nanotubes.<sup>30,31</sup> In the former case, the aim is the computation of equilibrium time-correlation functions of the heat flux,  $J_q$ , and to employ this quantity in the Green-Kubo relation to obtain the thermal conductivity. In the non-equilibrium MD approach, hot and cold reservoirs are coupled to the two ends of the system. By computing the average heat flux, the thermal

---

conductivity can be derived. There are, of course, some disadvantages present in the application of the non-equilibrium approach. One problem lies in the proper calculation of the heat flux. Therefore, we have used the reverse non-equilibrium MD approach in this work which imposes a certain flux to the system and the thermal gradient will be calculated as an effect in the end of the simulation.<sup>32</sup>

The understanding of the exotic and often highly intriguing properties of carbon nanotubes has prompted intensive and deep-going experimental and theoretical/computational research efforts in the fields of nanotube physics, chemistry and technology. These activities have led to the appearance of several thousand research publications over the last decade. In this connection we have tried here to answer open questions in the field of the heat transfer in carbon nanotubes such as: What is the origin of their high thermal conductivity and which factors and variables are controlling these values? Can carbon nanotubes be considered as one-dimensional (1D) systems? If they can be classified as quasi-one-dimensional systems, the following question arises: Is it allowed to adopt physical concepts for perfect one-dimensional monoatomic chains to explain the properties of nanotubes? Can we expect that carbon nanotubes conserve as a solid-state thermal rectifier? Finally, how is it possible to control and change the magnitude and direction of the heat flux?

- (1) Rafii-Tabar, H. *Computational Physics of Carbon Nanotubes*; Cambridge University Press: New York, 2008.
- (2) Leonard, F. *Physics Of Carbon Nanotube Devices*; William Andrew Inc.: New York, 2008.
- (3) Saito, R. *Physical Properties of Carbon Nanotubes*; Imperial College Press: London, 2004.
- (4) Reich, S.; Thomsen, C.; Maultzsch, J. *Carbon Nanotubes: Basic Concepts and Physical Properties*; WILEY-VCH, 2004.
- (5) Rotkin, S. V.; Subramoney, S. *Applied Physics of Carbon Nanotubes: Fundamentals of Theory, Optics and Transport Devices*; Springer: New York, 2005.
- (6) Hornyak, G. L.; Dutta, J.; Tibbals, H. F.; Rao, A. *Introduction to Nanoscience* Taylor & Francis, 2008.
- (7) Ventra, M.; Evoy, S.; Heflin, J. *Introduction to Nanoscale Science and Technology*; Springer, 2004.
- (8) Berendsen, H. J. C. *Simulating the Physical World*; Cambridge University Press: New York, 2007.
- (9) Frenkel, D.; Smit, B. *Understanding Molecular Simulation: From Algorithms to Applications, second edition*; Academic Press: California; Vol. 1.
- (10) Silva, E.; Forst, C.; Ju, L.; Xi, L.; Ting, Z.; Yip, S. *Mathematical Modelling and Numerical Analysis* **2007**, 427.
- (11) McGrother, S.; Goldbeck-Wood, G.; Lam, Y. M. *Computational materials science. From basic principles to material properties (Lecture Notes in Phys. Vol.642)* **2004**, 223.
- (12) Iijima, S. *Nature* **1991**, 354, 56.

- 
- (13) Sawaya, S.; Akita, S.; Nakayama, Y. *Nanotechnology* **2007**, *18*, 035702.
  - (14) Wang, M. S.; Peng, L. M.; Wang, J. Y.; Chen, Q. *Advanced Functional Materials* **2006**, *16*, 1462.
  - (15) Rochefort, A.; Avouris, P.; Lesage, F.; Salahub, D. R. *Physical Review B* **1999**, *60*, 13824.
  - (16) de Pablo, P. J.; Martinez, M. T.; Colchero, J.; Gomez-Herrero, J.; Maser, W. K.; Benito, A. M.; Munoz, E.; Baro, A. M. *Advanced Materials* **2000**, *12*, 573.
  - (17) Bernholc, J.; Brenner, D.; Nardelli, M. B.; Meunier, V.; Roland, C. *Annual Review of Materials Research* **2002**, *32*, 347.
  - (18) Chen, B. H.; Chuang, C. H.; Chang, S. C.; Tsau, F. H.; Jeng, M. S.; Chen, C. K. *Journal of Micro-Nanolithography Mems and Moems* **2009**, *8*, 021151.
  - (19) Xiao, J. R.; Gama, B. A.; Gillespie, J. W. *International Journal of Solids and Structures* **2005**, *42*, 3075.
  - (20) Meo, M.; Rossi, M. *Composites Science and Technology* **2006**, *66*, 1597.
  - (21) Meo, M.; Rossi, M. *Materials Science and Engineering a-Structural Materials Properties Microstructure and Processing* **2007**, *454*, 170.
  - (22) Lu, J. N.; Chen, H. B. *Chinese Journal of Chemical Physics* **2008**, *21*, 353.
  - (23) Rafii-Tabar, H. *Physics Reports-Review Section of Physics Letters* **2004**, *390*, 235.
  - (24) Xinhe, T.; Hammel, E.; Reiter, W. *Collection of Papers Presented at the 2009 15th International Workshop on Thermal Investigations of ICs and Systems. THERMINIC 2009* **2009**, *3*.
  - (25) Savin, A. V.; Hu, B. B.; Kivshar, Y. S. *Physical Review B* **2009**, *80*, 195423.
  - (26) Hou, Q. W.; Cao, B. Y.; Guo, Z. Y. *Acta Physica Sinica* **2009**, *58*, 7809.
  - (27) Fujii, M.; Zhang, X.; Xie, H. Q.; Ago, H.; Takahashi, K.; Ikuta, T.; Abe, H.; Shimizu, T. *Physical Review Letters* **2005**, *95*.
  - (28) Choi, T. Y.; Poulidakos, D.; Tharian, J.; Sennhauser, U. *Nano Letters* **2006**, *6*, 1589.
  - (29) Vijayaraghavan, A.; Marquardt, C. W.; Dehm, S.; Hennrich, F.; Krupke, R. *Carbon* **2010**, *48*, 494.
  - (30) Grujicic, M.; Cao, G.; Roy, W. N. *Journal of Materials Science* **2005**, *40*, 1943.
  - (31) Lukes, J. R.; Zhong, H. L. *Journal of Heat Transfer-Transactions of the Asme* **2007**, *129*, 705.
  - (32) Müller-Plathe, F. *Journal of Chemical Physics* **1997**, *106*, 6082.

# The thermal conductivity and thermal rectification of carbon nanotubes studied using reverse non-equilibrium molecular dynamics simulations

Mohammad Alaghemandi, Elena Algaer, Michael C Böhm and Florian Müller-Plathe

Eduard-Zintl-Institut für Anorganische und Physikalische Chemie, Technische Universität Darmstadt, Petersenstrasse 20, D-64287 Darmstadt, Germany

E-mail: [m.alaghemandi@theo.chemie.tu-darmstadt.de](mailto:m.alaghemandi@theo.chemie.tu-darmstadt.de)

Received 17 September 2008, in final form 3 November 2008

Published 25 February 2009

Online at [stacks.iop.org/Nano/20/115704](http://stacks.iop.org/Nano/20/115704)

### Abstract

The thermal conductivity of single-walled and multi-walled carbon nanotubes has been investigated as a function of the tube length  $L$ , temperature and chiral index using non-equilibrium molecular dynamics simulations. In the ballistic-diffusive regime the thermal conductivity follows a  $L^\alpha$  law. The exponent  $\alpha$  is insensitive to the diameter of the carbon nanotube;  $\alpha \approx 0.77$  has been derived for short carbon nanotubes at room temperature. The temperature dependence of the thermal conductivity shows a peak before falling at higher temperatures ( $>500$  K). The phenomenon of thermal rectification in nanotubes has been investigated by gradually changing the atomic mass in the tube-axial direction as well as by loading extra masses on the terminal sites of the tube. A higher thermal conductivity occurs when heat flows from the low-mass to the high-mass region.

### 1. Introduction

Recent advances in the know-how of micro/nanosystems have made possible a continuous reduction in the size of electrical devices in many industries [1]. It is now widely accepted that the thermal management in nanosized devices becomes increasingly important with decreasing size parameters [2]. New thermal management strategies are thus of considerable importance to guarantee high performance and lifetimes. These strategies include the development of novel carbon nanotube (CNT) materials with high thermal conductivity  $\lambda$  [3]. Due to the experimental difficulties in synthesizing high-quality and well-ordered nanotubes, it is still challenging to perform perfect thermal conduction measurements with the current equipment. Only a few research groups have reported experimental  $\lambda$  values of these nano-objects [4–9]. An alternative and supplement to experimental activities are theoretical approaches which have the advantage that the structures generated are clean, defect-free and perfectly characterized. Different molecular

dynamics (MD) simulations on the thermal conductivity of isolated single-walled carbon nanotubes (SWNT) have been reported in the literature [1–3, 10–14]. Unfortunately the calculated  $\lambda$  values vary from several hundred to several thousand  $\text{W m}^{-1} \text{K}^{-1}$ . This large width makes it necessary to clarify the confidence limits of the simulation results and the conditions for obtaining them.

In the present paper, we use a non-equilibrium molecular dynamics method to calculate the thermal conductivity  $\lambda$  and thermal conductance  $\sigma$  of carbon nanotubes. We first focus on the length  $L$ , temperature  $T$ , and diameter  $D$  dependence of  $\lambda$  for both single-walled and multi-walled carbon nanotubes. Since carbon nanotubes are a possible candidate for thermal rectifiers [15], which are significant for modern electronics, the second topic of the present contribution is a model study of the thermal rectification either by nanotubes with a mass gradient or by tubes embedded in an inhomogeneous medium. Possible future applications are expected in the areas of nanoscale calorimeters, microelectronic processors, macroscopic refrigerators and energy-saving buildings.

## 2. Theoretical background: reverse non-equilibrium molecular dynamics (RNEMD) approach

The RNEMD method has been discussed in detail in the literature, including all its advantages and shortcomings; see, for example, [16]. The idea of the method is to drive—as a primary perturbation—a heat flux through the simulated system. In the preparation of the steady state with a constant  $T$  gradient, energy is transferred continuously from one region of the system, denoted as the 'cold' region, to another one, the 'hot' region. The two regions are spatially separated, say, in the  $z$  direction. The cold and the hot region of the system are created by interchanging the velocity of the hottest atom in the cold region with the velocity of the coldest atom in the hot region. This implies that a known amount of heat is transferred between the two regions. By repeating the transfer periodically, an artificial heat flux  $j_z$  is created from the cold to the hot region

$$j_z = \frac{1}{2tA'} \sum_{\text{transfer}}^m \frac{m}{2} (v_{\text{hot}}^2 - v_{\text{cold}}^2) \quad (1)$$

where  $m$  is the mass of the atoms,  $t$  the time of the simulation and  $A'$  the cross-sectional area of the simulation box.  $v_{\text{hot}}$  and  $v_{\text{cold}}$  are the velocities of the selected atoms. The summation is over the exchange events. When the steady state has been reached, the same amount of energy per time and area (this is the definition of the heat flux  $j_z$ ) flows from the hot to the cold region by heat conduction. This equality of the two fluxes follows from energy conservation. As a result, a temperature gradient  $(dT/dz)$  is formed in the system. From the known imposed  $j_z$  and the calculated  $(dT/dz)$ , the thermal conductivity  $\lambda$  is calculated as  $\lambda = -j_z/(dT/dz)$ , assuming the validity of a linear response (Fourier's law). We are aware of the possible limitations of this empirical law in one-dimensional (1D) materials [17, 18]. In the present work intended to derive general, transferable trends, this violation should not lead to conceptual problems. Note that the applicability of the Fourier law depends on a number of quantities such as the length of the tube, disorder, or the phonon mean free path whose influence on  $\lambda$  is not understood completely yet.

## 3. Computational details

The intramolecular force field  $V(\dots)$  characterized by the geometric parameters  $r_0$ ,  $\theta_0$ ,  $\delta_0$  and force constants  $k_r$ ,  $k_\theta$ ,  $k_\delta$  contains harmonic bond stretching<sup>1</sup> ( $r_0 = 0.1418$  nm,  $k_r = 392.460$  kJ mol<sup>-1</sup> nm<sup>-2</sup>), harmonic bond angle bending<sup>2</sup> ( $\theta_0 = 120.0^\circ$ ,  $k_\theta = 527$  kJ mol<sup>-1</sup> rad<sup>-2</sup>) and harmonic dihedral angle<sup>3</sup> ( $\delta_0 = 0.0^\circ$ ,  $k_\delta = 167$  kJ mol<sup>-1</sup> rad<sup>-2</sup>) [19] terms. The non-bonded potential  $V(r_{ij})$  which includes Lennard-Jones terms<sup>4</sup> ( $\epsilon = 0.4396$  kJ mol<sup>-1</sup>,  $\sigma = 0.3851$  nm) is added to account for carbon-carbon interactions of the van der Waals

<sup>1</sup>  $V(r) = (k_r/2)(r - r_0)^2$ .

<sup>2</sup>  $V(\theta) = (k_\theta/2)(\theta - \theta_0)^2$ .

<sup>3</sup>  $V(\delta) = (k_\delta/2)(\delta - \delta_0)^2$ .

<sup>4</sup>  $V(r_{ij}) = 4\epsilon[(\sigma/r_{ij})^{12} - (\sigma/r_{ij})^6]$ .

type. They occur between interlayer atoms in the simulation of multi-walled nanotubes and in one of the simulations of the thermal rectification. The parameters  $\epsilon$  and  $\sigma$  have been taken from the so-called universal force field (UFF) [20] and have been used already by other groups [21] for the investigation of structural data of carbon nanotube systems.

All molecular dynamics simulations have been carried out with the YASP package [22], which uses the leapfrog algorithm [23] and orthorhombic periodic boundary conditions. Unless specified otherwise, all simulations have been performed at constant volume and temperature. The Berendsen method [24] with a coupling time of 1 ps has been adopted to guarantee a constant temperature. The coupling time accepted was sufficient to keep the measured mean temperature within 2 K of the target temperature. Unless specified otherwise, a target temperature of 300 K has been chosen. Normally, time steps of 1 fs have been employed. Non-bonded interactions, where necessary, have been evaluated from a Verlet neighbor list, which was updated every 15 time steps. Unless specified otherwise a cutoff radius of 1.0 nm has been adopted while the neighbor list cutoff was 1.1 nm. The exchange period of the RNEMD scheme was every 300 time steps (0.6 ps), the temperature profiles were sampled every 301 time steps. It has been checked that the temperature gradient was linear when adopting this exchange period. A non-equilibrium run covered typically 6 ns. The last 1000 ps of it have been used for the data production.

The systems studied here have been constructed by repeating the unit cell of zig-zag or armchair nanotubes with different diameters. The two ends of the nanotubes were connected via periodic boundary conditions. Thus, they are pseudoinfinite, which prevents the study of end effects. Thermal contact problems as encountered in experimental studies of CNTs are therefore beyond the capability of the RNEMD approach used. The smallest system considered contained 800 carbon atoms and the largest one 227 680 carbon atoms. The simulation cells were elongated in the  $z$  direction, which is also the direction of the energy flow; their length varied from 10 to 700 nm. We had to accept that the length parameters accessible are smaller than typical experimental values. Nevertheless they exceed the dimension employed in recent MD simulations of CNT networks [2, 3, 10–14].

## 4. Results and discussion

### 4.1. Length dependence of the thermal conductivity

The length dependence of the thermal conductivity  $\lambda$  at room temperature has been studied for single-walled carbon nanotubes with different chiral indices: (5, 5), (10, 0), (7, 7), (10, 10), (17, 0), (15, 15), and (20, 20). We have also included one triple- (i.e. multi-) walled armchair nanotube (MWNT) which is made of (5, 5), (10, 10) and (15, 15) SWNTs. For length parameters  $L$  from 5 to 350 nm the calculated thermal conductivity is listed in table 1 and shown in figure 1. In the diagram we see that the splitting between the  $\lambda$  curves is largest for short tube lengths  $L$ ; it is reduced with increasing  $L$ . Furthermore we notice that  $\lambda$  increases

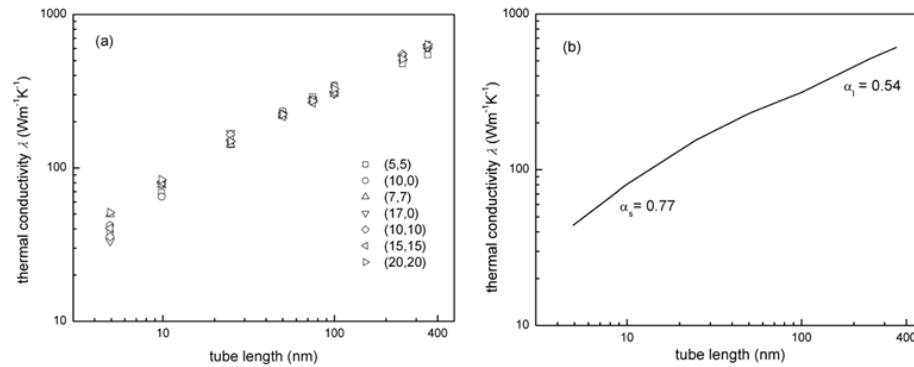


**Figure 1.** (a) Thermal conductivity  $\lambda$  versus tube length of (5, 5), (10, 0), (7, 7), (10, 10), (17, 0), (15, 15), and (20, 20) SWNTs at 300 K in a double-logarithmic scale. (b) This curve refers to the average for the seven systems studied in (a).

**Table 1.** Thermal conductivities  $\lambda$  and thermal conductances  $\sigma$  of different single-walled and one triple-walled nanotubes as a function of the tube length at 300 K.

Length (nm)	Chirality index							
	(5, 5)		(10, 0)		(7, 7)		(17, 0)	
	$\lambda$ ( $\text{W m}^{-1} \text{K}^{-1}$ )	$\sigma$ ( $10^{-8} \text{W K}^{-1}$ )	$\lambda$ ( $\text{W m}^{-1} \text{K}^{-1}$ )	$\sigma$ ( $10^{-8} \text{W K}^{-1}$ )	$\lambda$ ( $\text{W m}^{-1} \text{K}^{-1}$ )	$\sigma$ ( $10^{-8} \text{W K}^{-1}$ )	$\lambda$ ( $\text{W m}^{-1} \text{K}^{-1}$ )	$\sigma$ ( $10^{-8} \text{W K}^{-1}$ )
5	37.59 ± 0.46	0.553 ± 0.007	42.28 ± 1.10	0.721 ± 0.019	49.95 ± 1.39	1.028 ± 0.029	33.30 ± 0.72	0.965 ± 0.021
10	68.99 ± 0.44	0.507 ± 0.003	65.01 ± 0.82	0.669 ± 0.007	77.27 ± 1.71	0.795 ± 0.018	79.14 ± 1.63	1.147 ± 0.024
25	141.57 ± 1.46	0.483 ± 0.004	149.53 ± 0.56	0.501 ± 0.002	142.02 ± 0.82	0.579 ± 0.003	169.18 ± 4.41	0.964 ± 0.025
50	232.00 ± 1.31	0.336 ± 0.002	234.38 ± 0.83	0.393 ± 0.001	218.32 ± 1.13	0.443 ± 0.002	221.84 ± 0.86	0.632 ± 0.002
75	290.64 ± 1.23	0.281 ± 0.001	279.25 ± 1.32	0.311 ± 0.002	276.77 ± 1.18	0.375 ± 0.002	278.81 ± 1.07	0.528 ± 0.002
100	345.14 ± 1.01	0.237 ± 0.001	338.84 ± 1.81	0.268 ± 0.002	302.79 ± 1.12	0.307 ± 0.001	304.66 ± 2.49	0.433 ± 0.004
250	477.65 ± 0.92	0.138 ± 0.001	542.78 ± 1.65	0.181 ± 0.001	518.04 ± 0.78	0.210 ± 0.001	532.15 ± 3.16	0.302 ± 0.002
350	546.07 ± 0.57	0.113 ± 0.001	602.82 ± 0.82	0.144 ± 0.001	621.53 ± 1.29	0.180 ± 0.001	620.13 ± 1.83	0.252 ± 0.001

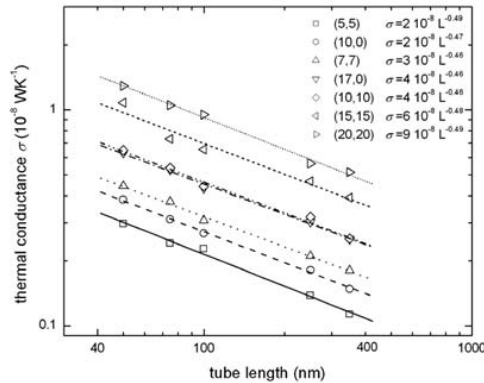
  

Length (nm)	Chirality index							
	(10, 10)		(15, 15)		(20, 20)		MWNT	
	$\lambda$ ( $\text{W m}^{-1} \text{K}^{-1}$ )	$\sigma$ ( $10^{-8} \text{W K}^{-1}$ )	$\lambda$ ( $\text{W m}^{-1} \text{K}^{-1}$ )	$\sigma$ ( $10^{-8} \text{W K}^{-1}$ )	$\lambda$ ( $\text{W m}^{-1} \text{K}^{-1}$ )	$\sigma$ ( $10^{-8} \text{W K}^{-1}$ )	$\lambda$ ( $\text{W m}^{-1} \text{K}^{-1}$ )	$\sigma$ ( $10^{-8} \text{W K}^{-1}$ )
5	35.56 ± 1.19	1.312 ± 0.035	40.41 ± 3.34	2.224 ± 0.147	51.15 ± 1.21	3.009 ± 0.071	27.36 ± 0.73	3.555 ± 0.094
10	78.68 ± 1.55	1.188 ± 0.023	80.26 ± 2.08	1.947 ± 0.046	83.77 ± 1.61	2.464 ± 0.048	45.86 ± 0.91	2.973 ± 0.098
25	164.83 ± 3.25	0.961 ± 0.019	152.32 ± 1.03	1.237 ± 0.009	149.05 ± 1.71	1.736 ± 0.020	104.05 ± 1.52	2.670 ± 0.073
50	223.93 ± 2.72	0.650 ± 0.008	216.13 ± 3.09	1.084 ± 0.013	223.08 ± 2.77	1.293 ± 0.016	131.61 ± 1.95	1.681 ± 0.054
75	279.24 ± 2.85	0.537 ± 0.006	265.29 ± 0.89	0.731 ± 0.003	271.95 ± 1.43	1.052 ± 0.006	—	—
100	305.87 ± 3.07	0.442 ± 0.004	312.19 ± 0.73	0.656 ± 0.002	326.77 ± 1.51	0.947 ± 0.004	—	—
250	549.70 ± 5.51	0.319 ± 0.003	537.88 ± 6.38	0.467 ± 0.001	511.63 ± 6.96	0.544 ± 0.008	—	—
350	611.97 ± 3.24	0.253 ± 0.001	630.35 ± 6.58	0.391 ± 0.001	635.35 ± 7.58	0.513 ± 0.001	—	—

with increasing tube length. This is consistent with the length dependence found in other MD studies [1, 2, 12, 14]. For a tube length, which is not much longer than the phonon mean free path ( $\approx 0.5 \mu\text{m}$ ), it has been shown experimentally [7] that the thermal conductivity does not converge to a constant boundary. Our results in figure 1 reproduce this behavior. The thermal conductivity increases with a power law  $L^\alpha$ . The room temperature exponent  $\alpha$  is approximately 0.77 for short ( $L < 25 \text{ nm}$ ) and 0.54 for longer ( $100 \text{ nm} < L < 350 \text{ nm}$ ) nanotubes. These results are in line with the theoretical room temperature findings of Wang et al [25] with an exponent  $\alpha$

of 0.83 for short ( $L < 100 \text{ nm}$ ) and 0.35 for long ( $L > 10 \mu\text{m}$ ) CNTs. The thermal conductivity of the armchair triple-walled carbon nanotube also increases with increasing  $L$ . The calculated exponent  $\alpha$  for the short ( $< 0.1 \mu\text{m}$ ) MWNT of 0.71 is similar to the values of the short SWNTs (0.77).

One of the open questions in the evaluation of the thermal conductivity  $\lambda$  of nanotubes is the choice of the cross-sectional area  $A$  for the heat flux. Unlike in bulk materials, there is some arbitrariness in this definition. In the present work we define the cross-sectional area as a ring with the same diameter as the SWNT under inclusion of a van der Waals diameter of 0.34 nm



**Figure 2.** Double-logarithmic representation for the thermal conductance  $\sigma$  of (5, 5), (10, 0), (7, 7), (10, 10), (17, 0), (15, 15), and (20, 20) SWNTs at 300 K with a tube length  $L$  between 50 and 350 nm.

for each carbon atom. This choice, however, is only one of many. As a matter of fact it is sometime more convenient to work with the thermal conductance  $\sigma = \lambda' \times A'/L$ , which has no ambiguity in its definition. In contrast to the 'nanotube' parameter  $A$ ,  $A'$  refers to the cross-sectional area of the simulation box which is a well-defined quantity.  $\lambda'$  is the crude thermal conductivity of the simulation box without using the ring cross-sectional area. Figure 2 shows the  $\sigma$  curves of the discussed carbon nanotubes at room temperature in a double-logarithmic representation. We notice that the thermal conductance decreases with increasing tube length. It does not converge in the length range studied ( $L < 350$  nm). This result is not surprising as  $\lambda$  depends on the length via a  $L^\alpha$  law  $\alpha < 1$ . Final division by  $L$  yields a  $L^{-\gamma}$  law for  $\sigma$  with  $\gamma = (1 - \alpha) < 1$ .

All computational results for the thermal conductivity  $\lambda$  and thermal conductance  $\sigma$  for SWNTs as well as for the MWNT chosen are summarized in table 1. It is seen immediately that the length dependence of  $\lambda$  and  $\sigma$  is large in comparison to the influence of the diameter and the chiral indices.

Our thermal conductance data for SWNTs can be fitted by a simple phenomenological expression. At a given temperature, here 300 K (figure 2), the thermal conductance for systems with a length between 50 and 350 nm obeys a power law relation

$$\sigma = \beta L^{-\gamma}, \quad (2)$$

with  $\gamma = (1 - \alpha) < 1$ . As the exponent  $\alpha$  for nanotubes of different diameters is more or less constant ( $\alpha \approx 0.54$ ) an almost universal exponent  $\gamma \approx 0.46$  occurs, too. The prefactor  $\beta$  has been found to depend linearly (figure 3) on the number of carbon atoms  $n$  in the circumference of the tube.  $n$  is given by the sum of the two chiral indices. The  $n$  dependence of  $\beta$  reads

$$\beta = 2(n - 1)10^{-9}. \quad (3)$$

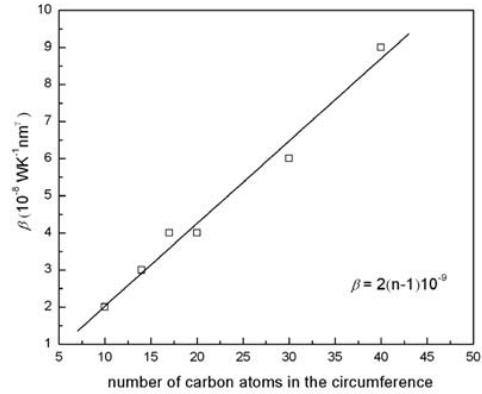


**Figure 3.** Prefactor  $\beta$  (equation (2)) for the thermal conductance versus number of carbon atoms ( $n$ ) in the circumference of SWNTs.

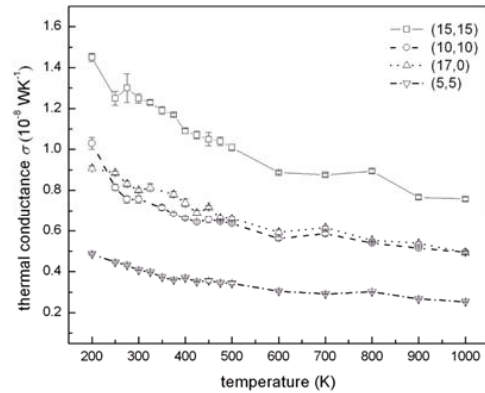


**Figure 4.** Thermal conductance  $\sigma$  versus temperature for (5, 5), (17, 0), (10, 10), and (15, 15) single-walled carbon nanotubes with a length of 30 nm.

In the present formulation, the unit of  $\beta$  is  $\text{W K}^{-1} \text{nm}^\gamma$ . Equations (2) and (3) can provide a quick estimate for the thermal conductance of SWNTs.

#### 4.2. Temperature dependence of the thermal conductance

The thermal conductance of (10, 10), (17, 0), (15, 15) and (5, 5) SWNTs with  $L = 30$  nm and of an armchair triple-walled CNT with  $L = 15$  nm formed by (5, 5), (10, 10), and (15, 15) SWNTs has been calculated for temperatures between 200 and 1000 K. As shown in figure 4, the MD based (i.e. classical)  $\sigma$  values of all nanotubes decrease monotonically with increasing temperature. Due to the neglect of quantum effects in the MD approach, the present results differ from the available experimental data. Up to 350 K the experimental curves decrease smoothly with decreasing temperature [4, 8, 9]. For

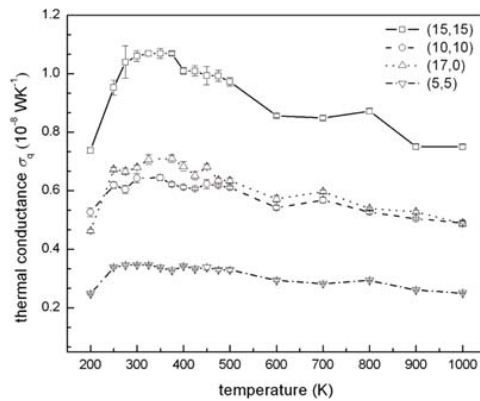


**Figure 5.** Thermal conductance  $\sigma_q$  versus temperature for (5, 5), (17, 0), (10, 10) and (15, 15) single-walled carbon nanotubes with 30 nm length after applying quantum corrections.

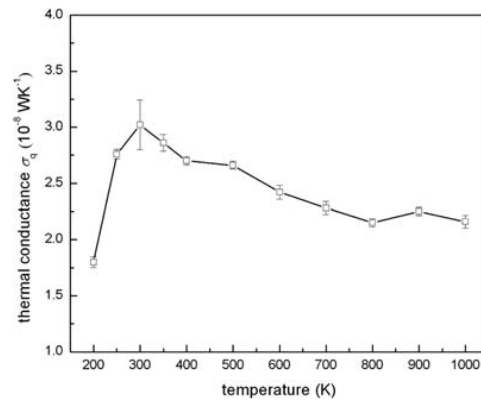


**Figure 6.** Thermal conductance  $\sigma_q$  versus temperature for an armchair triple-walled carbon nanotube with 15 nm length and 2 nm diameter after applying quantum corrections.

MD temperatures  $T_{MD}$  less than the Debye temperature  $T_D$  inherent errors of the present  $\sigma$  parameters have to be expected.  $T_D$  values ranging from 473 to 960 K have been reported for carbon nanotubes. Reasons for this width have been discussed in the literature [1, 26–28]. The implementation of quantum corrections of the zero-point type into the present MD results causes no principal problems. Before presenting such data we want to mention that the general findings presented up to now (i.e. length dependence of  $\lambda$  and  $\sigma$ ) are not changed under the influence of quantum effects. In the present study we have used the quantum corrections of Lukes and Zhong [1] which are based on the following ingredients. It is assumed that the total energy of the system at  $T_{MD}$  is given by twice the mean kinetic energy. Then this energy is equated to the phonon energy of the system by adopting the temperature  $T_q$  as fitting parameter.  $T_q$  is the so-called quantum temperature of the system [29]. Zero-point effects in this correction scheme are considered by an additional parameter. The quantum correction sketched leads to thermal conductance values  $\sigma_q$  where the MD  $\sigma$  numbers are multiplied by the ratio  $dT_{MD}/dT_q$  defined by the MD temperature  $T_{MD}$  and the quantum temperature  $T_q$ .

The quantum-corrected thermal conductance  $\sigma_q$  increases rapidly up to around 250 K (figure 5). Then the curves show a broad maximum followed by a slow decrease at higher temperatures ( $T > 400$  K). The  $\sigma_q$  curves are in reasonable agreement with measured data. However, we cannot see a sharp maximum as found in experimental reports [4, 9]. A reason might be the differences between the length and diameter of the nanotubes which have been used in the simulations and in experiment. Pop *et al* [9] (e.g.) have studied a SWNT with a length of 2.6  $\mu\text{m}$  and a diameter of 1.7 nm while we have used SWNTs with 30 nm length and diameters of 0.33, 0.67, and 1.01 nm for the (5, 5), (10, 10) and (15, 15) systems, respectively. It seems that the thermal conductance of short SWNTs is less temperature-sensitive than that of long CNTs. One also notes that the thermal conductance

of SWNTs with the same length and diameter coincide more or less. Figure 5 shows that the  $\sigma_q$  curves of the (10, 10) and (17, 0) SWNTs are quite similar. Thus it can be deduced the chiral indices of the nanotubes are not important in connection with the thermal conductance. This behavior differs from another transport property, i.e. the inverse resistivity which depends on the chirality index [30]. As predicted by equation (2) the conductance increases with the diameter of the SWNT. Figure 5 suggests that the  $\sigma_q$  of nanotubes with large diameter are more temperature-sensitive than the  $\sigma_q$  of small diameter systems. There is also an indication that the curve maxima are shifted to higher temperatures when the diameter is enhanced. They are found at around 250 K for the (5, 5), (10, 10), and (17, 0) nanotubes, while they are between 300 and 400 K for the (15, 15) system. The thermal conductance  $\sigma_q$  of the MWNT considered shows, the same behavior as found for the SWNTs (figure 6). The temperature dependence of  $\lambda$  and  $\sigma$  at higher temperatures, where quantum effects become less important, can be explained theoretically by so-called Umklapp processes in the phonon-phonon interaction. See [4, 8, 11].

#### 4.3. Thermal rectification in CNTs

Rectification describes a treatment process through a system that is faster in one than in the reverse direction. Rectification is well known in the flow of charge (diodes are rectifiers). But for a long time it has not been observed for heat transport. Recently, however, carbon and boron nitride nanotubes have been found to exhibit thermal rectification effects in an inhomogeneous surrounding [15]. The inhomogeneity was introduced by covering a single nanotube with a platinum compound in a conical geometry. It was found that the heat flow from the high load to the low load region was roughly 2% faster than in the opposite direction.

To model asymmetric heat propagation, we have simulated the loading of the  $L = 60$  nm (10, 10) nanotube with a heavy



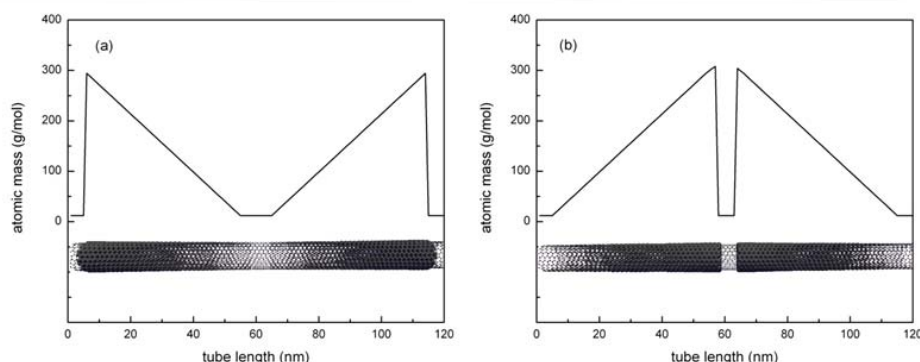


**Figure 7.** Mass distribution in the axial direction of a (10, 10) SWNT. (a) The heavy particles are located in the hot regions on either side of the periodic simulation cell. (b) The heavy particles are located in the cold region in the center of the periodic simulation cell. The RNEMD method requires atoms of identical mass in the hot and cold regions. Implications following from the sudden mass change at the sides (a) and at the tube center (b) are discussed in the text.

component by assigning different masses to the atoms. Please note that the theoretical peculiarities of the RNEMD method require an effective length parameter of  $2L$ . The first setup simulated implements a mass gradient by gradually increasing the atomic masses from 12 to 300 along the tube; see figure 7. Two distributions are realized, one having the heavy atoms in the cold region (center), the other having them in the hot regions (sides). The symmetric mass distribution is dictated by the periodicity of the system. The RNEMD method restricts velocity exchange to atoms of the same mass. Therefore, the atomic masses in the hot and cold slabs are the same. This system is referred to as having a mass gradient. We feel that the setup chosen might be helpful to understand rectification effects in glass or ceramic materials where a mass gradient can be generated via impurity doping at the boundaries of the material. For CNTs, of course, it should be accepted as an idealized model.

In the second system modeled, the nanotube itself has not been modified. It has been loaded with external extra atoms either placed in the hot or cold region of the simulation cell (figure 8). Totally 3336 external particles were distributed at each side of the nanotube. They form regular layers with alternating zig-zag and armchair arrangements. The shortest interatomic contacts within one layer amount to 0.6 nm, a separation which guarantees that the external particles do not contribute sizably to the heat transport in the stacking direction. These intralayer constants are too large for the atoms to 'feel' a harmonic potential with a force constant  $k_r$  of 100000.0 kJ mol<sup>-1</sup> nm<sup>-2</sup> becoming operative for an interatomic separation  $\leq 0.5$  nm. Contacts meeting this boundary are only found for interlayer pairs. But we want to mention that most of the external particles do not contribute to any bond. External particles have been fixed around the tube by a Lennard-Jones potential ( $\epsilon = 0.48$  kJ mol<sup>-1</sup>,  $\sigma = 0.7$  nm). They have a mass of 11, a value close to that of carbon. The small difference to the carbon mass, however, prevents that they participate in the velocity exchange. A (10, 10)

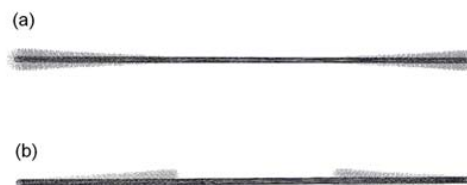


**Figure 8.** Representation of the extra atoms deposited externally on a (10, 10) carbon nanotube with  $L = 60$  nm. (a) Extra atoms are placed in the hot regions on either side of the periodic simulation cell. (b) Extra atoms are placed in the cold region in the direction towards the center of the periodic simulation cell.

SWNT with 60 nm length (the simulation box covers a length of 120 nm) has been used for the calculation of the thermal conductivity  $\lambda$  when heat flows from the high-mass to the low-mass region and vice versa. This (second) system is referred to as the externally loaded system.

In RNEMD, the heat flux is constant. Therefore, the thermal conductivity is proportional to  $\langle dT/dz \rangle^{-1}$ .

$$\lambda = -j_z / \langle dT/dz \rangle. \quad (4)$$

In inhomogeneous systems, the temperature gradient and, hence, the thermal conductivity can vary locally. Figure 9 shows the temperature profile in the axial direction of a nanotube with a mass gradient as symbolized in figure 7. The averaged temperature in this simulation amounts to 300 K. The heat flux has been simulated both into (figure 9(a)) and against (figure 9(b)) the direction of lower atomic masses.

In figure 9(a) a sudden drop of  $T$  is found in the terminal region while this drop occurs in the central part of figure 9(b). These temperature drops are related to the density drop in the systems. The local thermal conductivity  $\lambda_{loc}$  can be calculated by dividing the flux, which is imposed to the system, by the

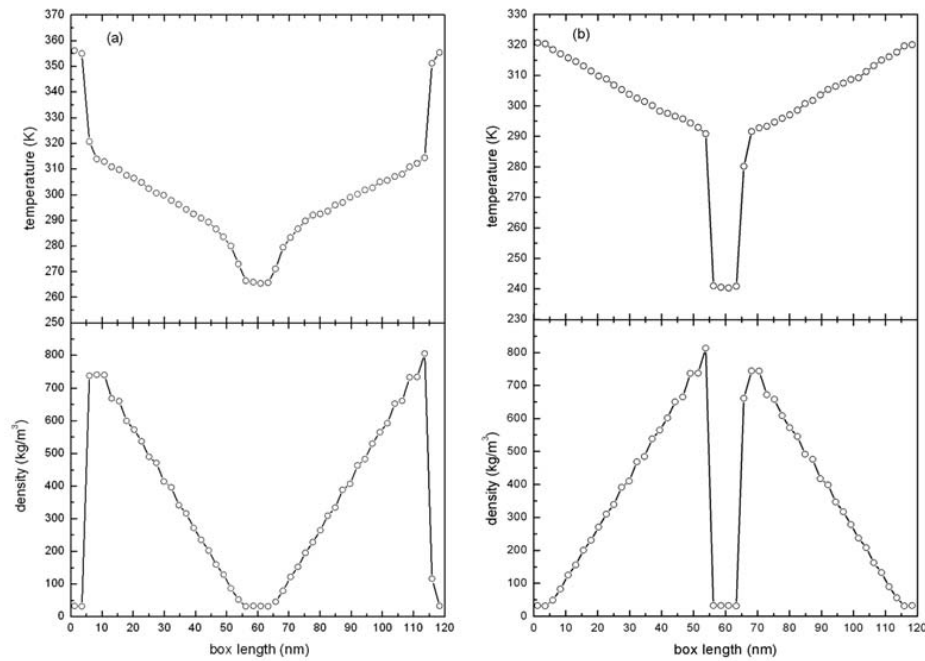


**Figure 9.** Temperature and density profiles in the (10, 10) single-walled nanotube with a mass gradient (figure 7) at an averaged temperature of 300 K. (a) Heat flows into the direction of lower atomic masses. (b) Heat flows into the direction of higher atomic masses.

temperature gradient ( $-dT/dz$ ) for the local area chosen. See again equation (4).

We first focus on  $\lambda_{loc}$  within the regions with a linear temperature profile. The sudden temperature drops will be discussed below. At 300 K, the local thermal conductivities are  $25.66 \text{ W m}^{-1} \text{ K}^{-1}$  when heat flows from the low-mass region to the high-mass region and  $23.24 \text{ W m}^{-1} \text{ K}^{-1}$  for the opposite flow (figure 9). In a second 500 K simulation (not shown) the respective values are 22.73 and  $21.77 \text{ W m}^{-1} \text{ K}^{-1}$ . The thermal rectification  $R_t$  is defined as

$$R_t = \frac{\lambda_{loc,L \rightarrow H} - \lambda_{loc,H \rightarrow L}}{\lambda_{loc,L \rightarrow H}} \times 100 \quad (5)$$

where  $\lambda_{loc,H \rightarrow L}$  stands for the thermal conductivity of the nanotube when heat flows from the high-mass to the low-mass end; vice versa for  $\lambda_{loc,L \rightarrow H}$ . At 300 (500) K we have calculated  $R_t$  numbers of 10.4 (4.4)%. Simulations at still higher temperatures confirm this trend, i.e. the rectification is reduced with increasing  $T$ . Detailed simulation results over a larger  $T$  interval will be presented in a future contribution.

The opposite direction for the preferred heat flux has been predicted in a recent theoretical study of a monoatomic one-dimensional chain [31]. The Fermi–Pasta–Ulam potential employed in this work is defined by a harmonic and a fourth-order coupling element. *A priori* this difference in the theoretical findings might be caused either by non-equivalent

potential energies adopted or by the strict one-dimensional order in the article cited. Peculiarities in the properties of perfect 1D materials are known since the 1960s [32, 33]. In order to comment on the above problem we have performed a single-file 1D simulation under the same computational conditions as adopted for the nanotubes. In the potential only the force constant  $k_r$  has been taken into account. Now the sign of  $R_t$  has changed and agrees with the data in [31]. With the present computational setup we derive a thermal rectification parameter of 3.5% for a preference of the heat flux from the heavy to the light atoms. Thus we have shown that the peculiarities in the physical properties of 1D systems are not restricted to electronic degrees of freedom as presented in [32, 33]. The present results impressively demonstrate that nanotubes—although characterized by a stacking direction—and 1D systems differ quite generally. To sum up: in contrast to 1D materials, we have—at least in the (10, 10) nanotube—a larger thermal conductivity when the ‘higher’ temperature is at the ‘lighter’ particles. Our simulations in progress, however, have shown that magnitude and direction of the thermal rectification depend on the diameter of the nanotube.

Let us come back to the results in figure 9. The sudden jumps in the temperature profiles always occur at the position where atoms of mass 12 are connected to atoms of mass 300. The large differences in the vibrational frequencies on the two sides of the interface are responsible for a slow and inefficient

phonon–phonon coupling. As a result, the thermal conductivity at the interface is small and the temperature gradient is steep (equation (4)). We note that the temperature jump is larger when the mass discontinuity occurs in the cold (figure 9(b)) and not in the hot region (figure 9(a)). It is not clear whether this behavior is caused by opposite directions in the mass gradient or by a large temperature differences in the hot and cold region.

An asymmetric geometrical shape can, in principle, introduce an asymmetric boundary scattering of the phonons [15]. An outcome of such an effect might be a thermal conductivity that is reduced in one direction while it is enhanced in the reverse direction. This possibility leads us to the second class of systems. They are externally loaded. Hence they form inhomogeneous nanotubes. The thermal conductivity at 300 K is larger in the direction of increasing external loading ( $169.19 \text{ W m}^{-1} \text{ K}^{-1}$ ) than in the reverse direction ( $141.20 \text{ W m}^{-1} \text{ K}^{-1}$ ). This trend coincides with our results for the nanotubes with a mass gradient; see above. Our findings, however, differ from a recent experiment [15], where one half of the nanotube has been gradually mass loaded on the surface by heavy molecules. Here, a 2% higher conductivity was found in the direction from high to low loading. On the basis of the limited simulation results we cannot explain this difference. We hope that additional RNEMD simulations as a function of the CNT geometry and the mass distribution will offer deeper insight into key-parameters controlling thermal rectification.

## 5. Conclusions

Using reverse non-equilibrium molecular dynamics simulations we have calculated the thermal conductivity and thermal conductance of single-walled and multi-walled carbon nanotubes as a function of the length, temperature, and chiral index. The calculated thermal conductivity follows a  $L^\alpha$  law, with  $\alpha$  values between 0.54 and 0.77. The effective exponent  $\alpha$  is quite insensitive to the diameter and chiral index of the carbon nanotubes. With increasing diameter the maxima in the thermal conductance curves are shifted to higher temperatures. Again the chiral index is only a weak influence parameter. There is a crossover of the power law at lengths of  $\approx 50$  nm. Short nanotubes exhibit a weaker temperature dependence of  $\lambda$  than long nanotubes. We have also studied the heat rectification in single-walled nanotubes. We have observed a more efficient heat current (i.e. higher thermal conductivity) when heat flows from low-mass to the high-mass region. The calculated rectification was between 3 and 16%. It depends on the temperature and on the way how the mass gradient was implemented. These results confirm the experimental finding of a preferential direction for the heat transport in inhomogeneous nanotubes. In the future they might be used as thermal rectifiers or even transistors for heat flow. Comparison of the thermal rectification as derived for nanotubes and perfect 1D chains emphasizes the different behavior of the two classes of components. The physical properties of nanotubes do not match perfect 1D behavior. This topic will be commented on in detail in our future contribution.

## Acknowledgments

We acknowledge valuable discussions with Dr Frederic Leroy and financial support from the Deutsche Forschungsgemeinschaft (DFG).

## References

- [1] Lukes J R and Zhong H 2007 *J. Heat Transfer* **129** 705
- [2] Che J, Çağın T and Goddard W A III 2000 *Nanotechnology* **11** 65
- [3] Yao Z, Wang J-S, Li B and Liu G-R 2005 *Phys. Rev. B* **71** 085417
- [4] Kim P, Shi L, Majumdar A and McEuen P L 2001 *Phys. Rev. Lett.* **87** 215502
- [5] Fujii M, Zhang X, Xie H, Ago H, Takahashi K and Ikuta T 2005 *Phys. Rev. Lett.* **95** 065502
- [6] Choi T-Y, Poulidakos D, Tharian J and Sennhauser U 2006 *Nano Lett.* **6** 1589
- [7] Yu C, Shi L, Yao Z, Li D and Majumdar A 2005 *Nano Lett.* **5** 1842
- [8] Hone J, Whitney M, Piskoti C and Zettl A 1999 *Phys. Rev. B* **59** 2514
- [9] Pop E, Mann D, Wang Q, Goodson K and Dai H 2006 *Nano Lett.* **6** 96
- [10] Berber S, Kwon Y-K and Tomanek D 2000 *Phys. Rev. Lett.* **84** 4613
- [11] Osman M A and Srivastava D 2001 *Nanotechnology* **12** 21
- [12] Padgett C W and Brenner D W 2004 *Nano Lett.* **4** 1051
- [13] Moreland J F, Freund J B and Chen G 2004 *Microscale Thermophys. Eng.* **8** 61
- [14] Maruyama S 2002 *Physica B* **323** 193
- [15] Chang C W, Okawa D, Majumdar A and Zettl A 2006 *Science* **314** 1121
- [16] Müller-Plathe F and Bordat P 2004 *Novel Methods in Soft Matter Simulations (Springer Lecture Notes in Physics vol 640)* ed M Karttunen, I Vattulainen and A Lukkarinen (Heidelberg: Springer) p 310
- [17] Chang C W, Okawa D, Garcia H, Majumdar A and Zettl A 2008 *Phys. Rev. Lett.* **101** 075903
- [18] Lepri S, Livi R and Politi A 1997 *Phys. Rev. Lett.* **78** 1896
- [19] Li C and Chou T-W 2003 *Int. J. Solids Struct.* **40** 2487
- [20] Rappe A K, Casewit C J, Colwell K S, Goddard W A III and Skiff WM 1992 *J. Am. Chem. Soc.* **114** 10024
- [21] Walther J H, Jaffe R, Halicioğlu T and Koumoutsakos P 2001 *J. Phys. Chem. B* **105** 9980
- [22] Müller-Plathe F 1993 *Comput. Phys. Commun.* **78** 77–94
- [23] Tarmyshov K and Müller-Plathe F 2005 *J. Chem. Inf. Model.* **45** 1943
- [24] Allen M P and Tildesley D J 1987 *Computer Simulation of Liquids* (Oxford: Oxford University Press)
- [25] Berendsen H J C, Postma J P M, van Gunsteren W F, Di Nola A and Haak J R 1984 *J. Chem. Phys.* **81** 3684
- [26] Wang J and Wang J-S 2006 *Appl. Phys. Lett.* **88** 111909
- [27] Charlier A and McRae E 1998 *Phys. Rev. B* **57** 6689
- [28] Benoit J M, Corraze B and Chauvet O 2002 *Phys. Rev. B* **65** 241405(R)
- [29] Hone J 2001 *Carbon Nanotubes (Topics in Applied Physics vol 80)* ed M S Dresselhaus, G Dresselhaus and P Avouris (Berlin: Springer) p 273
- [30] Maiti A, Mahan G D and Pantelides S T 1997 *Solid State Commun.* **102** 517
- [31] Suzuura H and Ando T 1999 *Mol. Cryst. Liq. Cryst.* **340** 731
- [32] Yang N, Li N, Wang L and Li B 2007 *Phys. Rev. B* **76** 020301
- [33] Rieder Z, Lebowitz J L and Lieb E H 1967 *J. Math. Phys.* **8** 1073
- [34] Lieb E H and Wu F Y 1968 *Phys. Rev. Lett.* **20** 1445

# Thermal rectification in mass-graded nanotubes: a model approach in the framework of reverse non-equilibrium molecular dynamics simulations

Mohammad Alaghemandi, Frédéric Leroy, Elena Algaer,  
Michael C Böhm and Florian Müller-Plathe

Eduard-Zintl-Institut für Anorganische und Physikalische Chemie, Technische Universität  
Darmstadt, Petersenstrasse 20, D-64287 Darmstadt, Germany

E-mail: [m.alaghemandi@theo.chemie.tu-darmstadt.de](mailto:m.alaghemandi@theo.chemie.tu-darmstadt.de) and  
[f.leroy@theo.chemie.tu-darmstadt.de](mailto:f.leroy@theo.chemie.tu-darmstadt.de)

Received 3 August 2009, in final form 27 November 2009

Published 18 January 2010

Online at [stacks.iop.org/Nano/21/075704](http://stacks.iop.org/Nano/21/075704)

## Abstract

The thermal rectification in nanotubes with a mass gradient is studied by reverse non-equilibrium molecular dynamics simulations. We predict a preferred heat flow from light to heavy atoms which differs from the preferential direction in one-dimensional monoatomic systems. This behavior of nanotubes is explained by anharmonicities caused by transverse motions which are stronger at the low-mass end. The present simulations show an enhanced rectification with increasing tube length, diameter and mass gradient. Implications of the present findings for applied topics are mentioned concisely.

## 1. Introduction

Rectification is a transport process that is faster in one direction than in the opposite one. This phenomenon has been used extensively in electric devices such as diodes. As a result of a predominant charge flow in one direction these elements can act as electric rectifiers. The recent detection of thermal rectification in externally mass-loaded carbon and boron nitride nanotubes has been a milestone in nanoscale solid-state science [1]. In analogy to the electric phenomenon, thermal rectification  $R_t$  describes a preferred direction for the heat flow in a material. The challenging experimental findings of Chang *et al* [1] therefore have focused the interest of theoreticians on thermal rectification. In a series of molecular dynamics (MD) simulation studies, Li and co-workers described the possibility of observing thermal rectification in carbon nanocones [2] or in nanotubes having an intramolecular junction [3]. Guided by the aim to understand the mechanism of rectification, Li and co-workers have detected thermal rectification in a perfect one-dimensional (1D) mass-graded monoatomic chain [4] interacting through the Fermi–Pasta–Ulam (FPU) potential [5]. In this model a harmonic term is supplemented by a fourth-order coupling element introducing anharmonic effects. Li

and co-workers showed in their articles that the overlap of the vibrational spectra of the two chain ends having different masses or different diameters is a key quantity for thermal rectification. The larger the vibrational overlap, the more intense is the heat flow. In objects with asymmetric mass or size distribution, therefore a more or less efficient overlap can be obtained, depending on how the system is oriented into a temperature gradient. Additionally, Li and co-workers pointed out the decisive role of anharmonic effects for thermal rectification. This is illustrated in detail in their MD study of the mass-graded 1D monoatomic FPU chain [6]. Indeed, low-frequency modes contributing predominantly to heat conduction can be generated when the anharmonic part of the FPU potential is excited. On the one hand, the mass-graded FPU chain is thought to be a suitable model for the understanding of thermal rectification in systems having an extent in one dimension. On the other hand, no attempt has been made up to now to correlate the theoretical findings for such a system with results for quasi-one-dimensional structures such as nanotubes.

In our recent MD study on the thermal conductivity in nanotubes [7], we have demonstrated that both external loading under otherwise constant atomic masses in the nanotube and

the implementation of a mass gradient  $\alpha = \Delta m(z)/\Delta z$  along the tube axis ( $z$ ) renders possible thermal rectification.  $m(z)$  symbolizes the particle mass at position  $z$ . In our study we have shown that systematic trends in thermal rectification can be derived more easily for a mass-graded quasi-1D system. At this stage of our research we could not give a microscopic explanation of the origin, direction and magnitude of thermal rectification. In [7] we have described only the general phenomenon. Now we have chosen mass-graded nanotube models to understand the underlying microscopic mechanisms involved in thermal rectification. Instead of externally mass-loaded nanotubes we have chosen a set-up where thermal rectification is rendered possible by a mass gradient along the tube axis.

Nanotube materials have been chosen by experimentalists and theoreticians to analyze whether concepts for 1D single-file chains can be transferred to quasi-1D materials which are experimentally accessible. The present contribution will show that, as far as thermal rectification is macroscopically concerned, the behavior of mass-graded monoatomic 1D systems is different from that of mass-graded quasi-1D systems such as nanotubes. Furthermore, by proposing a model based on spectral considerations, we show that the introduction of possible transverse atomic moves due to a cylindrical configuration and their coupling to longitudinal vibrations plays a central role in thermal rectification. They are responsible for a different behavior of the heat conduction in tubes and in perfect 1D systems.

## 2. Theoretical background: non-equilibrium MD simulations and rectification parameters

We have employed a reverse non-equilibrium molecular dynamics (RNEMD) approach [8, 9] to study thermal rectification in nanotubes with a mass gradient. To generate such a mass gradient  $\alpha$  we have modified gradually the atomic mass  $m(z)$  along the main axis of the systems, here chosen to be the  $z$  axis. As the theoretical background of the RNEMD technique can be found in the literature [8, 9] only the most important ingredient of this method will be reviewed here. The RNEMD formalism is based on a reversal of the experimental cause-and-effect picture. In contrast to conventional non-equilibrium MD schemes, the RNEMD model makes use of an imposed heat flux which allows the evaluation of the temperature gradient in the  $z$  direction. The evaluation of the heat flux in the presence of an imposed temperature gradient is not straightforward on a molecular scale.

The atoms in the nanotubes interact via harmonic radial, angular and torsion potentials. The equilibrium values of these parameters in nanotubes amount to 0.1418 nm, 120° and 0°. The associated force constants are 3 92460 kJ mol<sup>-1</sup> nm<sup>-2</sup>, 527 kJ mol<sup>-1</sup> rad<sup>-2</sup> as well as 167 kJ mol<sup>-1</sup> rad<sup>-2</sup>. These parameters have been determined by Li and Chou [10]. In analogy to our recent article on thermal conductivity in carbon nanotubes [7], we have employed them without further modifications.

The thermal rectification factor  $R_t$  is defined as

$$R_t = \frac{\lambda_{H \rightarrow L} - \lambda_{L \rightarrow H}}{\lambda_{L \rightarrow H}} \times 100 \text{ (in \%)} \quad (1)$$

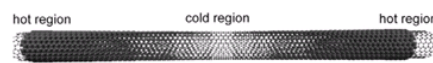


**Figure 1.** Schematic mass distribution in the axial direction of a (10, 10) nanotube. The heavy particles (symbolized by bold lines) are located in the hot regions on either side of the periodic simulation cell. The terminal light atoms (thin lines) at the chain ends are a manifestation of velocity exchanges in the RNEMD formalism that are restricted to particles of the same mass; see text. In the second case the heavy particles are located in the cold (central) region of the simulation cell.

where  $\lambda_{H \rightarrow L}$  stands for the thermal conductivity of the system when heat flows from the high-mass to the low-mass region, and vice versa for  $\lambda_{L \rightarrow H}$ . We are aware of the fact that equation (1) is only one possible choice to quantify thermal rectification. However, this definition is in line with the formula adopted by Chang *et al* in the first experimental verification of this phenomenon in nanotubes [1].

The thermal conductivity  $\lambda$  is related via the Fourier law  $\lambda = -j_z/(dT/dz)$  to the heat flux  $j_z$  through the system set into a temperature gradient along the  $z$  direction  $dT/dz$ . We should mention that, when using the RNEMD method, a linear temperature profile is observed only within the central region of the sample. Therefore, we have restricted the determination of  $\lambda$  to this linear region and disregarded the boundaries of the system. The physical origin of this behavior has been emphasized in detail in our recent study of nanotubes [7]. The velocity exchange in the RNEMD method is restricted to particles of the same mass. The imposed mass gradient in the nanotubes then requires light atoms (for the exchange) in the neighborhood of heavy ones. We refer to figures 7 and 9 of our recent study [7].

In section 4 we first analyze the thermal rectification factor  $R_t$  in nanotube systems with different chiral indices and thus different diameters as well as tube lengths. Caused by the above-mentioned peculiarity of the RNEMD method (i.e. mass equivalence of atoms whose velocity is swapped) an effective sample length is required which exceeds the target length by a factor of two. In one series of simulations we have adopted a linear mass gradient  $\alpha = 5.76 \text{ g mol}^{-1} \text{ nm}^{-1}$  starting with a mass of 12 g mol<sup>-1</sup> for the lightest atoms in each system. Additional values for  $\alpha$  will be commented on below. A typical mass profile we have adopted is depicted in figure 1. In one configuration, the gradient was oriented such that the heavy atoms were in the hot regions (sides) while in the second configuration heavy atoms were in the cold region (center). The symmetric mass distribution generated is dictated by velocity exchanges between atoms of the same mass; see above. In both configurations described, light atoms were chosen to be in the velocity exchange regions.

In purely harmonic mass-graded (1D) systems set into a temperature gradient, the energy transfer is exactly compensated when reversing the temperature gradient. Therefore, rectification cannot exist in this case [4]. A recent study in the framework of the mass-graded FPU chain, however, showed that the energy transfer in a lattice with

an anharmonic character is not compensated, when reversing the temperature gradient and thermal rectification arises [4]. In order to quantify such an uncompensated energy transfer, we have calculated the power spectra of the studied systems. Already in articles dealing with nanocones [2] or the mass-graded FPU chain [4], the reliability of such an approach has been proven. In contrast to previous articles [3, 4] where only power spectra of particular light and heavy atoms in the system were computed, we have evaluated the total power spectra. We have computed them as the Fourier transform of the mass-weighted Cartesian velocity auto-correlation function. In the harmonic approximation, it corresponds to the density of vibrational states of the system [11].

When increasing the temperature, the amplitudes of the transverse vibrations of the atoms increase. In additional simulations we have shown that—even in connection with a classical MD model—light atoms are more sensitive to this effect. Thus, we expect that anharmonic vibrations in tubes can be correlated to excited transverse vibrations of light atoms. Therefore, we state that, when light atoms are placed in the high temperature region, the transfer of energy from transverse vibrations to longitudinal vibrations is more efficient than for warmed-up heavy atoms. In order to check that model, we define—in addition to the parameter  $R_t$ —a ‘spectral’ rectification factor  $R_p$ :

$$R_p = \frac{P_Z^{H \rightarrow L} - P_Z^{L \rightarrow H}}{P_Z^{L \rightarrow H}} \times 100 \text{ (in \%)} \quad (2)$$

In analogy to equation (1)  $H \rightarrow L$  refers to a heat flow from the high-mass end to the low-mass end, and vice versa for  $L \rightarrow H$ . The projection of the power spectrum in the longitudinal direction  $P_Z$  is computed using

$$P_Z = \frac{\int G_Z(\omega) d\omega}{\int G(\omega) d\omega} \quad (3)$$

where  $G_Z(\omega)$  is the  $z$  projection of the Fourier transform of the mass-weighted Cartesian velocity auto-correlation function  $G(\omega)$ :

$$G(\omega) = \frac{1}{\sqrt{2\pi}} \int_{-\infty}^{\infty} dt e^{i\omega t} \left\langle \sum_{j=1}^N m_j \vec{v}_j(t) \vec{v}_j(0) \right\rangle \quad (4)$$

The symbol  $v_j(t)$  abbreviates the velocity of atom  $j$  at time  $t$ , while  $\omega$  denotes the vibrational wavenumber. The integration in equation (4) was carried out over the whole spectrum.  $P_z$  appears to be the fraction of the total power spectrum related to longitudinal atomic moves. Thus  $P_z$  is expected to quantify the transfer of the total vibrational energy to the longitudinal direction when the system is set into a temperature gradient. Other quantities based on the relaxation of correlation functions for transverse and longitudinal atomic moves under non-equilibrium conditions may similarly map this energy transfer. They will be considered in a forthcoming paper [12].

### 3. Computational conditions

All MD simulations have been performed with the YASP package [13, 14] using periodic boundary conditions. This implies that the end regions of the systems are connected. Unless specified otherwise, all simulations have been performed at constant volume and temperature. The Berendsen thermostat [15] has been used to maintain a constant temperature. The chosen coupling time of 1 ps has been sufficient to keep the measured mean temperature within 2 K of the target temperature. A time step of 1 fs has been employed. In order to build up a steady heat flux in the system, a velocity exchange in the RNEMD approach has always been performed after 300 time steps (i.e. 0.3 ps) while temperature profiles have been recorded for time intervals covering 301 steps. It has been checked that the temperature gradient was linear when adopting this exchange period. Non-equilibrium simulations required typically 6 ns. The last nanosecond has been used for the data production. To check the stability of the RNEMD data we have extended the simulation time to values larger than 10 ns. These test calculations have shown that 5 ns was sufficient to derive stable results, irrespective of the masses employed. We are aware of the different simplifications adopted in the present model simulations. But neither the rather short chain length nor the underestimation of anharmonicities have an influence on the general trends derived. When enhancing the length of the nanotubes or allowing for additional anharmonic couplings, we observed rectification effects that are somewhat more pronounced.

### 4. Microscopic model for thermal rectification

To simplify the analysis of the thermal rectification let us—for a moment—come back to the thermal conductivity in nanotube models. In figure 2 we have displayed  $\lambda$  and the thermal rectification factor  $R_t$  of nanotubes with different chiral indices. The average temperature in the simulations amounts to 300 K. The chiral indices considered are (5, 5), (7, 7), (10, 10), (15, 15) and (20, 20). They refer to tube diameters of 0.677, 0.948, 1.354, 2.031 and 2.708 nm, respectively. We have chosen lengths of 30, 50 and 80 nm for the mass gradient, which implies simulation box lengths of 70, 120 and 200 nm. In figure 2(a) we present the variation of the thermal conductivity in the nanotube systems with respect to the tube diameter for a heat flow from the light end to the heavy end and vice versa. It can be seen that the thermal conductivity is larger when heat flows from the light end of the tubes to the heavy end. This behavior differs from the mass-graded FPU-based findings of Li and co-workers [4] in perfect 1D chains. These authors have found that the heat flux from heavy to light atoms exceeds the flux in the reverse direction. In the mass-graded anharmonic FPU chain one has the situation that heating the heavy mass end yields a more efficient excitation of low-frequency modes contributing to heat conduction. Our simulation results for the nanotubes in figure 2(a) show that this reasoning cannot be applied to the quasi-1D tube systems. In a previous work Li and co-workers [6] pointed out the decisive role of anharmonic effects for thermal rectification.

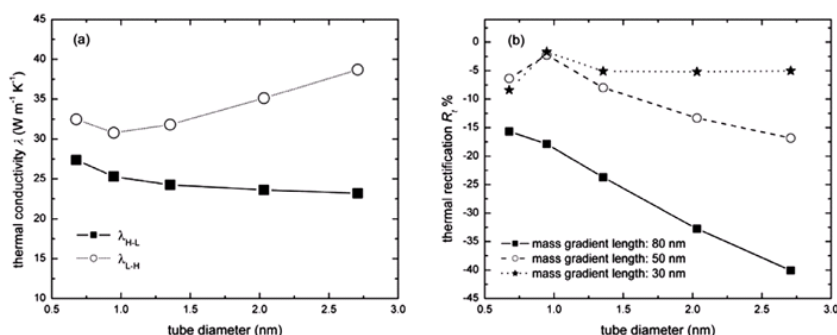


**Figure 2.** (a) Thermal conductivity  $\lambda$  of (5, 5), (7, 7), (10, 10), (15, 15) and (20, 20) nanotubes (from left to right) with a mass gradient length of 80 nm and  $\alpha = 5.76 \text{ g mol}^{-1} \text{ nm}^{-1}$  for a heat flow from the light part to the heavy one (upper curve) and vice versa (lower curve). (b) Diameter dependence of the thermal rectification  $R_t$  for the same nanotubes as considered in the left diagram with a mass gradient length of 30, 50 and 80 nm. The lines in all diagrams serve as guides for the eyes. The error bars in the simulations are less than the dimension of the adopted symbols.

Anharmonic—or more generally coupling—mechanisms are of different origin in perfect one-dimensional and cylindrical structures. Indeed, in tubes coupling can arise from transverse vibrational displacements while such modes are absent in a linear arrangement. The validity of this assumption will be explained below. Macroscopically, the implications of this difference in the degrees of freedom for rectification effects are illustrated in figure 2(b). Here it is shown that the thermal rectification factor  $R_t$  in nanotubes has a negative value throughout. Before continuing with our theoretical model, one should note that the magnitude of the rectification is enhanced by tube diameter and tube length. This is visualized in figure 2(b) where the  $R_t$  numbers have been computed on the basis of the  $\lambda$  values plotted in figure 2(a).

Now let us consider the 'spectral' rectification parameter  $R_p$  to render possible a microscopic explanation for the findings summarized in figure 2. The variation of  $R_p$  as a function of the tube diameter and tube length is reported in figure 3. It must be noticed that  $R_p$  has the same sign as  $R_t$  and that its variation follows the same trend as encountered for  $R_t$ . We believe that this one-to-one correspondence between  $R_t$  and  $R_p$  validates our model. It shows that the transfer of vibrational energy from transverse atomic motions to longitudinal ones plays a crucial role for thermal rectification. Moreover, it has to be compared to the mass-graded FPU chain where the introduction of the anharmonic term in the potential energy renders possible thermal rectification [4]. In the case of a mass-graded nanotube, the possibility of transverse atomic motions and their coupling to longitudinal moves plays the same role. However, in a monoatomic 1D chain, the heat transfer is dictated by the fact that a warm heavy atom can excite a lighter atom more efficiently than a warm light atom can excite a heavier atom. As a consequence, the rectification factor is positive. In a nanotube arrangement the thermal rectification shows an opposite trend. This follows from the fact that the enhanced anharmonicities of light atoms can be transmitted more easily via the transverse–longitudinal coupling.

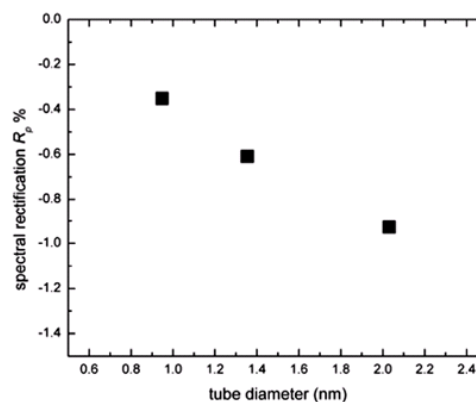


**Figure 3.** Spectral rectification factor  $R_p$  calculated from equation (2) for (7, 7), (10, 10) and (15, 15) nanotubes (from left to right) with a mass gradient length of 80 nm and  $\alpha = 5.76 \text{ g mol}^{-1} \text{ nm}^{-1}$ .

When increasing the tube diameter, the number of transverse modes is enhanced. Following the model described above, we can anticipate that the energy transfer to the longitudinal tube direction will be enhanced accordingly. Since a mass-graded tube exhibits a higher heat flow from the low-mass end to the high-mass end, we expect that an enlargement of the tube diameter renders possible an increase in the magnitude of the thermal rectification factor  $R_t$ . This is exactly what is observed in the RNEMD results reported in figure 2(b), where  $R_t$  is increasing in absolute value when the tube diameter is enhanced.

Due to the construction of our samples, the number of lightest atoms remains constant when the tube length is increased while the number and the mass of heavier atoms are increased. Thus the energy demand for the atoms to feel

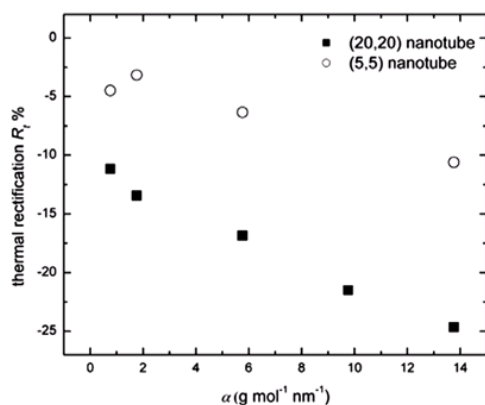


**Figure 4.** Thermal rectification as a function of the mass gradient  $\alpha$  for (20, 20) and (5, 5) nanotubes with a length of 50 nm for the mass gradient at an averaged temperature of 300 K.

the anisotropy of the local potential is higher for the heavy particles than for the light ones. Therefore, the anharmonic character of the lattice is enhanced when the higher thermal energy is experienced by the light atoms. As a matter of fact the magnitude of the thermal rectification is increased when the tube is longer. This is shown in figure 2(b).

In addition to the influence of the diameter and length of the nanotubes on the magnitude of  $R_t$ , the slope of the mass gradient  $\alpha$  plays a significant role, too. Again we have analyzed the heat flow from the heavy-mass part to the low-mass one and vice versa for (5, 5) and (20, 20) nanotubes with a length of 50 nm at an average temperature of 300 K. We found that both thermal conductivities  $\lambda_{H \rightarrow L}$  and  $\lambda_{L \rightarrow H}$  decrease with increasing mass difference between bonded atoms. It is well known that the energy transfer is maximized for atoms of identical mass. One should also remark that a similar behavior

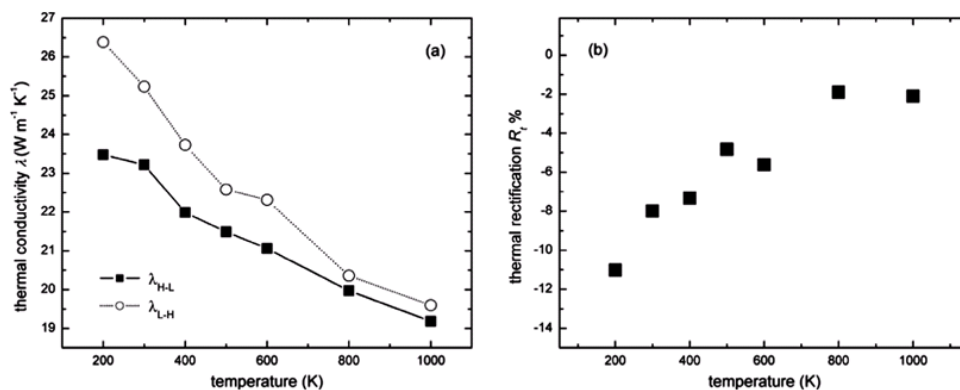


**Figure 5.** (a) Temperature dependence of the thermal conductivity  $\lambda$  for a heat flow from heavy to light atoms and vice versa in a (10, 10) nanotube with a length of 50 nm and a mass gradient  $\alpha$  of  $5.76 \text{ g mol}^{-1} \text{nm}^{-1}$ . (b) Temperature dependence of the thermal rectification in the (10, 10) nanotube given under (a).

would exist in monoatomic 1D chains since the energy transfer is reduced by an increasing mass difference along the system's main axis. However, in the case of the nanotubes studied here, the splitting between the two thermal conductivities is almost constant for all  $\alpha$  parameters chosen. As explained previously  $\lambda_{L \rightarrow H}$  is always higher than  $\lambda_{H \rightarrow L}$ . Figure 4 shows that the thermal rectification factor is negative and increases in magnitude when the mass gradient increases. Indeed, we found that, due to the diameter effect described, the difference between  $\lambda_{H \rightarrow L}$  and  $\lambda_{L \rightarrow H}$  is larger for the larger tube diameter, i.e. for the (20, 20) nanotube.

Next we consider the influence of the temperature on the two directions of the heat transfer and on the thermal rectification. The temperature dependence of the calculated thermal conductivities and thermal rectification factors is given in figures 5(a) and (b). The splitting between the two curves  $\lambda_{H \rightarrow L}$  and  $\lambda_{L \rightarrow H}$  is reduced when increasing the temperature. The final result is an attenuation of rectification effects. At higher temperatures it becomes irrelevant whether the energy for the heat conduction is stored in the high- or low-mass region of the nanotube. This effect seems to overcompensate the influence of anharmonicities in the potential, which should be stronger at high temperatures.

## 5. Conclusions

In the present paper we have explained the microscopic origin for the thermal rectification in mass-graded nanotube systems by performing reverse non-equilibrium molecular dynamics simulations. We have observed a more efficient heat current (i.e. higher thermal conductivity) in nanotubes when heat flows from the low-mass to the high-mass region. The opposite behavior has been found in mass-graded 1D chains. We have emphasized that the thermal conductivity in quasi-1D networks such as nanotubes and perfect 1D chains is controlled by different influence parameters. Only in nanotubes can we have a transfer of the vibrational energy to the longitudinal



axis under the influence of anharmonic effects perpendicular to this direction. Such an energy transfer is absent in single-file chains. At least in connection with thermal conductivities and rectification we have to conclude that nanotubes cannot serve as model structures to study the physical peculiarities of 1D systems. Such an exclusion also holds for electronic properties [16, 17]. The influence of the tube length, diameter, mass gradient and temperature on the thermal rectification in mass-graded nanotubes has been quantified. The rectification factor  $R_t$  is positively correlated with the length, the diameter and the mass gradient while it is negatively correlated with the temperature.

We are convinced that the model systems studied are helpful in understanding thermal rectification effects in real systems where a mass gradient can be generated via impurity doping or isotopic substitution. It is well known that an enrichment of isotopes in a natural matrix leads to a significant reduction of  $\lambda$ . This has been verified in a number of experimental studies [18–21]. For a random distribution of isotopes, rectification effects do not occur. But when going to a spatially ordered (i.e. localized) arrangement of added isotopes or impurities, thermal rectification is expected. The enrichment of isotopes at one side of a glass or ceramic material might lead to a more efficient energy balance. With this prediction let us go back to the first experimental observation of thermal rectification [1]. It is our hope that the present theoretical findings provide an explanation for the measured thermal rectification in externally mass-loaded nanotubes. Rectification in these materials arises from enhanced amplitudes of transverse modes due to their interaction with the external particles. This mechanism represents the source of an asymmetric energy transfer necessary to observe thermal rectification in such a material. The sign of the rectification factor is a direct effect of the cylindrical arrangement. More generally, the understanding of vibrations in a nanotube as we have described here, may be of interest for any system with a coupling between the vibrational modes of the tube and the vibrational modes of the species adsorbed either on the internal or the external surface.

## Acknowledgment

Financial support from the Deutsche Forschungsgemeinschaft (DFG) is gratefully acknowledged.

## References

- [1] Chang C W, Okawa D, Majumdar A and Zettl A 2006 *Science* **314** 1121
- [2] Yang N, Zhang G and Li B W 2008 *Appl. Phys. Lett.* **93** 243111
- [3] Wu G and Li B W 2007 *Phys. Rev. B* **76** 085424
- [4] Yang N, Li N, Wang L and Li B W 2007 *Phys. Rev. B* **76** 020301
- [5] Fermi E, Pasta J and Ulam S 1955 Studies of non linear problems *Document LA-1940*
- [6] Li B W, Wang J, Wang L and Zhang G 2005 *Chaos* **15** 015121
- [7] Alaghemandi M, Algaer E, Böhm M C and Müller-Plathe F 2009 *Nanotechnology* **20** 115704
- [8] Müller-Plathe F 1997 *J. Chem. Phys.* **106** 6082
- [9] Müller-Plathe F and Bordat P 2004 *Novel Methods in Soft Matter Simulations (Springer Lecture Notes in Physics vol 640)* ed M Karttunen, I Vattulainen and A Lukkarinen (Heidelberg: Springer) p 310
- [10] Li C Y and Chou T W 2003 *Int. J. Solids Struct.* **40** 2487
- [11] Jobic H, Smirnov K S and Bougeard D 2001 *Chem. Phys. Lett.* **344** 147
- [12] Alaghemandi M, Leroy F, Müller-Plathe F and Böhm M C 2010 *Phys. Rev. B* submitted
- [13] Müller-Plathe F 1993 *Comput. Phys. Commun.* **78** 77
- [14] Tarmyshov K B and Müller-Plathe F 2005 *J. Chem. Inf. Model.* **45** 1943
- [15] Berendsen H J C, Postma J P M, van Gunsteren W F, DiNola A and Haak J R 1984 *J. Chem. Phys.* **81** 3684
- [16] Böhm M C and Schütt J 1997 *Phys. Lett. A* **232** 106
- [17] Böhm M C, Schütt J and Philipp S 1998 *Int. J. Quantum Chem.* **69** 727
- [18] Onn D G, Witek A, Qiu Z, Anthony T R and Banholzer W F 1992 *Phys. Rev. Lett.* **68** 2806
- [19] Anthony T R, Fleischer J L, Olson J R and Cahill D G 1991 *J. Appl. Phys.* **69** 8122
- [20] Ozhogin V I, Inyushkin A V, Taldenkov A N, Tikhomirov A V, Popov G E, Haller E and Itoh K 1996 *JETP Lett.* **63** 490
- [21] Chang C W, Fennimore A M, Afanasiev A, Okawa D, Ikuno T, Garcia H, Li D, Majumdar A and Zettl A 2006 *Phys. Rev. Lett.* **97** 085901

## Thermal rectification in nanosized model systems: A molecular dynamics approach

*Mohammad Alaghemandi\*, Frédéric Leroy, Florian Müller-Plathe and Michael C. Böhm*

Eduard-Zintl-Institut für Anorganische und Physikalische Chemie,  
Technische Universität Darmstadt, Petersenstrasse 20, D-64287 Darmstadt, Germany

\*E-mail: [m.alaghemandi@theo.chemie.tu-darmstadt.de](mailto:m.alaghemandi@theo.chemie.tu-darmstadt.de)

The thermal conductivity in a set of mass-graded nanosized model systems has been studied by non-equilibrium molecular dynamics (MD) simulations in order to understand the phenomenon of thermal rectification which has been detected in externally mass-loaded nanotubes. We have found that the preferred direction of the heat transport in mass-graded nanotubes occurs from light to heavy atoms while the opposite direction of the heat transfer is observed in anharmonic mass-graded single-file chains. Mass-graded polyacetylene-like chains behave like single-file chains as long as the mass gradient is hold by the backbone atoms. The thermal rectification in nanotubes with a gradient in the bond force constant ( $k_r$ ) has been studied, too. They are characterized by a preferred heat transfer from the region with large  $k_r$  to the domain with small  $k_r$ . Thermal rectification has been studied also in planar and 3D mass-graded systems where the heat flow followed a preferred direction similar to that observed in nanotubes. Additionally, a more realistic system has been implemented. Here a different number of carbon nanotubes have been grafted on both sides of a graphene sheet. We have found that the transfer of the vibrational energy as well as the generation of low-energy modes at atoms with large masses is responsible for the sign of the thermal rectification. Its origin has been rationalized with the help of (projected) vibrational density of states. On the basis of the present MD simulations we suggest a possible design of materials showing a strong preference for the heat transfer into one direction.

---

## 4.1. Introduction

Rectification is a transport process that is faster in one direction than in the opposite. This phenomenon is known since many decades for the current of charges; diodes are electric rectifiers. The first experimental articles on thermal rectification ( $R_t$ ), i.e. the non-equivalence of the heat transport in two opposite directions, however, have been published in the seventies. This phenomenon has been found in metal-metal and dielectric-dielectric systems.<sup>1,2</sup> For a current review on solid-state thermal rectification in bulk materials we refer to 3. The recent detection of thermal rectification in externally mass-loaded carbon and boron nitride nanotubes<sup>4</sup> has led to a breakthrough in nanoscience that initiated also new experimental activities on bulk materials such as transition metal oxides.<sup>5</sup> To come back to nanosized materials, the rectification effects observed here have led to an increasing interest in the physical properties of carbon nanotubes (CNTs).<sup>6-9</sup> Li and coworkers have shown in a number of theoretical studies that the origin of a different heat conduction in opposite directions depends on the type of the system studied.<sup>3, 10-12</sup> A geometric anisotropy, e.g., can be built by a conic fragment in a tube with otherwise constant diameter. Very recently such a geometric anisotropy has been studied theoretically for asymmetric graphene ribbons.<sup>13, 14</sup> The implementation of an impurity gradient can establish a mass anisotropy. Another possibility to generate thermal rectification is the insertion of external masses at the boundaries of a low-dimensional system. Such a setup has been used in Ref. 4. The above factors are either responsible for an anisotropy in the static potential energy surface (PES) or in the kinetic energy part leading to a PES anisotropy in a dynamic description.<sup>15</sup> Modifications in the local vibrational modes yield the necessary anisotropy for the heat conduction.

In recent molecular dynamics (MD) simulations,<sup>16</sup> the present authors have analyzed the thermal conductivity ( $\lambda$ ) as well as the thermal conductance ( $\sigma$ ) of CNTs as a function of the chain length ( $l$ ), diameter ( $d$ ) and temperature ( $T$ ). This research has led to our first contact with thermal rectification in externally mass-loaded CNTs and nanotubes with a mass gradient ( $\alpha$ ).<sup>17</sup> We have found that the signs of  $R_t$ ,

$$R_t = \frac{\lambda_{H \rightarrow L} - \lambda_{L \rightarrow H}}{\lambda_{L \rightarrow H}} \times 100, \quad (\text{in } \%) \quad (1)$$

of mass-graded nanotubes and mass-graded one-dimensional (1D) single-file chains differ.  $\lambda_{H \rightarrow L}$  symbolizes the thermal conductivity from heavy to light atoms; vice versa for  $\lambda_{L \rightarrow H}$ . Modified definitions of thermal rectification for the mapping of other physical situations will be given in the next section. The predicted preferred heat transport in single-file chains occurs from atoms with heavy masses to light particles leading to  $R_t > 0$ .<sup>10</sup> The negative sign of  $R_t$  calculated for nanotubes indicates that the energy transport is here more efficient when placing the light atoms at higher temperatures. In the present manuscript we have adopted an  $R_t$  definition

---

where the number of the degrees of freedom in the high and low  $T$  reservoir is identical.  $R_t \neq 0$  is then caused by different efficiencies of the degrees of freedom for the transport of energy.

Differences in the physical properties of a hypothetical 1D single-file chain and nanotube models or any other quasi 1D system raise a general question. It concerns the transferability of physical concepts derived for 1D single-file chains to quasi 1D systems that are experimentally feasible. In a brief report<sup>17</sup> we have explained why mass-graded quasi 1D nanotubes cannot serve as a model system for perfect 1D single-file chains at least in connection with heat transport processes. The influence of anharmonicities in the potential, which are a possible prerequisite for thermal rectification, is different in mass-graded single-file chains and quasi 1D systems.

The different signs of  $R_t$  in hypothetical 1D single-file chains and quasi 1D networks such as CNTs are not unexpected. Theoretical articles emphasizing the physical peculiarities of hypothetical 1D systems have been published over many decades. More than eighty years ago Jordan and Wigner<sup>18</sup> have shown that the electronic quantum statistics in single-file chains is essentially arbitrary. It differs from the conventional fermionic statistics of electronic systems that are more than one-dimensional. The topology dependence of this statistics has been analyzed by one of the present authors.<sup>19,20</sup> Lieb and Wu<sup>21</sup> have demonstrated the absence of a  $T$  gradient in the interior of single-file chains when adopting the harmonic approximation. Deviations from this behavior have been found in the framework of the Fermi-Pasta-Ulam (FPU) potential,<sup>22</sup> where the harmonic terms are supplemented by fourth-order coupling elements.<sup>10</sup> Another peculiarity of perfect 1D systems has been reported by W. Kohn in the fifties.<sup>23</sup> Manifestations of the so-called Kohn anomaly, i.e. a characteristic mode softening at half band-filling, on the electrical conductivity have been commented on in Refs. 24, 25. To sum up: in theoretical articles published over many decades, it has been demonstrated that the physics of single-file chains differs not only from the physics of two- (three-) dimensional materials but also from the one established in many quasi 1D systems experimentally accessible. Possible one-to-one correlations between the properties of hypothetical single-file chains and quasi 1D materials have become a challenging field of chemical physics.

In the present MD study we analyze the correlation between the dimension of a system and the sign or magnitude of the thermal rectification. As one class of model compounds we have chosen nanotubes. In the past years it has been accepted quite generally that nanotubes are suitable models to map the physical peculiarities of 1D systems.<sup>6-9</sup> But already in our recent article<sup>17</sup> we have shown that this direct correlation cannot be justified when comparing the  $R_t$  parameters of mass-graded nanotubes and 1D single-file chains. In the present contribution our recent findings will be extended into several directions. We have considered a larger collection of nanosized systems. In addition to quasi 1D nanotubes we have studied quasi 1D chains with a polyacetylene-like structure as well as some 2D and 3D networks. Please note that each atom in

---

the present MD simulation has three spatial degrees of freedom (i.e. Cartesian  $x$ ,  $y$ ,  $z$  coordinates) irrespective of the actual dimension of the nanosystem. The anisotropy in most of the present model systems is kinetic energy driven as it has been generated via a mass-gradient  $\alpha$ . For a (10,10) nanotube model we have generated a PES anisotropy via changes in the force constant under conservation of the masses. Thermal rectification under 2D conditions has been modeled for a graphene sheet with a mass-gradient. Crystalline and amorphous Lennard-Jones (LJ) solids have been employed to study 3D networks. As a final example we have chosen (6,6) nanotubes in contact with a graphene interlayer that differ in the number of CNT chains on both sides of the interlayer; see Fig. 1. On one side we have four (6,6) CNTs, on the other only a single one. In the CNT-graphene system displayed in Fig. 1 neither the particle masses nor the force constants have been modified. Here the PES anisotropy is of pure topological origin. The systems mentioned show that we have chosen idealized models to identify key parameters for thermal rectification. Despite this simplification, our general conclusions should be transferable to real systems.

For the determination of thermal conductivities, which are a prerequisite to calculate the  $R_t$  parameters, see Eq. (1), we have adopted MD simulations of the reverse non-equilibrium (RNEMD)<sup>26, 27</sup> and dual thermostat (DTMD) [28] type. Both techniques have been used successfully in our group to derive the thermal conductivities of polymers, LJ fluids or molecular liquids.<sup>29-33</sup> The two methods are part of the MD program YASP which has been adopted as computational tool.<sup>34</sup> In Ref. 11 we have suggested that the sign of  $R_t$  in mass-graded nanotubes can be explained by a transfer of vibrational energy under the influence of anharmonicities from transverse to longitudinal modes. This transfer mechanism is more efficient when placing the light atoms at higher temperatures. Some sparse theoretical studies of mode-coupling to explain heat conduction have been reported in the past decade.<sup>35, 36</sup>

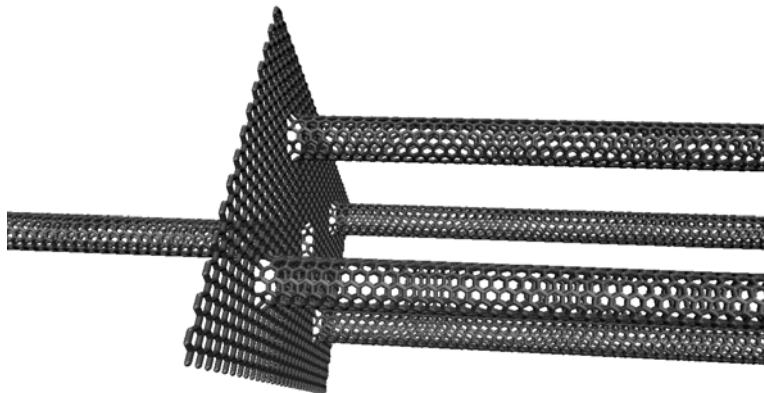


**Figure 1.** Schematic picture of a (6,6) carbon nanotube rectifier where four nanotubes (rhs.) and a single chain (lhs.) are separated by a graphene interlayer.

---

We have used the Fourier-transform of the mass-weighted Cartesian velocity auto-correlation function to explain this mechanism. Up to now it seems to be not possible to make a priori predictions on the preferred direction of the heat flow. Central aim of the present article is the identification of key quantities controlling the transfer of energy in nanosized systems. On the basis of our findings we formulate some general rules on the preferred direction of the energy flow.

## 4.2. Theoretical tools

As mentioned in the introduction we have employed two MD techniques to derive the thermal conductivity and thus the thermal rectification of nanosized systems. Most of the simulation results have been determined by the reverse non-equilibrium MD method.<sup>26,27</sup> Only for the CNT-graphene system of Fig. 1 we have adopted the dual-thermostat technique.<sup>28</sup> To calculate the thermal conductivity, we have assumed the validity of the Fourier law with its linear  $T$  profile. Thus we have related  $\lambda$  to the heat flux  $j_z$  into the direction of the  $T$  gradient, here the  $z$  direction, and to the inverse of the temperature gradient  $\langle dT / dz \rangle$ .

$$\lambda = -j_z / \langle dT / dz \rangle \quad (2)$$

Many years ago it has been verified theoretically<sup>21</sup> that such a linear  $T$  profile does not exist in perfect 1D single-file chains when using the harmonic approximation. This restriction, however, does not occur in the studied nanosized systems with their anharmonicities. They are an outcome of the coupling between the harmonic potential terms employed in our MD approach.<sup>37</sup> The implication of anharmonic terms on the thermal conductivity of polymeric glasses has been analyzed in very recent study.<sup>38</sup> Later we come back to the role of vibrational couplings; see also the remarks in the introduction. The validity of the Fourier law in quasi 1D systems has been discussed critically both in experimental and theoretical articles.<sup>39, 40</sup> Even if a linear  $T$  gradient does not exist at the chain ends, it occurs in the central part of these systems. The heat flow in the present work has been calculated only in this linear regime; again we refer to 16. Here a more detailed discussion of the shape of the temperature profile in nanotube models set into a  $T$  gradient has been given. As they are not important for the aim of the present analysis – and to save the space of the journal – such  $T$  profiles have not been commented on in the article at hand. To reemphasize; the  $R_t$  numbers discussed below have been determined for spatial domains where a linear response is strictly valid.

As both the RNEMD and DTMD techniques have been described in the literature,<sup>26-28</sup> it suffices to review the basic facts. Advantages and disadvantages as well as the error bars of the methods have been described in a number of articles.<sup>26-33</sup> The heat flux  $j_z$  in the RNEMD method is the outcome of an artificial exchange of particle velocities in different regions. For this purpose, the

system is partitioned along the  $z$  direction into equidistant slabs. One terminal slab is defined as the “hot slab”, another one as the “cold slab”. At certain time intervals the velocities of the coldest particles in the hot slab and the hottest particles in the cold one are exchanged. These swapping processes require identical masses of the respective particles. This however implies that the overall  $z$  dimension of the simulation cell for systems with a mass-gradient is twice the dimension of the region characterized by a  $T$  gradient; again we refer to recent articles on the RNEMD method.<sup>26, 27</sup> By repeating these exchange processes periodically, we can derive the heat flux  $j_z$  which offers an access to the thermal conductivity  $\lambda$  via Eq. (2) in the steady state.

In analogy to the RNEMD method, we have two reference regions, the hot and cold one, in the DTMD technique.<sup>28</sup> They are locally coupled to Berendsen thermostats.<sup>41</sup> The temperatures in the two reference slabs are kept constant. After equilibration of the system, a linear  $T$  profile is formed in the intervening region. Parallel to the DTMD method we have adopted Eq. (2) to derive  $\lambda$ . As mentioned above, the DTMD simulations have been restricted to the CNT system portrayed in Fig. 1. To have a measure for the thermal rectification in this species, a modification of Eq. (1) has been necessary. The parameter  $R'_t$  in Eq. (3) guarantees that – at least technically – the same number of degrees of freedom on both sides of the graphene sheet has been taken into account. Due a drop in the temperature at the graphene interlayer, it is necessary to restrict the balance region for the heat transfer to the CNTs.

$$R'_t = \frac{j_{4 \rightarrow 1} - 4j_{1 \rightarrow 4}}{4j_{1 \rightarrow 4}} \times 100, \quad (\text{in } \%) \quad (3)$$

$j_{4 \rightarrow 1}$  symbolizes the heat flux in the right CNT fragment with four chains towards the single chain unit on the lhs. under exclusion of the interlayer; vice versa for  $j_{1 \rightarrow 4}$ .

It remains to define a thermal rectification parameter for the RNEMD simulations on the (10,10) nanotube with a constant carbon mass (12 gmol<sup>-1</sup>). Here we have generated a PES anisotropy by gradually changing the bond force constant  $k_r$  between bonded carbons. The  $R_{\text{tf}}$  formula used

$$R_{\text{tf}} = \frac{\lambda_{s \rightarrow l} - \lambda_{l \rightarrow s}}{\lambda_{l \rightarrow s}} \times 100, \quad (\text{in } \%) \quad (4)$$

is a straightforward generalization of Eq. (1).  $\lambda_{s \rightarrow l}$  abbreviates the thermal conductivity from the region with small bond force constants to the domain with large ones; vice versa for  $\lambda_{l \rightarrow s}$ .

After having introduced the two MD techniques employed and the parameters describing thermal rectification, we now define the quantities chosen to explain its origin in the presence (absence) of a mass-gradient. For some nanotube systems we have calculated the power and projected power spectra by adopting the Fourier transform of the mass-weighted Cartesian velocity auto-correlation function. In the harmonic approximation these spectra map the density

of vibrational states.<sup>42</sup> Let us make the hypothesis that thermal rectification in mass-graded nanotubes is the outcome of an energy transfer from transversal to longitudinal modes. This coupling leads to an enhanced vibrational density of states (DOS) into the longitudinal direction, i.e. into the direction of the  $T$  gradient. For recent approaches based on mode-coupling we refer to the literature.<sup>35, 36</sup> The coupling mechanism is more efficient when placing the light particles at high temperatures. The decisive role of the overlap of the vibrational spectra in the hot and cold spatial domains for thermal rectification had been mentioned already by Li et al.<sup>10</sup>

To explain the physical origin for the direction of the thermal rectification we define – in addition to the quantities  $R_t$ ,  $R_{t\boxminus}$ , and  $R_{tr}$  – a spectral rectification parameter  $R_p$  by using (projected) power spectra.

$$R_p = \frac{P(z)_{H \rightarrow L} - P(z)_{L \rightarrow H}}{P(z)_{L \rightarrow H}} \times 100 \quad (\text{in } \%) \quad (5)$$

The indices  $H \rightarrow L$ ,  $L \rightarrow H$  have the same meaning as in Eq. (1), i.e. they indicate the direction of the heat flow in a system with a mass gradient.  $P(z)$  stands for the projection of the vibrational spectrum onto the longitudinal  $z$  direction. It is defined as

$$P(z) = \frac{\int G_z(\omega) d\omega}{\int G(\omega) d\omega} \quad (6)$$

with  $G_z(\omega)$  abbreviating the  $z$ -projection of the Fourier transform of the mass-weighted Cartesian velocity auto-correlation function  $G(\omega)$ .

$$G(\omega) = \frac{1}{\sqrt{2\pi}} \int_0^\infty dt e^{i\omega t} \left\langle \sum_{j=1}^N m_j \vec{v}_j(t) \vec{v}_j(0) \right\rangle \quad (7)$$

$m_j$  stands for the mass of the  $j^{\text{th}}$  particle and  $v_j(t)$  for its velocity at time  $t$ .  $\omega$  symbolizes the vibrational wave number. The Fourier transform in Eq. (7) covers the whole vibrational spectrum. The physical information carried by  $P(z)$  can be explained as follows. As  $P(z)$  represents the fraction of the total power spectrum confined to longitudinal modes, it quantifies the transfer of the total vibrational energy to this direction when the system is set into a  $T$  gradient.

At the end of this section we want to clarify the validity and limitations of the present MD simulations. i.) The YASP force field,<sup>34</sup> see next section, contains – with one exception – only harmonic potential parameters for the bond lengths, angles and torsions. Thus we have to ask whether we can use such a potential to study a physical phenomenon that is caused by anharmonicities? Yes we can: any coupling of harmonic potential parameters causes a certain degree of anharmonicity.<sup>37, 38</sup> We are aware of the fact that anharmonicities are underestimated by the force field employed. Nevertheless



---

they are sufficient to explain thermal rectification. ii.) We have mentioned above that we have used mass-dependent particle vibrations to predict the general direction of thermal rectification. iii.) Let us dwell on the neglect of quantum effects in the present classical MD study. At the temperatures chosen, quantum effects are not decisive as they merely lead to a constant shift of all thermal conductivities.<sup>43, 44</sup> iv.) To avoid a prohibitive computer time demand for the MD runs, we have chosen lengths of the simulation cells that are shorter than the dimensions in the micrometer range realized in experimental studies.<sup>45-50</sup> The length dependence of  $\lambda$  and  $\sigma$  has been studied in the recent articles.<sup>16, 51</sup> On the basis of these results our length restriction can be justified in a study intended to explain general trends.

### 4.3. Computational details

In the introduction we have already emphasized the model character of many systems adopted in the present theoretical contribution. All particles in the “carbon-like” mass-graded networks interact via a common force-field, i.e. neither the harmonic force constants nor the geometrical parameters depend on the particle mass. A (10,10) nanotube model is an exception; it has been studied as a function of the bond force constant  $k_r$ . All other force constants and the respective carbon masses have been kept fixed in this series of simulations. The only model, where we have chosen force constants and geometrical parameters that depend on the topology of the atoms is the 1D chain with a polyacetylene-like arrangement where the “effective” carbons are saturated by “effective” hydrogens; see Fig. 2. Note that the periodic boundary conditions employed lead to a  $C_nH_n$  system and not to a  $C_nH_{n+2}$  one as encountered for a system with a finite length. The descriptor “effective” symbolizes that we have chosen force constants and atomic increments for the bond length that are characteristic for carbon (hydrogen), even if we have modified the respective masses to introduce an anisotropy in the kinetic energy.

Although the intramolecular force field for all effective carbon systems has been optimized for CNTs, we have used the same parameters for all other carbon-like materials. This choice allowed us to restrict our analysis to the topological influence on rectification. In our study they appear decoupled from possible modifications of the potential energy surface due to chemical bonding.

With exception of the polyacetylene model all quasi-1D and 2D systems studied are described by three harmonic force constants  $k_r = 392460 \text{ kJmol}^{-1}\text{nm}^{-2}$ ,  $k_\theta = 527 \text{ kJmol}^{-1}\text{rad}^{-2}$  and  $k_\delta = 167 \text{ kJmol}^{-1}\text{rad}^{-2}$  for the bond stretching, angle bending and the dihedral behavior. The associated geometrical parameters at the PES minimum amount to  $r_0 = 0.1418 \text{ nm}$ ,  $\theta_0 = 120.0^\circ$  and  $\delta_0 = 0.0^\circ$ .<sup>52-54</sup> The force field and geometrical parameters for the polyacetylene-like chains can be found in Table 1; the data have been taken from Ref. 55.  $V(\tau)$  maps the torsional behavior of the potential;  $k_\tau$  is the corresponding force constant. In contrast to the dihedral term for the other networks  $V(\tau)$  is not defined by a quadratic term. For the MD simulations of the crystalline and amorphous 3D LJ solids we have adopted  $\varepsilon = 1.197 \text{ kJmol}^{-1}$  and  $\sigma = 0.335 \text{ nm}$ . These parameters have been developed for Ar.<sup>56</sup>

**Table 1.** Force field parameters and equilibrium values for the geometry of polyacetylene.<sup>55</sup>

$V(r) = (k_r/2)(r - r_0)^2$		
bond	distance/nm	$k_r / \text{kJmol}^{-1}\text{nm}^{-2}$
C-C	0.1446	328668.02
C=C	0.1346	549398.71
C-H	0.108 0	200000.00
$V(\theta) = (k_\theta/2)(\theta - \theta_0)^2$		
bond angle	$\theta_0 / \text{deg}$	$k_\theta / \text{kJmol}^{-1}\text{rad}^{-2}$
C-C=C	125.3 0	1198.36
H-C-C	116.29	505.89
H-C=C	118.41	505.89
$V(\tau) = (k_\tau/2)[1 - \cos 3(\tau - \tau_0)]$		
dihedral angle	$\tau_0 / \text{deg}$	$k_\tau / \text{kJmol}^{-1} \text{ rad}^{-2}$
C-C-C-C	180.0	562.0

We have used the program system YASP<sup>34</sup> for all MD simulations. It employs the leapfrog algorithm<sup>57</sup> and orthorhombic cyclic boundary conditions. They have been used for all systems irrespective of their formal dimension. Unless mentioned explicitly, the MD runs have been performed for a constant volume and temperature. Constant temperatures have been guaranteed by the Berendsen thermostat<sup>41</sup> with a coupling time of 1 ps. This choice rendered possible the generation of a measured mean temperature which fluctuates by less than 5 K around the target temperature. The sufficient accuracy of the thermostat has been verified in a number of test simulations. In the majority of simulations we have chosen a target temperature of 300 K. In the 3D Lennard-Jones

---

solid,  $T$  has been reduced to 30 K. The time-step in the MD simulations amount to 1 fs. The non-bonded interactions, when necessary, have been determined with the help of a Verlet neighbor list which has been updated every 15 time steps. We have chosen a cutoff radius of 1.0 nm. The neighbor list cutoff exceeds this value by 0.1 nm. The particle exchange in the RNEMD simulations takes place every 300 time step (0.3 ps). The temperature profiles have been sampled every 301 time steps. Whenever adopting this exchange period, the presence of a linear temperature gradient has been checked. A non-equilibrium simulation typically covered 6 ns. The last 2000 ps of this interval have been selected for the data production. In additional test simulations over 10 ns we have shown that 6 ns is sufficient to guarantee steady state simulation results. This is valid for all masses and systems studied. The error bars displayed in the different diagrams always refer to the maximum value. They refer to the standard deviation of the simulations.

#### 4.4. Calculated thermal rectification parameters

##### 4.4.1. Mass-graded nanotubes

We start the presentation of calculated thermal rectification parameters with mass-graded nanotubes of different chiral indices and tube lengths ( $l$ ). The data have been derived by RNEMD simulations which require an effective length parameter that exceeds the length of the domain with the  $T$  gradient by a factor of 2; see Fig. 2 for a schematic representation. The mass-graded nanotubes are generated by gradually enhancing the atomic mass along the tube axis ( $z$ ). The first atoms in the nanotubes have a mass of 12 gmol<sup>-1</sup>. We end with atomic masses of several hundreds. The constant mass-gradient  $\alpha = \Delta m(z) / \Delta z$  (in gmol<sup>-1</sup>nm<sup>-1</sup>) in the simulations spans a range from 1.76 to 13.76. The two combinations of the mass and temperature profile analyzed have been symbolized in Fig. 2. In this diagram we show a (10,10) nanotube as well as a polyacetylene-like chain as representative examples. The “polyacetylene” results will be discussed in Sec. 4.4.4. In one series of simulations we have placed the heavy particles at the ends of the simulation box at high temperatures while the light central masses occurred in the cold region. In the second series of RNEMD simulations the reverse combination of masses and temperatures has been studied. The symmetric mass distribution in Fig. 2 is dictated by a characteristic feature of the RNEMD technique. Note that it restricts velocity exchanges to particles of identical mass.<sup>26,27</sup>

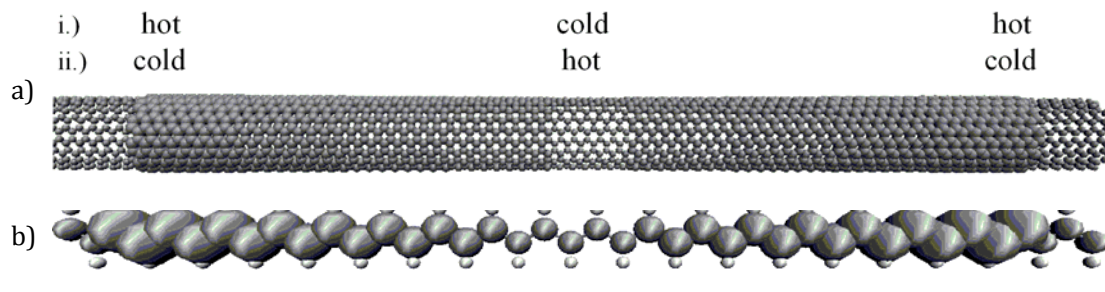


**Figure 2.** (a) Schematic representation of the mass profile in the axial ( $z$ ) direction of a (a) (10,10) nanotube and (b) for a polyacetylene-like topology. The chain atoms in b refer to effective carbons, the outer ones to effective hydrogens. The bigger circles represent heavier atoms. In the top of the diagram we show the two temperature profiles considered. i.) The heavy particles in both terminal regions are placed at high temperatures, the central light particles are located in the cold region. ii.) In the second  $T$  profile the heavy particles are located in the cold terminal region while the light central particles are hot.

The thermal rectification in nanotubes depends on a number of factors.<sup>16, 17</sup> In Fig. 3 we have plotted  $R_t$  of nanotubes with chiral indices (5,5), (7,7), (10,10), (15,15) and (20,20) as a function of the tube diameter ( $d$ ) for an average temperature of 300 K. The four curves refer to a length of 30, 50, 70 and 90 nm for the region with a mass gradient. In the whole simulation series we have adopted  $\alpha = 5.76 \text{ gmol}^{-1}\text{nm}^{-1}$ . The negative sign of  $R_t$  in Fig. 3 indicates that the preferred heat transport proceeds from the light to the heavy particles. The splitting between the four curves is enhanced with increasing tube diameter. Elongation of the tube length shifts  $R_t$  to larger negative values. For the two shorter chains we predict an enlargement of  $R_t$  when going from the (5,5) to the (7,7) chain. This peak in the  $R_t$  curve is suppressed with an increasing length of the mass-graded region. Note that the splitting between the peak in the (7,7) system and the (5,5), (10,10) neighbors exceeds the error bars of the RNEMD approach.

In the next series of RNEMD calculations we have studied the thermal rectification  $R_t$  in a (10,10) nanotube as a function of the mass gradient  $\alpha$  for an effective length of 30, 50, 70 and 90 nm. The computational results have been displayed in Fig. 4. With increasing  $\alpha$  the parameter  $R_t$  becomes more negative. In analogy to the diameter dependence of  $R_t$  in Fig. 3, an increasing chain length causes an enhanced splitting between the curves. The thermal rectification for a mass-graded length of 30 nm depends only weakly on  $\alpha$ . Differences in the influence of  $d$  and  $\alpha$  on  $R_t$  become evident when comparing Figs. 3 and 4. The parameter  $R_t$  is a linear function of  $\alpha$  with a negative slope while we have observed  $R_t$  maxima in Fig. 3 for the (7,7) nanotube as long as the length of the mass gradient is small enough ( $\leq 70 \text{ nm}$ ).

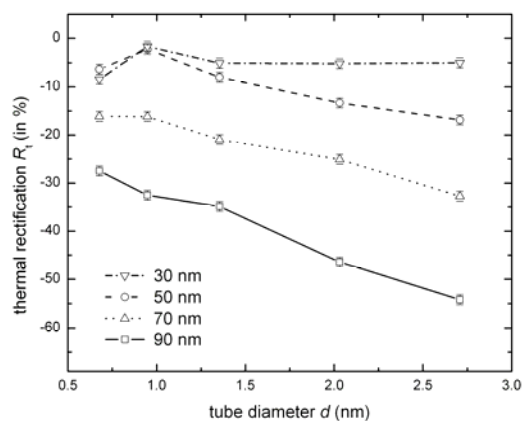


**Figure 3.** Diameter dependence of the thermal rectification  $R_t$  in (5,5), (7,7), (10,10), (15,15) and (20,20) nanotubes (from left to right) with a mass gradient length of 30, 50, 70 and 90 nm. The mass gradient  $\alpha$  adopted in this series of RNEMD simulations amounts to  $5.76 \text{ gmol}^{-1}\text{nm}^{-1}$ . The average temperature is 300 K. In all diagrams we have plotted only the maximum error bar; see comment at the end of Sec. 4.3 The lines in all diagrams only serve as a guide for the eye.

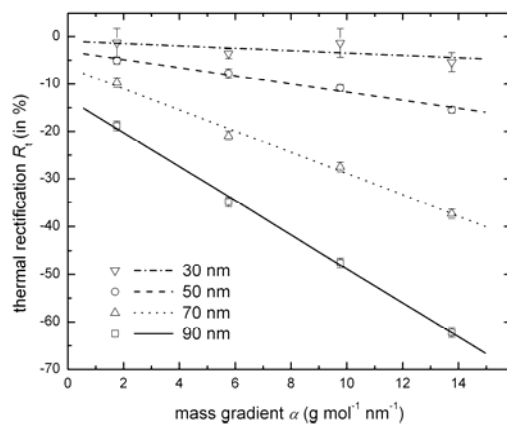


**Figure 4.** Thermal rectification  $R_t$  in a (10,10) nanotube as a function of the mass gradient  $\alpha$ . We have considered the following lengths for the mass gradient area: 30, 50, 70 and 90 nm. The average temperature is 300 K. The data could be fitted to a straight line.

The influence of the temperature on  $R_t$  has been plotted in Fig. 5. Thermal rectification in mass-graded nanotubes is reduced with increasing  $T$ . The  $T = 200 \text{ K}$  splitting between the (10,10), (15,15) and (20,20) curves exceeds the curve splitting at 800 K by a factor larger than two. The theoretical results in Fig. 5 can be interpreted as follows. Thermal rectification profits from differences in the eigenfrequencies of the classical oscillators. With increasing  $T$  these differences become smaller with respect to the thermal energy. Outcome of this frequency

leveling is an attenuation of the thermal rectification if  $T$  is enlarged. This implies that a large selectivity for the direction of the heat transfer (i.e. large  $|R_t|$ ) requires low temperatures. Of course we have to keep in mind that both the force field and the restriction to the classical limit have an influence on the absolute numbers; the general trends, however, are conserved when allowing parameter changes.

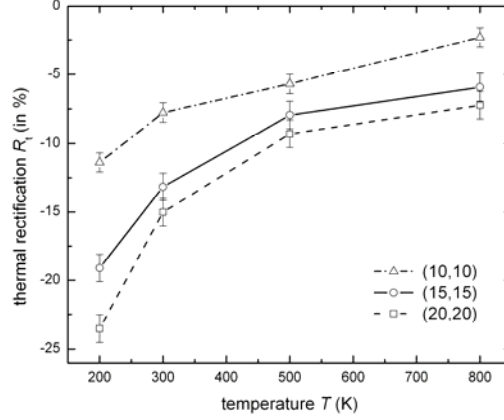


**Figure 5.** Temperature dependence of the thermal rectification  $R_t$  for (10,10), (15,15) and (20,20) nanotubes with an effective length of 50 nm and a mass-gradient  $\alpha$  of  $5.76 \text{ gmol}^{-1}\text{nm}^{-1}$ .

#### 4.4.2. Nanotube simulations with a gradient in the bond force constant

Let us stay with nanotube models for a moment. The implementation of a mass gradient is not the only way to induce thermal rectification. In the following we present RNEMD data for a (10,10) nanotube with a gradient  $\beta = \Delta k_r(z) / \Delta z$  in the bond force constant  $k_r$  under conservation of a universal carbon mass of  $12 \text{ gmol}^{-1}$ . In contrast to the implementation of a mass gradient with its kinetic energy modification this setup yields an anisotropy in the potential energy. The two extremal  $\beta$  values are  $1666.7$  and  $6666.7 \text{ kJmol}^{-1}\text{nm}^{-3}$ . The mean value for the bond force constant in all (10,10) chains amounts to  $400000 \text{ kJmol}^{-1}\text{nm}^{-2}$  which is very close to  $k_r$  adopted in the simulations of mass-graded chains. The minimum and maximum values of  $k_r$  amount to  $200000$  and  $600000 \text{ kJmol}^{-1}\text{nm}^{-2}$  for largest  $\beta$  value (i.e.  $6666.7 \text{ kJmol}^{-1}\text{nm}^{-3}$ ). The thermal rectification  $R_{\text{tf}}$  for systems with a gradient in the force constant has been defined in Eq. (4). Fig. 6 represents the  $\beta$  dependence of  $R_{\text{tf}}$  for a (10,10) nanotube with an effective length of 60 nm. The simulations have been performed for an average temperature of 300 K. We predict  $R_{\text{tf}} < 0$  for all  $\beta$  values which indicates that the heat current in this nanochain model is more efficient from the region with large force constants to the lower  $k_r$  region. This trend has been expected when remembering that the energy of (harmonic) oscillators scales with  $\sqrt{k/\mu}$  which  $\mu$  denoting the reduced mass. This formula is valid both in a classical and

quantum description.<sup>57</sup> To sum up; the local curvature of the PES is affected in the same direction when decreasing the bond force constant or increasing the reduced mass. An enhanced difference in the force constant  $k_r$  at two neighboring atoms implies a higher thermal rectification  $R_{tr}$ . The reduced efficiency for the heat transport guarantees an enhanced selectivity.

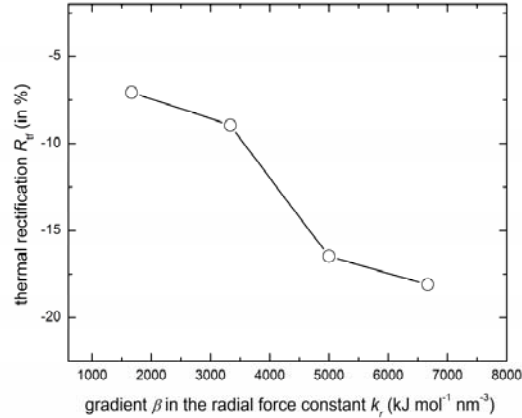


**Figure 6.** Thermal rectification parameter  $R_{tr}$  in a (10,10) nanotube as a function of the gradient  $\beta$  in the bond force constant  $k_r$ . The RNEMD simulations have been performed for an effective chain length of 60 nm at  $T = 300$  K.

#### 4.4.3. Mass-graded 2D and 3D models

Let us leave the nanotube models for an analysis of the thermal rectification  $R_t$  in 2D and 3D systems with a mass gradient. Recent work on 2D networks can be found in Refs. 13, 14. We begin with a graphene sheet of 12.76 nm width and an effective length of 50 nm. The chosen width of graphene coincides almost perfectly with the circumference of a (30,30) nanotube. The simulations summarized below have been performed for an average temperature of 300 K and a mass-gradient  $\alpha$  of  $5.76 \text{ gmol}^{-1}\text{nm}^{-1}$ . The chosen  $\alpha$  leads to masses between 12 and  $300 \text{ gmol}^{-1}$ . The thermal rectification for the 2D graphene system has the same (negative) sign as determined in all mass-graded nanotubes. Nevertheless it is much smaller in magnitude ( $R_t = -3.7 \%$ ) than in the (30,30) nanotube ( $R_t = -17.3 \%$ ) with the same "transversal" dimension. To explain this difference we postulate that "transversal" vibrational coupling effects within a plane are less strong than transversal couplings in a bend topology like in a tube. On the one hand this coupling might find its origin in the non-zero transverse mean stress due to the tube curvature. On the other hand, this behavior is well-known for quantum oscillators.<sup>58</sup> Thus it seems that the present classical data fit to the results of a quantum description.

To analyze thermal rectification  $R_t$  under 3D conditions, we have chosen a Lennard-Jones solid formed by 10000 particles in a simulation box of dimension  $5 \times 5 \times 15 \text{ nm}^3$ . The length of the

---

mass gradient in the  $z$  direction amounts to 6.3 nm. We have chosen  $\alpha = 45.87 \text{ gmol}^{-1}\text{nm}^{-1}$  starting with an atomic mass of 12 and ending with  $300 \text{ gmol}^{-1}$ . The 3D system has been equilibrated at 500 K. In a sudden quenching the temperature has been reduced to 30 K to create a glass. Before we have started the RNEMD simulations to derive  $R_t$ , we have performed a final equilibration. The non-equilibrium run in the amorphous solid covered 1 ns. For the crystalline solid this interval has been enlarged to 6 ns. In analogy to the mass-graded quasi 1D nanochains and graphene, we predict a more efficient energy transfer when heat flows from the light-mass to the heavy-mass region. For the amorphous LJ solid we derive  $R_t = -36.5 \%$  which is reduced to  $-28.0 \%$  in the crystalline system. When assuming that the thermal rectification in all mass-graded systems with a dimension higher than 1D is caused by transversal vibrational couplings, it follows that this mechanism is more efficient in amorphous systems, i.e. in the absence of geometrical constraints. The enhanced selectivity (i.e. large  $|R_t|$ ) in the amorphous system correlates with the higher  $\lambda$  in the crystalline material with its “undisturbed” vibrational modes. At the end of this section we shortly mention a possible application of the predicted mass dependence of thermal rectification. Experimentally a mass gradient can be generated via isotopic substitution. The implications of this process on the thermal conductivity have been studied in a number of articles. For diamond, e.g., it has been verified that  $\lambda$  can be reduced by 30% in samples, with a random distribution of an enhanced  $^{13}\text{C}$  concentration in the natural matrix.<sup>59</sup> Isotopically enriched polycrystalline diamond films have been analyzed in Ref. 60. The isotope effect on  $\lambda$  of silicon has been described in a conference proceeding.<sup>61</sup> More experimental results can be found in articles on germanium single crystals<sup>62, 63</sup> and on the isotope effect on the thermal conductivity of boron nitride nanotubes.<sup>64</sup> All these articles have shown the sensitive correlation between  $\lambda$  and randomly distributed isotopes. When going from a random distribution of added isotopes to a spatially ordered mass-graded one, thermal rectification is expected. The potential of thermal rectification for the energy efficiency of buildings should become evident on the basis of our suggestion. Spatially ordered isotope substitution in windows might lead to a reduction of the heat transfer from the heated inside to outside.

#### 4.4.4. Mass-graded polyacetylene-like models

In this sub-section we go back to systems with a transverse dimension smaller than in the nanotube case. For this purpose we have chosen a mass-graded chain with a polyacetylene-like topology; see Fig. 2. Four different mass distributions i.) to iv.) have been studied. In the first series of simulations i.) the effective carbon mass has been changed linearly whereas we have conserved the outer, i.e. hydrogen, mass which amounts to  $1 \text{ gmol}^{-1}$ . The second simulation series ii.) is characterized by a mass gradient at the outer effective hydrogens while we have



fixed the mass of the backbone (i.e. carbon) atoms to  $12 \text{ gmol}^{-1}$ . iii.) refers to the situation where we have adopted the same mass gradient  $\alpha$  at the inner chain and outer atoms; its slope is identical. iv.) Finally we have simulated a chain with opposite directions for the mass enhancement at the two types of atoms. We have adopted the same  $\alpha = 20 \text{ gmol}^{-1} \text{ nm}^{-1}$  for both atomic species. This value has been conserved in all simulations described in the present subsection. A length of 500 nm for the polyacetylene-like arrangement has been taken throughout. Again we have chosen an average temperature of 300 K. The first series of simulations, i.e. mass-graded inner atoms, has led to  $R_t = 44.6 \%$ . The positive value indicates a more efficient heat transfer in the direction from the heavy inner atoms to the light ones. This direction has been expected. It coincides with the findings for the 1D single-file chain described by the FPU potential.<sup>10</sup> The sign of  $R_t$  is dictated by the mass-graded inner part of the polyacetylene-like model while the hydrogens with a constant mass do not support rectification effects. The chain model with a constant C mass and mass-graded effective hydrogens ii.) reproduces the findings for the mass-graded nanotubes. The negative sign of  $R_t$  ( $-7.3 \%$ ) indicates the influence of mass-dependent transverse couplings. The transverse vibrations arise from larger torques due to high masses at the outer atoms of the chain. The energy transfer is stronger when having the light effective hydrogens at higher temperatures. When going to model chain iii.) with the same direction for the mass gradient at both types of atoms, we derive the same heat transfer as encountered in a mass-graded nanotube chain ( $R_t = -28.2 \%$ ). The enhancement of  $|R_t|$  relative to the simulations of type ii.) indicates that transverse coupling effects are stronger in the absence of a large mismatch in the masses of the effective carbons and hydrogens. We refer to Ref. 65 where the implications of mass differences on the thermal conductivity have been analyzed. In the last simulation series iv.) with opposite directions of the two mass-gradients we reproduce again the rectification pattern in anharmonic single-file chains, i.e.  $R_t$  is positive ( $35.4 \%$ ). Note that we have chosen a  $R_t$  definition for iv.) where  $R_t > 0$  symbolizes a preferred heat transfer from heavy carbons (light hydrogens) to light carbons (heavy hydrogens). Under consideration of the simulations i.) and ii.) one probably might have expected an  $R_t$  value for the last series iv.) exceeding  $R_t$  of model i.) with mass-graded carbons. The  $R_t$  reduction from  $44.6 \%$  in i.) to  $35.4 \%$  in iv.), however, reflects the suppression of coupling effects with increasing mass differences within the effective C-H units; see again Ref. 65. To reemphasize: with the mass-graded polyacetylene-like model chains it has been possible to reproduce either the direction of the thermal rectification in 1D single-file chains (mass gradient in the central chain) or the negative  $R_t$  elements of quasi 1D nanotubes (mass gradient at the outer atoms). This possible switching in the sign of  $R_t$  gives quasi 1D systems a better ability of modeling thermal conductivities than the FPU anharmonic single-file chain.

#### 4.4.5. Topological thermal rectification

At the end of this section we leave the analysis of idealized models and discuss the nanochain system of Fig. 1. As we have used a uniform particle mass of  $12 \text{ gmol}^{-1}$  and the same force constants within all units of the network, thermal rectification can be only of topological origin. In section II we have given the prescription to define the rectification parameter  $R_t$ , see Eq. (3), for this CNT-graphene interlayer material. Only this system has been studied by the DTMD method.<sup>28</sup> The temperatures of the hot and cold bath amount to 325 and 375 K. The  $T$  profiles for the two directions of the heat transfer have been displayed in Fig. 7. In the CNT part we predict a  $T$  profile that is more or less linear indicating the applicability of the Fourier law in these units. In the diagram this has been verified via a linear least-square fit to the data points adopted. At the graphene interlayer, however, we have a sudden drop of  $T$ . The large temperature jump at the graphene sheet is a manifestation of a sizeable interfacial thermal resistance in the connecting region between the nanotubes and the graphene layer. A physical interpretation of this effect will be given in the next section in connection with our analysis of vibrational polarization under the influence of mode-mode coupling. To continue with the phenomenon of thermal rectification we derive a topological rectification parameter  $R_t$  of 30.3%. From the definition of the thermal rectification in the present system  $R_t \neq 0$  means that we have an imbalance in the thermal resistance at the graphene layer for the two directions of the heat flow. The layer-caused resistance is more important if the transferred energy is small (1→4 direction). It is less decisive for the propagation of larger energy packages. For the heat flow from the four nanotubes to a single one, the system might also benefit from interference of waves exciting in the four channels.

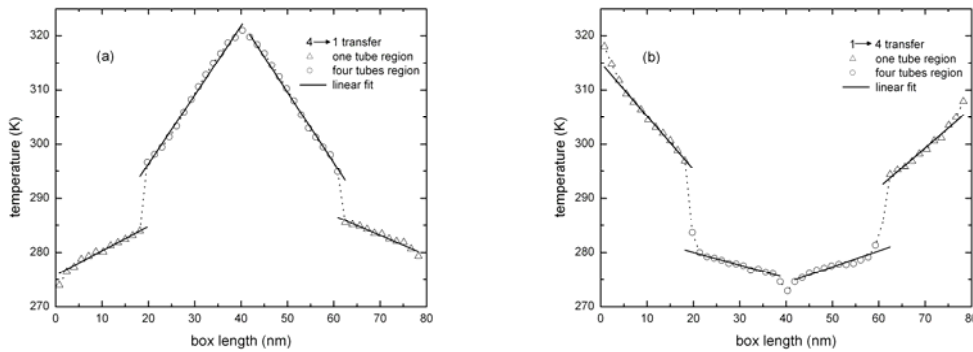


**Figure 7.** Temperature profiles in the CNT-graphene system of Fig. 1 for the two different directions of the heat transfer. On the lhs. we have shown the  $T$  profile for the heat transfer from four CNTs to a single one. Vice versa for the diagram on the rhs. The slight left-right asymmetry follows from the fact that DTMD simulations require an even number of slabs in the  $z$  direction. The straight lines have been determined via a least-square fit.

---

#### 4.5. Analysis of the projected density of vibrational states – the spectral rectification parameter $R_p$

As a possible step towards a microscopical explanation for the thermal rectification in the nanotube and polyacetylene-like models, we have calculated the spectral rectification parameter  $R_p$  defined in Eq. (5). Recent theoretical studies employing the coupling between modes into different directions have been mentioned already in the introduction.<sup>35, 36</sup> In Fig. 8 we have plotted  $R_p$  for the same nanotubes as considered in Fig. 3. We have chosen an effective chain length of 50 nm and the same  $\alpha$  as employed in the evaluation of  $R_t$ . The comparison of the two diagrams shows that the thermal rectification parameter  $R_t$  and its spectral pendant  $R_p$  are both of negative sign. Note however that the latter is smaller in magnitude. The two  $|R_p|$  numbers become larger when enhancing the tube diameter. The local maximum of  $R_t$  for the (7,7) nanotube, however, is not reproduced by  $R_p$ . Nevertheless we are convinced that the similarity of the two plots supports our model that thermal rectification in mass-graded nanotubes is a manifestation for a polarization of the vibrational energy from the transversal direction to longitudinal one.  $R_t (R_p) < 0$  implies that this mechanism is more efficient when placing the light atoms at higher  $T$ . It differs from thermal rectification in mass-graded single-file chains described by the FPU model<sup>10</sup> where transversal couplings are absent. Here the preferred direction for the energy transport profits from the fact that the excitation of light atoms by heavy ones is more efficient for a heat transfer from heavy to light atoms. The inequivalence between both transfer paths yields  $R_t > 0$  in mass-graded single file-chains. The enhancement of  $|R_t|$  ( $|R_p|$ ) with increasing tube diameter in Figs. 3 and 8 simply shows that the predicted energy transfer from transversal to longitudinal modes is intensified with an increasing number of atoms, i.e. vibrational degrees of freedom. It is clear that the same argument is valid to explain the thermal rectification in the mass-graded 2D (graphene-like sheet) and the 3D models (LJ solids). Precise statements on the saturation of  $R_p$  as a function of  $d$  as well as the origin of the local maxima in Fig. 3 would require additional (time-consuming) simulations.

Let us go to Fig. 9 where we have plotted  $R_p$  of a (10,10) CNT with a constant atomic mass of  $12 \text{ gmol}^{-1}$  as a function of the gradient  $\beta$  in the bond force constant  $k_r$ . In analogy to the  $R_t$  diagram in Fig. 6, the spectral rectification parameter  $R_p$  is negative and in magnitude is an increasing function of  $\beta$ . A physical explanation for this behavior has been commented on already in Sec. 4.4.2.

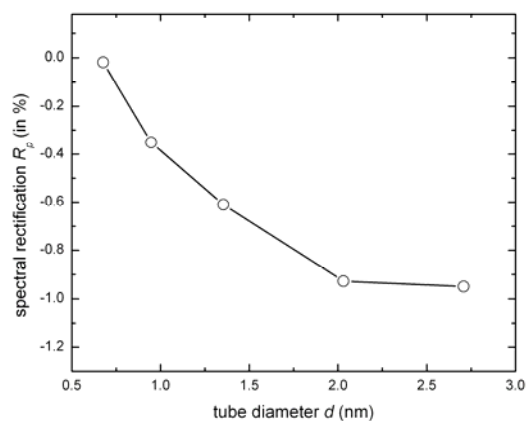


**Figure 8.** Spectral rectification parameter  $R_p$  derived for (5,5), (7,7), (10,10), (15,15) and (20,20) nanotubes (from left to right) with a length of 50 nm for mass gradient and  $\alpha = 5.76 \text{ gmol}^{-1}\text{nm}^{-1}$ . The average temperature is 300 K. The error bar of the simulations is smaller than the dimension of the circle.

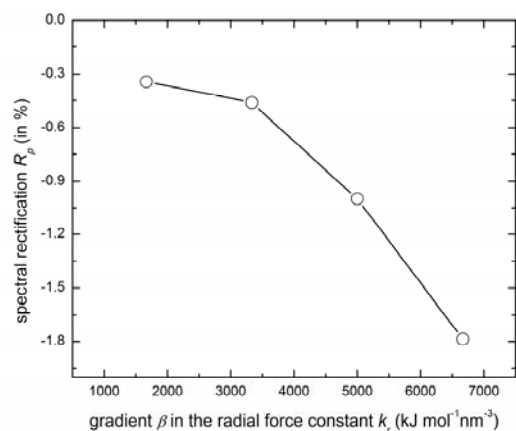


**Figure 9.** Thermal rectification parameter  $R_p$  in a (10,10) nanotube as a function of the gradient  $\beta$  in the bond force constant  $k_r$ . The simulations have been performed at an average temperature of 300 K.

At the end of this section let us analyze the spectral rectification  $R_p$  for the simulations ii.) and iv.) of the polyacetylene-like chain. Remember that we have derived  $R_t < 0$  for the model with a mass gradient at the outer atoms (i.e. for ii.) and  $R_t > 0$  in the case of iv.) with opposite mass gradients at the two types of atoms. Also remember that  $R_t > 0$  for this example symbolizes that the preferred heat transfer goes from the heavy chain atoms (light outer atoms) to the light inner centers (heavy outer atoms). For both model studies, we have found that  $R_t$  and the spectral parameter  $R_p$  are of the same sign. The polyacetylene-like model ii.) can be explained by the same arguments as outlined for the mass-graded nanotubes. The energy transfer from transversal to longitudinal modes is more efficient if the “transversal” neighbors are light. This

---

mechanism is operative both for neighbors that differ from the reference atoms (i.e. polyacetylene topology) and for identical neighbors (i.e. nanotubes).  $R_t$  ( $R_p$ )  $> 0$  for the simulation series iv.) shows that the direction of the thermal (spectral) rectification is controlled by the mass-graded chain atoms and not by the outer ones. Again we refer to the published data for the 1D single-file chain.<sup>10</sup>

On the basis of the theoretical results in this section we are able to explain the temperature drop at the graphene interlayer in the (6,6) carbon nanotube rectifier shown Fig. 1. The variation of the temperature as a function of the box coordinate has been given in Fig. 7. The large thermal resistance at the interlayer seems to express that the vibrational transfer from the longitudinal modes in the nanotubes into the in-plane modes in the graphene layer and back is rather weak. Such a topological barrier does not exist in all other nanotubes studied. Here each atom contributes both to transverse and longitudinal modes which guarantees that vibrational polarization in these networks is quite efficient. The outcome of this effect has been quantified by the spectral rectification parameter  $R_p$ . We strongly feel that this is a useful quantity to explain the direction of the thermal rectification in nanosized materials. Without exception we have found that  $R_t$  and  $R_p$  are of the same sign and of similar shape when derived as a function of model quantities such as the tube diameter, mass gradient or gradient in the (bond) force constant.

#### 4.6. Conclusions

In the present contribution we have employed two MD techniques to study thermal rectification in nanosized model systems. The majority of data has been derived by the reverse non-equilibrium MD formalism. The dual thermostat method has been chosen to analyze the CNT-graphene interlayer model portrayed in Fig. 1. The two central topics of our theoretical work can be expressed as follows. A: We have suggested correlation schemes to explain the direction of the thermal rectification in nanosized materials of different topologies. Thereby we have covered structures ranging from a more-or-less one-dimensional boundary to 3D Lennard-Jones solids. For the design of materials with certain thermal properties, it is a prerequisite to understand the key quantities determining the transfer of heat. B: We have adopted the flow of energy to study the transferability of physical concepts developed for 1D single-file chains to low-dimensional materials experimentally accessible. In this context we have concisely touched theoretical contributions on different physical peculiarities of perfect 1D systems published over many decades.

Topic A. We have suggested two factors controlling the direction of the thermal rectification in nanosized materials. i.) We first mention the vibrational coupling due to anharmonicities on the PES. In mass-graded nanotube models this mechanism leads to a transfer of vibrational energy

---

from the transversal to the longitudinal direction. Final outcome of this phenomenon is a preferred energy transfer from light to heavy particles. ii.) In mass-graded single-file chains as well as in certain models with a polyacetylene-like topology this coupling is either not possible or inefficient. The preferred heat transfer from heavy to light atoms in these systems can be explained by the generation of low-energy modes. For single-file chains described via the FPU potential this mechanism has been discussed already in the literature.<sup>10</sup> Both for i.) and ii.) we have the situation, that the present classical simulations lead to the same predictions than expected in a quantum description of the systems.<sup>37, 58</sup> The so-called topological rectification arises from thermal resistance of the interlayer, where vibrational transfer from the longitudinal modes in the nanotube to the in-plane vibrations in the graphene layer is poorly efficient.

The detailed analysis of the different parameters controlling thermal rectification should be considered as a useful input for the design of materials with a preferred direction of the heat transfer or fulfilling specific thermal requests. We have shown that thermal rectification can be induced either by the implementation of a mass gradient (isotope substitution), by a gradient in the force constants (impurity dopings), by external masses or by modifications in the topology.

B: It concerns the transferability of physical concepts that have been developed for hypothetical 1D single-file chains to real systems. At least for the transfer of energy we have quantified the conditions allowing or preventing such a correlation. In connection with thermal rectification we have demonstrated that mass-graded nanotubes do not map the behavior of 1D mass-graded FPU chains. Such a topological discrimination is known for many physical quantities and concepts. Recent contributions of one of the present authors to this discussion have been mentioned in the introduction.<sup>18, 19, 25</sup> It is interesting that the topological implications for thermal rectification can be related to the topology dependence of electronic quantum statistics. In quasi 1D chains a second dimension is necessary to allow the transfer of vibrational energy from the transversal to the longitudinal direction. In quantum statistics a second dimension is needed if electrons of the same spin should pass one another. In other words; the restriction to one dimension prevents them to pass (antisymmetry constraints are not operative) and it prevents the accumulation of vibrational density of states via polarization effects ( $R_t > 0$  in mass-graded single-file chains). The present data for the nanotube system with a gradient in the bond force constant as well as the polyacetylene-like chains with different mass distributions have let to new insight into conditions allowing a correlation from the 1D boundary to topologies experimentally accessible. Again we want to emphasize that the present analysis has been restricted to the transfer of energy. Nevertheless we are convinced that these data are another step to understand the peculiar physical properties of low-dimensional materials.

We are aware of the simplifications and model assumptions that had to be accepted in the article at hand. Despite the approximations employed, our simulations have reached the boundaries of today's computational facilities. We feel that the constraints accepted in the

---

simulations can be justified in a theoretical model study intended to explain general trends and physical concepts. The determination of results that are accurate in an absolute sense has not been the aim of the present research.

### Acknowledgment

The present research project has been supported by the Deutsche Forschungsgemeinschaft (DFG).

### 4.7. References

- (1) K. Balcerek and T. Tyc, *Phys. Stat. Sol. A* **47**, K125 (1978).
  - (2) A. Jeżowski and J. Rafalowicz, *Phys. Stat. Sol. A* **47**, 229 (1978).
  - (3) C. Dames, *J. Heat Transfer* **131**, 061301 (2009).
  - (4) C. W. Chang, D. Okawa, A. Majumder and A. Zettl, *Science* **314**, 1121 (2006).
  - (5) W. Kobayashi, Y. Teraoka and I. Terasaki, *Appl. Phys. Lett.* **95**, 171905 (2009).
  - (6) R. Saito, G. Dresselhaus and M. S. Dresselhaus, *Physical Properties of Carbon Nanotubes*, London, Imperial College Press (1998).
  - (7) J. F. Harris, *Carbon Nanotubes and related Structures*, Cambridge, Cambridge University press 1999).
  - (8) S. Reich, C. Thomsen and J. Maultzsch, *Carbon Nanotubes, Basic Concepts and Physical Properties*, Weinheim, Wiley-VCH (2004).
  - (9) J-C. Charlier, X. Blasé and S. Roche, *Reviews Mod. Phys.* **79**, 677 (2007).
  - (10) N. Yang, N. Li, L. Wang and B. Li, *Phys. Rev. B* **76**, 020301 (2007).
  - (11) G. Wu and B. Li, *Phys. Rev. B* **76**, 085424 (2007).
  - (12) G. Wu and B. Li, *J. Phys. Cond. Matt.* **20**, 175211 (2008).
  - (13) N. Yang, G. Zhang and B. Li, *Appl. Phys. Lett.* **95**, 033107 (2009).
  - (14) J. Hu, X. Ruan and Y. P. Chen, *Nano Lett.* **9**, 2730 (2009).
  - (15) G. Fischer, *Vibronic Processes in Inorganic Chemistry*, edited by C. D. Flint, Kluwer, Dordrecht, 1989, p. 7.
  - (16) M. Alaghemandi, E. Algaer, M. C. Böhm and F. Müller-Plathe, *Nanotechnology* **20**, 115704 (2009).
  - (17) M. Alaghemandi, F. Leroy, E. Algaer, M. C. Böhm and F. Müller-Plathe, *Nanotechnology*, (2009), submitted.
  - (18) P. Jordan and E. Z Wigner *Physik* **47**, 631 (1928).
  - (19) J. Schütt and M. C. Böhm, *Phys. Lett. A* **219**, 79 (1996).
  - (20) M. C. Böhm and J. Schütt, *Phys. Lett. A* **232**, 106 (1997).
  - (21) E.H. Lieb and F.Y. Wu, *Phys. Rev. Lett.* **20**, 1445 (1968).
-

- 
- (22) E. Fermi, J. Pasta and S. Ulam, Studies of non linear problems Document LA-1940 (1955).
- (23) W. Kohn, Phys. Rev. Lett. **2**, 393 (1959).
- (24) K. Dieterich and M. Wagner, Phys. Stat. Sol. B. **127**, 715, (1985).
- (25) M. C. Böhm and A. Staib, Phys. Rev. B **42**, 1930 (1990).
- (26) F. Müller-Plathe and P. Bordat, In Novel Methods in Soft Matter Simulations; Eds., M. Karttunen, I. Vattulainen and A. Lukkarinen, Lecture Notes in Physics, Heidelberg, Springer, **640**, 310 (2004).
- (27) F. Müller-Plathe, J. Chem. Phys. **106**, 6082 (1997).
- (28) T. Terao, E. Lussetti and F. Müller-Plathe, Phys. Rev. E. **75**, 057701 (2007).
- (29) P. Bordat, D. Reith and F. Müller-Plathe, J. Chem. Phys. **115**, 8978 (2001).
- (30) M. Zhang, E. Lussetti, E. S. du Souza and F. Müller-Plathe, J. Phys. Chem. B **109**, 15060 (2005).
- (31) M. Zhang and F. Müller-Plathe, J. Chem. Phys. **123**, 124502 (2005)
- (32) E. Algaer, M. Alaghemandi, M. C. Böhm and F. Müller-Plathe, J. Phys. Chem. A **113**, 11487 (2009).
- (33) E. Algaer, M. Alaghemandi, M. C. Böhm and F. Müller-Plathe, J. Phys. Chem. B **113**, 14596 (2009).
- (34) (a) F. Müller-Plathe, Comput. Phys. Commun. **78**, 77 (1993). (b) K. Tarmyshov and F. Müller-Plathe, J. Chem. Inf. Model. **45**, 1943 (2005).
- (35) S. Lepri, Phys. Rev. E **58**, 7165 (1998).
- (36) J.-S. Wang and B. Li, Phys. Rev. E **70**, 021204 (2004).
- (37) T. López-Ciudad, R. Ramírez, J. Schütt and M. C. Böhm, J. Chem. Phys. **119**, 4328 (2003).
- (38) S. Shenogin, A. Bodapati, P. Keblinski and A. J. H. McGaughey, J. Appl. Phys. **105**, 034906 (2009).
- (39) C. W. Change, D. Okawa, H. Garcia, A. Majumder and A. Zettl, Phys. Rev. Lett **101**, 075903 (2008).
- (40) S. Lepri, R. Livi and A. Politi, Phys. Rev. Lett. **78**, 1896 (1997).
- (41) H. J. C. Berendsen, J. P. M. Postma, W. F. van Gunsteren, A. Di Nola and J. R. Haak, J. Chem. Phys. **81**, 3684 (1984).
- (42) H. Jobic, K. S. Smirnov and D. Bougeard, Chem. Phys. Lett. **344**, 147 (2001).
- (43) J. R. Lukes and H. Zhong, Journal of Heat Transfer **129**, 705 (2007).
- (44) J.-S. Wang, Phys. Rev. Lett. **99**, 160601 (2007).
- (45) P. Kim, L. Shi, A. Majumdar and P. L. McEuen, Phys. Rev. Lett. **87**, 215502 (2001).
- (46) M. Fujii, X. Zhang, H. Xie, H. Ago, K. Takahashi and T. Ikuta, Phys. Rev. Lett. **95**, 065502 (2005).
- (47) T.-Y. Choi, D. Poulidakos, J. Tharian and U. Sennhauser, Nano Lett. **6**, 1589 (2006).
- (48) C. Yu, S. L. hi, Z. Yao, D. Li and A. Majumdar, Nano Lett. **5**, 1842, (2005).



- 
- (49) J. Hone, M. Whitney, C. Piskoti and A. Zettl, Phys. Rev. B. **59**, 2514 (1999).
- (50) E. Pop, D. Mann, Q. Wang, K. Goodson and H. Dai, Nano Lett. **6**, 96 (2006).
- (51) J. Wang and J.S. Wang, Appl. Phys. Lett. **88**, 111909 (2006).
- (52) C. Li and T.-W. Chou, Inter. J. Solids and Struct. **40**, 2487 (2003).
- (53) A. K. Rappe, C. J. Casewit, K. S. Colwell, W. A. Goddard III and W. M. Skiff, J. Am. Chem. Soc. **114**, 10024 (1992).
- (54) J. H. Walther, R. Jaffe, T. Halicioglu and P. Koumoutsakos, J. Phys. Chem. B **105**, 9980 (2001).
- (55) G. Sese and C.R.A. Catlow, Mol. Simu. **9**, 99 (1992).
- (56) I. Hanasaki, A. Nakatani and H. Kitagawa, Science and Technology of Advanced Materials **5**, 107 (2004).
- (57) M. P. Allen and D. J. Tildesley, Computer Simulation of Liquids, Oxford, Oxford University Press (1987)
- (58) P. Atkins and J. de Paula, Physical Chemistry, Oxford, W. H. freeman & Co (2006).
- (59) D. G. Onn, A. Witek, Y. Z. Qiu, T. R. Anthony and W. F. Banholzer, Phys. Rev. Lett. **68**, 2806 (1992).
- (60) T. R. Anthony, J. L. Fleischer, J. R. Olson and D. G. Cahill, J. Appl. Phys. **69**, 8122 (1991).
- (61) A. V. Inyushkin, A. N. Taldenkov, A. M. Gibin, A. V. Gusev and H.-J. Pohl, The 11th International Conference on Phonon Scattering in Condensed Matter (Phonons2004) (WILEY-VCH, Weinheim) (2004).
- (62) V. I. Ozhogin, A. V. Inyushkin, A. N. Taldenkov, A. V. Tikhomirov, G. E. Popov, E. Haller and K. Itoh, JEPT Letters **63**, 490 (1996).
- (63) V. I. Ozhogin, N. A. Babushkina, L. M. Belova, A. P. Zhernov, E. E. Haller and K. M. Itoh, J. Exp. Theo. Phys. **88**, 135 (1996).
- (64) C. W. Chang, A. M. Fennimore, A. Afanasiev, D. Okawa, T. Ikuno, H. Garcia, D. Li, A. Majumdar and A. Zettl, Phys. Rev. Lett. **97**, 085901 (2006).
- (65) S. Maruyama, Y. Igarashi, Y. Taniguchi and J. Shiomi, J. Thermal Science and Technology **1**, 138 (2006).

## On the correlation between thermal conductivity and bondlength alternation in carbon nanotubes: A combined reverse non-equilibrium molecular dynamics – crystal orbital analysis

*Mohammad Alaghemandi<sup>1</sup>, Joachim Schulte<sup>2</sup>, Frédéric Leroy<sup>1</sup>, Florian Müller-Plathe<sup>1</sup>  
and Michael C. Böhm<sup>1</sup>*

<sup>1</sup>Eduard-Zintl-Institut für Anorganische und Physikalische Chemie,  
Technische Universität Darmstadt, Petersenstrasse 20, D-64287 Darmstadt, Germany  
<sup>2</sup>Bruker Biospin GmbH, Silberstreifen, D-76287 Rheinstetten, Germany

The thermal conductivity ( $\lambda$ ) of carbon nanotubes (CNTs) with chirality indices (5,0), (10,0), (5,5) and (10,10) has been studied by reverse non-equilibrium molecular dynamics (RNEMD) simulations as a function of different bondlength alternation patterns ( $\Delta r$ ). The  $\Delta r$  dependence of the bond force constant ( $k_{rx}$ ) in the MD force field has been determined with the help of an electronic band structure approach. From these calculations it follows that the  $\Delta r$  dependence of  $k_{rx}$  in tubes with not too small diameter can be mapped by a simple linear bondlength – bondorder correlation. A bondlength alternation with an overall reduction in the length of the nanotube causes an enhancement of  $\lambda$  while an alternation scheme leading to an elongation of the tube is coupled to a reduction of the thermal conductivity. This effect is more pronounced in CNTs with larger diameters. The formation of a polyene-like structure in the direction of the longitudinal axis has no strong influence on  $\lambda$ . The combined analysis of RNEMD and crystal orbital results shows that  $\Delta r$  dependent modification of  $\lambda$  and the electrical conductivity are uncorrelated. This behavior is in line with a heat transfer that is not carried by electrons. General trends in the calculated  $\lambda$  values are explained with the help of (projected) power spectra which provide an access to (projected) densities of vibrational states (DOS).  $\lambda$  is enhanced with increasing DOS values into the longitudinal tube direction.

---

## 5.1. Introduction

The fascinating properties of carbon nanotubes (CNTs) have absorbed the interest of many research groups<sup>1-4</sup>. From an experimental point of view, their high electrical conductivity as well as superconducting transitions have attracted scientific activities since almost two decades. From a theoretical point of view, these nanosized systems have been employed widely to check the transferability of physical concepts derived for perfect one-dimensional (1D) single-file chains to experimentally feasible quasi 1D systems. In recent articles<sup>5,6</sup> we have analyzed the justification of this procedure for the thermal conductivity ( $\lambda$ ). The thermal conductivity of CNTs has been studied both experimentally<sup>7-12</sup> as well as by molecular dynamics (MD) simulations of the non-equilibrium (NE) type<sup>13-21</sup>. The observation of thermal rectification ( $R_t$ ) in externally mass-loaded carbon and boron nitride nanotubes<sup>22</sup> has led to a renaissance in the research of the heat transfer in nanotubes<sup>5,6,21,23-29</sup>.  $R_t \neq 0$  characterizes a difference in the heat transport into two opposite directions. The length ( $l$ ), diameter ( $d$ ) and temperature ( $T$ ) dependence of  $\lambda$  in carbon nanotubes has been quantified by (reverse) non-equilibrium MD (RNEMD) simulations. Our articles on nanotubes have led to a theoretical concept to explain the direction and magnitude of  $R_t$ <sup>5,6</sup>. For our analysis we have calculated the power spectra as well as projected power spectra of CNTs on the basis of the velocity-velocity auto-correlation function. In the harmonic approximation the (projected) power spectra map the (projected) density of vibrational states (DOS)<sup>30</sup>.

Although the recent MD simulations on the thermal conductivity of nanotubes provided deep insight into the correlation between  $\lambda$  and quantities such as the tube length, diameter or temperature, one possible key parameter has not been considered up to now. It is the influence of the bondlength or – even more important – the bondlength alternation on  $\lambda$ . Experimental studies of quasi 1D organic molecular crystals<sup>31</sup> and low-dimensional inorganic transition metal oxides<sup>32-36</sup> have shown sizable modifications of  $\lambda$  via dimerization or distortion coordinates. Bondlength alternations as well as other types of symmetry reductions in carbon nanotubes have been studied in detail by electronic (band) structure calculations ranging from model Hamiltonians of the Su-Schrieffer-Heeger type<sup>37,38</sup> over semiempirical all-valence techniques<sup>39,40</sup> to sophisticated procedures in the framework of density functional theory (DFT)<sup>41-44</sup>. From the manifold of band structure data on CNTs the following general trends can be deduced. A: The alternation in the bondlengths is enhanced with decreasing tube

---

diameter  $d$ . The largest differences between short and long bonds amount to roughly 5 pm. B: The deviations from equidistant C-C lengths in zig-zag tubes are larger than in armchair materials. C: The potential energy surface around the equidistant configuration is rather flat. D: For the majority of CNTs the tangential C-C bonds oriented mainly around the belt ( $r_1$ ) are longer than the axial C-C bonds mainly pointing into the direction of the tube axis ( $r_2$ ); see figure 1. E: There is no general correlation between bondlength alternation and the opening of a band gap ( $\Delta E$ ) in CNTs that are metallic in the equidistant configuration. The last item indicates that the alternation of the bondlength in CNTs cannot be identified in any case with the so-called Peierls-transition of 1D systems, i.e. a metal-insulator transition due to an enhancement of the lattice periodicity<sup>45</sup>. This result leads us back to the question touched above, i.e. the justification to adopt CNTs as a model to map the physical peculiarities of perfect one-dimensional single-file chains. Some of the cited band structure studies of theoretical physicists have been related to the milestone concept of Peierls. From electronic structure calculations of hydrocarbon  $\pi$  systems, however, it is well-known that these species show a strong tendency to form C-C bonds with characteristic alternation patterns. X-ray studies showing the bond alternation in conjugated  $\pi$  systems are legion<sup>46-48</sup>. First theoretical concepts to explain this behavior in terms of bondlength - bondorder correlations have been published 50 years ago<sup>49,50</sup>. In the past two decades it has been demonstrated by quantum chemical calculations that the bond alternation in hydrocarbon  $\pi$  systems depends sensitively on the competition between  $\pi$ - and  $\sigma$ -electronic effects<sup>51-55</sup>. The alternation of the bondlengths predicted for CNTs is thus not unexpected. It should be considered merely as a  $\pi$  electronic property leading to polyene, allylic or Kekule-like structures and not as a 1D solid state process.

The present work is the first theoretical study to analyze the correlation between bond alternation and thermal conductivity in carbon nanotubes. For this purpose we have supported reverse non-equilibrium molecular dynamics simulations<sup>56,57</sup> with the results of crystal orbital (CO) calculations derived by an efficient semiempirical electronic Hamiltonian of the intermediate neglect of differential overlap (INDO) type<sup>58,59</sup>. The INDO Hamiltonian employed is of the Hartree-Fock (HF) type. In contrast to DFT methods HF techniques tend to overestimate band gaps. DFT gaps are usually too small<sup>60</sup>. The CO formalism provides information that is easy to consider in the design of the force field of the RNEMD method. The capability of the INDO CO model has been

---

demonstrated for many low-dimensional systems<sup>61</sup>. They include fullerenes and fullerides<sup>62-64</sup>, graphite intercalates<sup>65</sup> as well as organic charge transfer salts<sup>66</sup>. In analogy to the broad application of the INDO CO Hamiltonian, the RNEMD approach has been also used to study the transport quantities of different materials<sup>67-71</sup>. Originally this approach has been developed for atomic liquids. Later it had been extended to molecular fluids as well as to crystalline and amorphous polymers. The reverse non-equilibrium method has been implemented into the MD code YASP<sup>72,73</sup>. All RNEMD simulations of the present study have been performed with it.

In our recent RNEMD study of nanotubes<sup>5,6</sup> we have used calculated (projected) power spectra to explain the preferred direction of the heat transfer in model systems with a mass gradient or other anisotropies. A possible correlation between  $\lambda$  and (projected) DOS values as a function of the bond alternation would offer an additional route to demonstrate the influence of longitudinal phonons on the heat transfer in nanotubes.

The CNTs chosen for the present analysis are shown in figure 1. We have considered zig-zag nanotubes with chiral indices (5,0) and (10,0) as well as (5,5) and (10,10) armchair tubes. From band structure calculations it is known that the zig-zag arrangement usually implies a finite gap ( $\Delta E$ ) between occupied and empty dispersion curves while armchair tubes are metallic<sup>1-4,43</sup>. The alternation patterns of the bondlengths studied are also shown in figure 1. For the armchair tubes we have studied the distortion coordinate  $\Delta r_1 = r_1 - r_2$  for both  $\Delta r_1 > 0$  and  $\Delta r_1 < 0$ . The first displacement symbolizes the formation of a longitudinal “allylic” configuration of the  $r_2$  bonds. In our calculations the length reduction of  $r_2$  is coupled to an elongation of the  $r_1$  bonds under the constraint that the averaged bondlength per C atom ( $r_0$ ) is conserved. The MD force field employed is based on  $r_0 = 141.8 \text{ pm}$ <sup>74</sup>. Negative  $\Delta r_1$  values in the armchair tubes describe a polyene structure with short bonds  $r_1$  orthogonal to the tube axis. For the zig-zag chains only the dimerization pattern  $\Delta r_2 = r_1 - r_2$  with  $\Delta r_2 > 0$  has been modeled. In analogy to the armchair tubes we have analyzed a polyene formation. But now the short bonds  $r_2$  are oriented into the direction of the tube axis. The  $\Delta r_1$  coordinate with  $\Delta r_1 > 0$  implies a reduction in the tube length while the  $\Delta r_1 < 0$  modulation is accompanied by an enhancement of  $l$ . Modifications of the diameter due to this displacement coordinate are less pronounced. Here we have a compensation between bondlengths shortening and elongation. For the second dimerization coordinate  $\Delta r_2$  such compensation occurs for the tube length  $l$  while the diameter  $d$  is

enhanced with increasing bond alternation. Other displacement patterns possible in CNTs remain unconsidered in the work at hand. For an older publication of one of the present authors on multi-mode Peierls transitions under quasi 1D conditions we refer to the literature<sup>75</sup>. Out-of-plane deformations in small diameter CNTs have been studied by different research groups<sup>76,77</sup>. However these studies have not been related to heat transport phenomena. In order to derive systematic simulation results we have calculated the thermal conductivity of the four CNTs in figure 1 over a large interval of the bondlength alternations  $\Delta r$ . The maximum  $\Delta r$  considered in this work exceeds the largest bond alternation calculated for CNTs by roughly a factor of two.

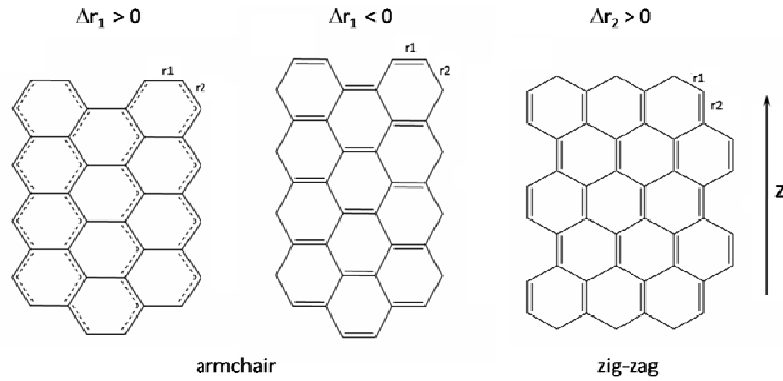


**Figure 1.** Schematic representation of the alternation in the bondlengths considered in the armchair (left and middle) and zig-zag (right) nanotubes. For the armchair systems the coordinate  $\Delta r_1 > 0$  maps the formation of an allylic structure of the  $r_2$  bonds under elongation of the  $r_1$  bonds that are orthogonal to the tube axis. The dimerization  $\Delta r_1 < 0$  is based on a shortening of the  $r_1$  bonds under elongation of the  $r_2$  bonds. Note that  $\Delta r_1 > 0$  leads to a reduction of the overall tube length while  $\Delta r_1 < 0$  implies an elongation of  $l$ . For the zig-zag CNTs the dimerization coordinate  $\Delta r_2$  has been considered only for  $\Delta r_2 > 0$ , i.e. a reduction in the length of the  $r_2$  bonds coupled to an enhancement of the  $r_1$  length. The predominant geometric modification of this alternation pattern is an enhancement of the tube diameter. All bondlength alternations considered have been performed under conservation of the averaged bondlength  $r_0$  at each carbon atom. For the alternation pattern  $\Delta r_1$  this leads to  $r_1 + 2r_2 = 3r_0$  while we have  $2r_1 + r_2 = 3r_0$  for the  $\Delta r_2$  alternation. The bond alternation is defined as  $\Delta r = r_1 - r_2$  for both types of nanotubes.

---

## 5.2. Theoretical tools

Detailed descriptions of the RNEMD method developed by one of the present authors have been given in the literature<sup>56,57</sup>. Thus it is not necessary to recapitulate its basic ingredients here. In the present context we should mention only that the derivation of  $\lambda$  requires the formation of a linear temperature gradient. More than four decades ago Lieb and Wu have demonstrated the absence of such a T profile in the interior of a homogenous single-file chain if the potential is purely harmonic<sup>78</sup>. Such a T shape, however, is not established in quasi 1D systems. The coupling between the different degrees of freedom per atom generates the anharmonicities avoiding the peculiar T profile of the “harmonic” single-file chain. This is valid even if the potential of the quasi 1D system is purely harmonic. We refer to our recent RNEMD studies of  $\lambda$  in nanotubes<sup>5,21</sup> as well as to contributions of other authors<sup>13-20</sup>.

The intramolecular force field for the CNTs<sup>74</sup> is characterized by the geometric parameters  $r_x$  ( $x = 1, 2$ ),  $\theta_0$  and  $\delta_0$ . The associated force constants are abbreviated by  $k_{rx}$ ,  $k_\theta$  and  $k_\delta$ . The (variable) C-C bondlengths  $r_x$  allow us to define deviations from the value  $r_0 = 141.8$  pm at the equidistant configuration<sup>74</sup>. Bond force constants  $k_{rx}$  have been chosen that are a function of the C-C bondlength.  $k_{rx}$  is enhanced with reduced bondlength (i.e. increasing double bond character). In the present work we have calculated the thermal conductivity of the CNTs as a function of the bond alternation  $\Delta r = r_1 - r_2$ . For the bond angle the approximation  $\theta_0 = 120^\circ$  has been adopted throughout to avoid a superposition of different influence factors on  $\lambda$ .  $\theta_0 = 120^\circ$  is approximately value if  $\Delta r$  is not too large for armchair tubes. Only for the (5,0) zig-zag chain the optimized angles differ somewhat from  $120^\circ$ <sup>43</sup>. The overall trends derived below, however, are not influenced by an unrelaxed bond angle. The last coordinate considered in the CNT force field is the dihedral angle  $\delta_0 = 0^\circ$ . The force constants for the equidistant configuration have been determined by Li and Chou<sup>74</sup>. To consider the bond alternation in this force field we have used a correlation suggested long time ago for hydrocarbon  $\pi$  systems<sup>49,50,79</sup>. The geometry dependence of the bond force constant is approximated via a simple “diagonal” formula

$$k_{rx} = k_{r'} + 116600 P_\pi \quad (\text{in kJmol}^{-1}\text{nm}^{-2}) \quad (1)$$

with  $k_{r'}$  denoting the bond force constant of a C-C single bond ( $k_{r'} = 334720$  kJmol<sup>-1</sup>nm<sup>-2</sup>)<sup>80</sup>.  $P_\pi$  is the  $\pi$  bondorder of the nanotube bonds. We have  $P_\pi = 0.0$  for a C-C single bond

and  $P_\pi = 1.0$  for a full double bond. To relate the interpolation (1) to the bondlength we make use of a popular bondlength - bondorder relation<sup>49,50,79</sup>

$$r = 150.6 - 17.8 P_\pi \text{ (in pm)} \quad (2)$$

where the first term on the rhs. denotes the length of a C-C single bond. With this interpolation we derive a double bond character  $P_\pi = 0.495$  for CNTs with equidistant C-C lengths of 141.8 pm. With  $P_\pi = 0.495$  we meet  $k_{rx} = 392460 \text{ kJmol}^{-1}\text{nm}^{-2}$  which corresponds to the force constant published by Li and Chou for CNTs with equidistant bonds<sup>74</sup>.

The validity of the above linear interpolation has been checked by band structure calculations with an INDO CO Hamiltonian<sup>58,59</sup>. The ( $\pi$ ) bondorder used in eqs. (1) and (2) is a well-defined quantity of this Hamiltonian. As  $P_\pi$  cannot be extracted easily from the CO results in the case of non-planar  $\pi$  systems, we have used an approach over so-called Wiberg bond indices ( $W$ )<sup>81</sup>. The  $\pi$  bondorder has been determined via  $W$  by assuming a  $\sigma$  bondorder  $P_\sigma$  of 1.0. Other quantities taken from the INDO CO calculations are the band gap ( $\Delta E$ ) in the zig-zag chains and the electronic density of states at the Fermi energy ( $N_F$ ) in the metallic armchair systems. These numbers allow us to relate the  $\Delta r$  dependence of the thermal conductivity to the  $\Delta r$  dependence of the electrical conductivity. In system with a finite gap  $\sigma$  scales with  $\exp(-\Delta E/k_B T)$  with  $k_B$  denoting the Boltzmann constant. In metallic configurations  $\sigma$  is proportional to  $N_F$ . Despite the adoption of the above CO quantities we want to emphasize that a new detailed electronic structure analysis of CNTs has not been intended in the present work. This has been done in detail by more sophisticated CO methods<sup>1-4,41-43</sup>. Our band structure data have a supplementary function which is feasible already with a rather low computational effort.

For mass-graded nanotubes we have demonstrated that the thermal conductivity can be correlated with a projection of the density of vibrational states into the direction of the  $T$  gradient, here chosen as the  $z$ -axis ( $D_z$ )<sup>5,6</sup>.  $D_z$  is defined as

$$D_z = \frac{\int G_z(\omega) d\omega}{\int G(\omega) d\omega} \quad (3)$$

with  $G_z(\omega)$  denoting the  $z$ -projection of the Fourier transform of the mass-weighted Cartesian velocity-velocity-auto-correlation function. The parameter  $\omega$  stands for the vibrational wave number. Prescriptions to calculate  $G_z(\omega)$  and  $G(\omega)$  can be found in the literature<sup>5,6,30</sup>. The  $D_z$  parameter in quasi 1D systems can be used as a measure for the coupling between transverse and longitudinal vibrational modes. In our recent studies



---

this interaction had been an outcome of different orientations of a mass gradient relative to the direction of the T gradient<sup>5,6</sup>. In the work at hand we want to consider changes of  $D_z$  as a function of the bond alternation  $\Delta r$ .

### 5.3. Computational conditions

All RNEMD simulations have been performed with the simulation package YASP<sup>72,73</sup>. The force field accepted for CNTs with equidistant C-C bonds has been taken from ref. <sup>74</sup>. The  $\Delta r$  dependence of the harmonic bond force constants  $k_{rx}$  has been described in the last section. For the harmonic bond angle bending we have adopted  $k_\theta = 527 \text{ kJmol}^{-1}\text{rad}^{-2}$ , the harmonic dihedral term amounts to  $k_\delta = 167 \text{ kJmol}^{-1}\text{rad}^{-2}$ . As a result of the rigid nanotube geometry it was not necessary to consider non-bonding interactions in the MD force field. In the integration of Newton's equation of motion we have used the leapfrog algorithm<sup>82</sup> with a time step of 1 fs. A single nanotube of a length of 50 nm has been placed in the orthorhombic periodic simulation box in all RNEMD simulations. Thus our box is pseudo-infinite in the axial direction but has no lateral interaction with its periodic images. The temperature has been controlled by the Berendsen thermostat<sup>83</sup> ( $\tau = 1 \text{ ps}$ ,  $T = 300 \text{ K}$ ). A velocity exchange between hot and cold atoms has been performed every 300 time steps. This setup leads to an exchange period of 0.3 ps. An interval of 301 time steps has been allowed between two samplings of the temperature profiles in the tube. A non-equilibrium run in the RNEMD approach required roughly 5 ns. The last 2 ns of this interval have been selected for the collection of the data.

The INDO results reported in the next section are of the 1D type in order to match the setup of the MD simulations which have been performed for a single nanotube. We have derived the 1D band structure data with the help of a program that can be used for 1D, 2D and 3D solids<sup>59</sup>. The 1D CO calculations have been performed in a mesh of 50 k-points. We have used the same geometry in the CO calculations as employed in the MD simulations. To analyze possible modifications in the electronic structure of the CNTs under the influence of neighboring tubes, we have extended the CO approach to a monoclinic lattice. Neither hexagonal nor tetragonal unit cells are compatible with the rotational axis in the four nanotubes studied. Each tube in the 3D calculations is surrounded by six nearest neighbors. The shortest intertube separations ( $\approx 310 \text{ pm}$ ) have been taken a recent DFT study<sup>41</sup>. We have used the tubegene program to generate the 3D structure of the CNTs without bond alternation<sup>84</sup>. For the consideration of bond

---

alternation we have written a new code. The  $\bar{k}$ -points have been constructed by the approach developed by one of us<sup>85</sup>. The total number of  $\bar{k}$ -points considered in the 3D CO runs amounts to 256. The  $\bar{k}$ -mesh in the present 1D and 3D calculations is larger than the grid adopted in the majority of published band structure works<sup>37-44</sup>. Our 3D calculations have shown that the intertube couplings are without sizeable influence on the  $\pi$  bondorders. The band gap in the zig-zag chains is reduced by roughly 10 to 20%. Such modifications are however not relevant for the intention of the present analysis. Thus we have restricted the presentation of the CO data to the 1D case.

## 5.4. Results and discussion

### 5.4.1. Crystal orbital data

We start our discussion with the CO results which have been derived to estimate the justification of the linear interpolation for the determination of  $\Delta r$  ( $r_1$ ,  $r_2$ ) dependent bond force constants in the RNEMD step. Before presenting the CO data we want to reemphasize that the potential energy surface of the CNTs around the equidistant configuration  $\Delta r = 0$  is rather flat<sup>39,42,43</sup>. Thus one has to expect a dynamic bondlength alternation  $\Delta r \neq 0$  under the influence of the electron-phonon coupling even if the alternation coordinate does not lead to a lowering of the potential energy. Such a scenario has been analyzed recently by different techniques<sup>76,77,86,87</sup>.

In figure 2 we have plotted the  $\pi$  bondorder  $P_\pi$  of the  $r_1$  and  $r_2$  bonds of the two armchair tubes as a function of the alternation coordinate  $\Delta r_1$  in the positive direction, see figure 1, generating a longitudinal allylic configuration. A linear bondlength - bondorder correlation is valid for all  $\Delta r_1$  values selected. Both armchair tubes show roughly the same correlation in figure 2. The gradient of the  $r_2$  bondorder that exceeds the  $r_1$  one by roughly a factor of two follows from the fact that the  $\Delta r_1$  alternation leads to the formation of two shorter ( $r_1$ ) and one longer ( $r_2$ ) bond at each C atom under conservation of  $3r_0$  for the averaged lengths.

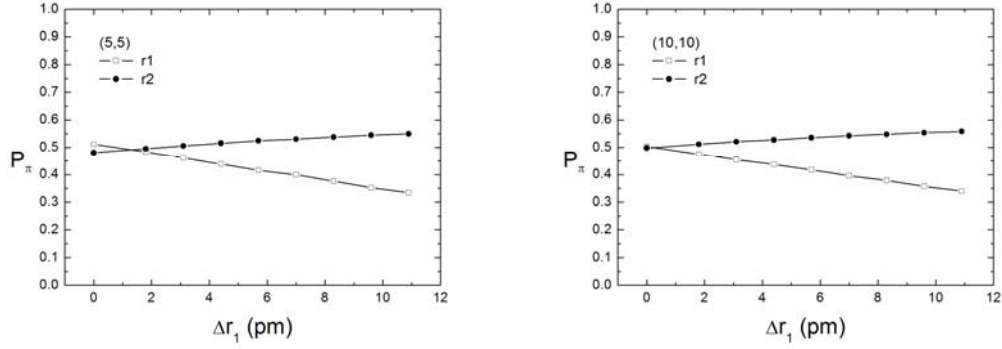


**Figure 2.** CO  $\pi$  bondorder  $P_\pi$  in the (5,5) and (10,10) armchair nanotubes as a function of the bondlength alternation  $\Delta r_1$  with values  $> 0$  leading to a longitudinal allylic structure.

The  $\pi$  bondorder in the armchair tubes for negative  $\Delta r_1$  values are plotted in figure 3. Only for larger absolute  $\Delta r_1$  the linear bondlength - bondorder correlation is slightly violated. Supplementary test simulations have shown that such minor effects can be neglected in the design of the MD force field. The following message can be extracted from figures 2 and 3. A: The popular bondlength - bondorder correlation of planar  $\pi$  systems seems to be valid also for nonplanar topologies, here for the cylindrical arrangement of CNTs. B: On the basis of these bondorders it is therefore possible to approximate the influence of the bond alternation on the MD force field in terms of a simple interpolation formula. In the present combined RNEMD-CO study intended to visualize general trends, we have accepted a common prefactor for  $P_\pi$  in eq. (2) that is close to values reported for planar  $\pi$  systems<sup>49,50,79</sup>. An optimization of this parameter for each individual tube has not been performed.

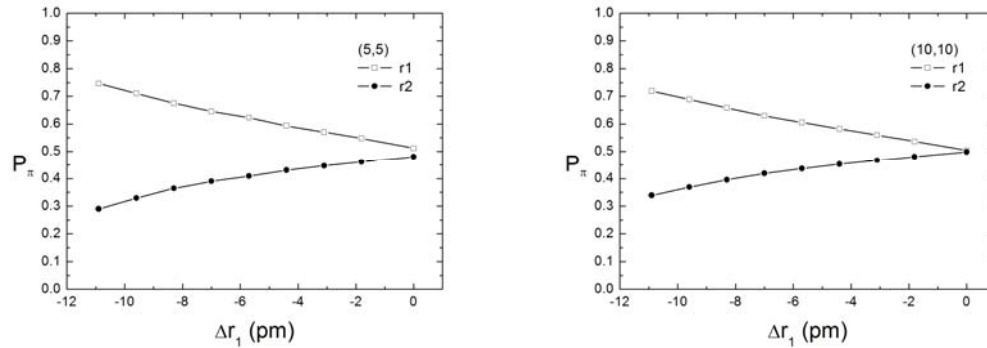


**Figure 3.** CO  $\pi$  bondorder  $P_\pi$  in the (5,5) and (10,10) armchair nanotubes as a function of the bondlength alternation  $\Delta r_1$  with  $\Delta r_1 < 0$  leading to a transversal polyene structure.

In figure 4 we have plotted  $P_\pi$  of the two zig-zag tubes as a function of  $\Delta r_2 > 0$  which maps the formation of a axial polyene configuration. For the (10,0) system we predict an approximate linear bondlength - bondorder correlation with a small change of the gradient at  $\Delta r_2 \approx 5$  pm. An explanation for this behavior will be given in the following. For the moment let us emphasize that the  $P_\pi$  splitting in the (10,0) tube in figure 4 gives an almost perfect mirror image of the  $\Delta r_1 < 0$  profile in both armchair tubes of figure 3. Again we see that an universal scaling law seems to be valid for CNTs irrespective of their chirality index as long as the tube diameter is not too small.

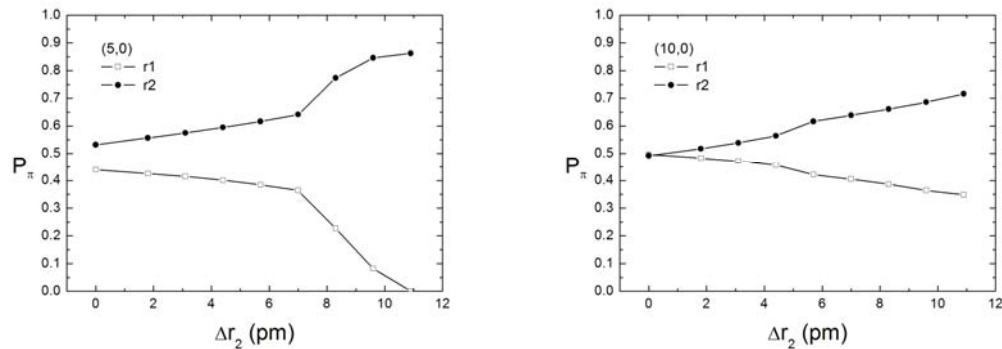


**Figure 4.** CO  $\pi$  bondorder  $P_\pi$  in the (5,0) and (10,0) zig-zag nanotubes as a function of the bondlength alternation  $\Delta r_2$  leading to a transversal polyene structure.

The latter restriction follows from the  $\pi$  bondorder profile of the (5,0) system in figure 4. Here the diameter is much smaller than in the other examples. In the series (5,0), (5,5), (10,0) and (10,10)  $d$  values of 391, 677, 782, and 1354 pm are realized (equidistant configuration). The stronger the deviations from planarity in a given system are<sup>62</sup>, the more pronounced is the  $\pi$ - $\sigma$  hybridization. This mixing is also supported by “through-space” coupling with other bonds of the tube. The combined effects are responsible for a  $\pi$  bondorder profile in the (5,0) system that differs from the others. In additional RNEMD simulations for the (5,0) CNT we have considered reoptimized  $\Delta r$  dependent scaling factors in the definition of the bond force constant  $k_{r1}$ . In the next section it will become clear that such a  $\Delta r$  dependence of  $k_{r1}$  has no large effect on the thermal conductivity. The splitting between the two  $\pi$  bondorders for  $\Delta r = 0$  in the (5,0) tube indicates an intrinsic instability of the equidistant configuration. Indeed we have found that the lowering of the energy due to bond alternation is largest for the (5,0) tube. This agrees with the findings of other CO calculations<sup>40,43</sup>. We wish to point out

that also in the (5,5) chain the two  $\pi$  bondorders at  $\Delta r = 0$  differ slightly; see figures 2 and 3.

The calculated band gap  $\Delta E$  for the two zig-zag chains is helpful for understand the  $P_\pi$  profiles in figure 4. The  $\Delta r$  dependence of  $\Delta E$  of these CNTs has been displayed in figure 5. The band gap depends on the magnitude of the bond alternation  $\Delta r$  (displacement coordinate  $\Delta r_2$ ). The predicted modulation of  $\Delta E$  is a manifestation of  $\Delta r$  dependent hybridization effects in the valence and conduction band. A quantitative analysis of such hybridization effects under the influence of a non-planar geometry for fullerenes and fullerides has been given by one of us<sup>62</sup>. The correlation between  $\Delta E$  and  $\pi$ - $\sigma$  hybridization in CNTs has been mentioned by several authors<sup>41-43</sup>. When comparing figures 4 and 5 we notice that changes in the  $P_\pi$  gradient correlate with changes of  $\Delta E$ . This effect is less pronounced in the (10,0) tube but rather strong in the (5,0) material. The right  $\Delta E$  minimum in the (10,0) chain is coupled to a second small hump in  $P_\pi$  for  $\Delta r > 11$  pm.

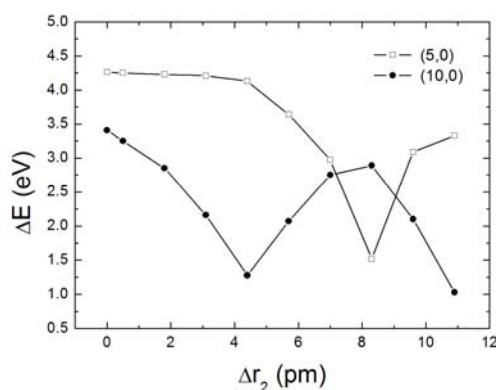


**Figure 5.** Band gap  $\Delta E$  in the zig-zag nanotubes of chirality (5,0) and (10,0) as a function of the bondlength alternation  $\Delta r_2$  leading to an axial polyene structure. The straight lines connecting the data points are only a guide for the eye.

The present band structure calculations have shown that the bondlength – bondorder correlation verified long time ago for planar  $\pi$  networks is also valid in CNTs if the tube diameter is not too small<sup>49,50,79</sup>. Consequently the force constants in the MD force field can be scaled by a universal relation that does not depend on the chirality index of the tube. With the help of electronic structure data, however, it would be possible to map system specific electronic fine effects by modifications in the prefactor of  $P_\pi$  in the given interpolation formulas.

## 5.4.2. Thermal conductivity

Below we discuss the dimensionless normalized thermal conductivity  $\lambda_n = \lambda/\lambda_0$  of the four CNTs as a function of the displacement coordinates  $\Delta r_1$  and  $\Delta r_2$ . The label  $\lambda_0$  denotes the thermal conductivity of the system for equidistant C-C bonds with  $r_0 = 141.8$  pm. We have  $\lambda_0 = 188.1, 232.0, 233.9$  and  $234.1$   $\text{Wm}^{-1}\text{K}^{-1}$  for the (5,0), (5,5), (10,0) and (10,10) nanotubes, respectively. But before presenting the  $\Delta r$  dependence of  $\lambda$  we first consider the normalized thermal conductivity of the (10,10) system as a function of the C-C bondlength under conservation of the equidistant arrangement. The two extreme  $r$  values employed refer to a C-C double bond ( $r = 132.8$  pm) and to a long C-C single bond ( $r = 153.1$  pm).

The  $r$  dependence of  $\lambda_n$  of the equidistant (10,10) tube has been plotted in figure 6. We see that  $\lambda_n$  is enhanced with decreasing  $r$  (enhanced bond force constant, reduced tube length). As the frequency of (harmonic) oscillators scales with  $\sqrt{k}$ , such a result has been expected<sup>5</sup>. Note that this square root dependence is valid both in the classical limit as accepted in the present MD simulations as well as for quantum (harmonic) oscillators.

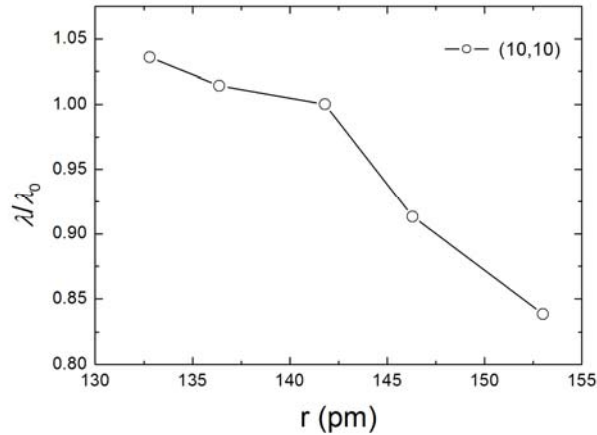


**Figure 6.** Normalized thermal conductivity  $\lambda_n = \lambda/\lambda_0$  of the (10,10) nanotube as a function of the length  $r$  of the C-C bonds under conservation of equidistant C-C bonds. The RNEMD simulations have been performed at an averaged temperature of 300 K.  $\lambda_0$  stands for the thermal conductivity of the nanotube with a bondlength  $r_0$  of 141.8 pm at the minimum of the potential energy surface. The curve shape for the (10,0) system is similar to the (10,10) profile.

In figure 7 we have plotted the  $\Delta r$  dependence of  $\lambda_n$ . We start with the  $\lambda_n$  values of the (5,5) and (10,10) armchair tubes. Similar to the  $r$  dependent  $\lambda_n$  in figure 6, the thermal

conductivity depends on the bondlength (alternation). The  $\Delta r$  dependence of  $\lambda_n$  in the (10,10) system is larger than in the thinner tube. In the  $\lambda_n$  plot for the armchair CNTs  $\Delta r_1$  values  $> 0$  and  $< 0$  have been modeled. In analogy to the  $r$  variation in figure 6, the thermal conductivity is enhanced with decreasing tube length ( $\Delta r_1 > 0$ ). Due to the definition of  $\Delta r_1$ , however, the sign of the slope of the  $\lambda_n$  curves in figure 6 and 7 differs.

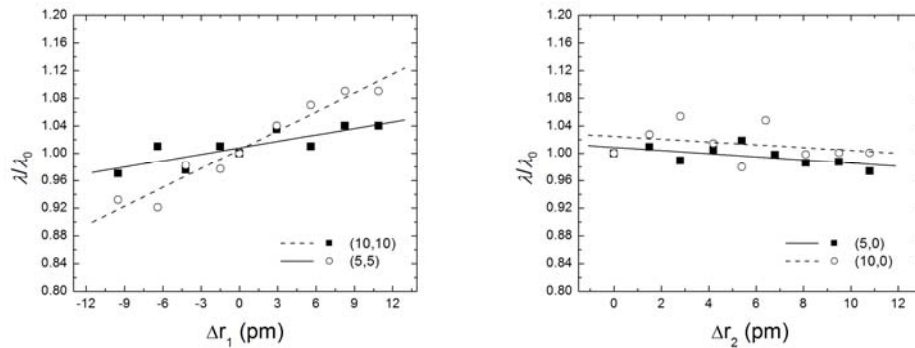


**Figure 7.** Normalized thermal conductivity  $\lambda_n = \lambda/\lambda_0$  of all CNTs plotted in figure 1 as a function of the bond alternation  $\Delta r$ . The RNEMD simulations have been performed at an averaged temperature of 300 K.

Where comparing the  $\lambda_n$  profiles for the (10,10) tube in figure 6 (i.e. length dependence of  $\lambda$  under conservation of equidistant C-C bonds) and figure 7 (i.e. bondlength alternation) we can deduce that the gradient of  $\lambda_n$  is not exclusively determined by the length of the tube. Furthermore we see that the  $\Delta r$  dependence of  $\lambda_n$ , see figure 7, depends on the tube diameter. In the next section we will come back to this topic.

Finally let us consider the  $\Delta r_2$  dependence of  $\lambda_n$  in the two zig-zag tubes. For these CNTs we observe a rather weak response of  $\lambda$  on  $\Delta r$ . The formation of a longitudinal polyene structure causes a – although weak – reduction in the thermal conductivity. Obviously this behavior cannot be explained with the overall tube length. Note that  $\lambda$  is even somewhat reduced when the longitudinal polyene structure is formed. If bare length arguments would be valid to explain the changes of  $\lambda_n$ , an enhancement of the thermal conductivity with increasing  $\Delta r_2$  would be expected. The opposite trend for  $\lambda$  in figure 7 is simple to explain. The heat transfer is most efficient in an “homogenous” system, i.e. for identical bonds in the direction of the T gradient<sup>6</sup>. Longitudinal 1D homogeneity is fulfilled for the displacement coordinate  $\Delta r_1$ , but not for  $\Delta r_2$ . In our recent RNEMD simulations of the heat transfer in nanotubes we have observed such a reduction of  $\lambda$  due to bonds in the direction of the T gradient that were not identical<sup>5,6</sup>.

---

We are left with the following peculiarities for the heat transfer in CNTs as a function of the bond alternation  $\Delta r$ . A: The  $\Delta r_2$  dependence of  $\lambda$  in zig-zag chains, which exhibit the largest bond alternation in the CNT family, is rather weak. B: The strong  $\Delta r_1$  dependence of  $\lambda$  in large diameter armchair systems is coupled to rather small displacement coordinates. C: The weak  $\Delta r_2$  dependence of  $\lambda$  in the non-metallic zig-zag chains is accompanied by forbidden band gaps  $\Delta E$  that depend on  $\Delta r_2$ ; see figure 5. The electrical conductivity in these tubes scales with  $\Delta E$ . D: The rather large  $\Delta r_1$  dependence of  $\lambda$  in the metallic armchair systems does not correlate with a  $\Delta r$  dependence of the electronic density of states at the Fermi energy  $N_F$ . The latter findings indicate that the  $\Delta r$  dependence of  $\lambda$  and  $\sigma$  is decoupled. This behavior is characteristic for systems where the thermal conductivity is not driven by charge carriers. In recent RNEMD simulations we have verified the decisive influence of phonons on  $\lambda$  in different polymer materials ranging from CNTs<sup>5,6</sup> to polystyrene or polyamides<sup>68,70,71,88</sup>.

### 5.4.3. Correlation between $\lambda$ and the projected phonon DOS

In the following we explain the  $\Delta r$  dependence of  $\lambda$  on the basis of the projected density of vibrational states  $D_z$ . Already in recent works<sup>5,6</sup> we have suggested that  $\lambda$  is enhanced with an increasing intensity transfer from transversal to longitudinal modes, here measured by the parameter  $D_z$ . Mode coupling theories which explain trends in  $\lambda$  as well as the direction of thermal rectification have been published by different authors<sup>23,24,89</sup>. We have restricted the present analysis to the (10,10) armchair tube where the  $\Delta r$  dependence of  $\lambda$  has been largest.

The  $D_z$  parameter for this CNT has been given in table 1. We have evaluated  $D_z$  for the longitudinal allylic ( $\Delta r_1 = 8.3$  pm) as well as for the transverse polyene arrangement ( $\Delta r_1 = -6.4$  pm). The first set of  $D_z$  values has been derived from an equilibrium MD simulation (EMD) with a constant temperature of 300 K, the second one in the presence of a temperature gradient with an average temperature of 300 K as used in the RNEMD simulations. To reemphasize, we interpret the splitting of the  $D_z$  in terms of a  $\Delta r$  dependent transfer of vibrational intensity between transverse and longitudinal modes. In the EMD simulations we predict roughly the same  $D_z$  parameter for the two configurations. When RNEMD calculations are performed in the presence of a T gradient, a splitting between the two numbers is observed. A more efficient polarization of



vibrational intensity in the allylic configuration leads to an enhanced density of vibrational states into the longitudinal direction. In other words, the enlarged  $D_z$  indicates that longitudinal modes are now easier to excite thermally. When relating the present results to our findings in mass-graded nanotubes<sup>5,6</sup> we feel that modifications of  $\lambda$  both as a function of  $\Delta r$  or of a mass gradient can be explained in terms of the projected phonon DOS  $D_z$ . The above arguments also render possible an explanation of the different  $\lambda_n$  gradients for the (5,5) and (10,10) tubes in figure 7. The transversal-longitudinal mode coupling is strengthened with an increasing number of atoms in the belt. As a matter of fact the  $\lambda_n$  enhancement in the (10,10) tube as a function of  $\Delta r_1$  exceeds the  $\lambda_n$  enhancement in the small diameter system.

**Table 1.** Projected phonon density of states in the (10,10) nanotube for the alternation coordinate  $\Delta r_1 > 0$  and  $\Delta r_1 < 0$ .  $\Delta r$  parameters of 8.3 pm and -6.4 pm have been chosen for  $\Delta r_1 > 0$  and  $\Delta r_1 < 0$ . They refer to the minimum and maximum values of  $\lambda/\lambda_0$  shown in figure 7. The  $D_z$  numbers in the left column have been derived under equilibrium conditions at 300 K. The  $D_z$  collection in the right column has been determined in the presence of a T gradient in the CNT.

Configuration	$D_z$ (in %) EMD	$D_z$ (in %) RNEMD
longitudinal allylic structure ( $\Delta r_1 = 8.3$ pm)	36.9	37.3
transverse polyene ( $\Delta r_1 = -6.4$ pm)	36.9	37.0

At the end of this section we come back to the bondlength dependence of  $\lambda_n$  (figure 6) as well as to the  $\Delta r_2$  dependence of the thermal conductivity in the zig-zag tubes. The enhancement of  $\lambda_n$  with reduced bondlength (and increased bond force constants) has been traced back to the  $\sqrt{k}$  dependence of vibrational frequencies. Phonon polarization via transverse-longitudinal mode coupling is irrelevant here. This has been checked by  $D_z$  numbers that are not changed as a function of the C-C bondlength  $r$ . The (weak)  $\Delta r_2$  dependence of  $\lambda_n$  in the zig-zag tubes has been commented on briefly in the last section. The  $\lambda_n$  reduction with increasing  $\Delta r_2$  is an outcome of an increasing localization of longitudinal modes. Delocalized modes can be formed most efficiently for a homogenous bonding framework.

---

## 5.5. Conclusions

We have studied modifications in the thermal conductivity of armchair and zig-zag carbon nanotubes as a function of different bond alternations by reverse non-equilibrium molecular dynamics simulations. To incorporate this geometry dependence into a given force field we have performed supporting electronic band structure calculations. On the one hand, the crystal orbital data have shown that the bond force constants can be modulated via a simple “diagonal” bondlength - bondorder correlation. On the other hand, the CO results have been employed to show that geometry dependent modifications of the thermal and electrical conductivity are decoupled, which means that the Wiedemann-Franz law is not valid for carbon nanotubes. The validity of this empirical relation is often used to emphasize that the heat transfer is controlled by charge carriers, i.e. electrons or holes.

The dependence of the thermal conductivity on bond alternation can be classified as follows: The formation of a longitudinal polyene structure in zig-zag tubes (distortion coordinate  $\Delta r_2$ ) leads to a small reduction of  $\lambda$ . This rather weak  $\Delta r_2$  response of  $\lambda$  is caused by the competition of two influence parameters acting into opposite directions. The length of the nanotube is reduced in the longitudinal polyene configuration, a geometrical modification supporting an enhancement of  $\lambda$ ; see the  $r$  dependence of  $\lambda$  in figure 6. This enhancement factor, however, is overcompensated by an attenuation of  $\lambda$  with an increasing difference between the  $r_1$  single and  $r_2$  double bonds. Vibrational transfer under the influence of mode coupling is of minor importance only. As a matter of fact we predict a shape for the  $\lambda$  profile in the zig-zag tubes that does not depend on the diameter. For the distortion coordinate  $\Delta r_1$  in the armchair systems which conserve the homogeneity of the bonds in the longitudinal direction, we have found a stronger and diameter-dependent modification of  $\lambda$  as a function of the bond alternation. The larger gradient of  $\lambda$  in the (10,10) nanosystem is in line with the expectations deduced from a mode coupling approach.

We have adopted projected phonon density of states to explain the  $\Delta r$  dependence of  $\lambda$  in the armchair tubes.  $D_z$  (and in the framework of our theory  $\lambda$ ) increased with an increasing transfer of vibrational intensity from transverse to longitudinal modes. It goes without saying that this effect becomes more efficient with increasing tube diameter. We are confronted with the situation that the  $\Delta r$  dependent modulation of the thermal conductivity is weak in zig-zag chains which, however, exhibit larger bond

---

alternation than those realized in the armchair systems. In large-diameter armchair tubes  $\lambda$  is significantly changed as a function of  $\Delta r_1$ . But here only a small bond alternation occurs.

From theoretical studies published recently, it can be deduced that  $\lambda$  will be coupled to displacement coordinates  $\Delta r$  even if  $\Delta r$  does not lead to a reduction of the potential energy<sup>76,77,86,87</sup>. Transmitter of such a process is the electron-phonon coupling. Let us end with a short prediction on the anisotropy of the thermal conductivity in the presence of bond alternation. We expect that the displacement coordinate  $\Delta r_1$  has a sizable influence on the anisotropy  $\lambda_l/\lambda_t$  in armchair tubes.  $\lambda_l$  is the longitudinal thermal conductivity and  $\lambda_t$  is the transversal conductivity in a three-dimensional CNT system.  $\Delta r_1 > 0$  implies an enhancement of  $\lambda_l$  (shortening of the tube length) and a reduction of  $\lambda_t$  (magnification of  $d$ ). Note that we have neglected a possible intertube contribution to  $\lambda_t$ . Such RNEMD simulations on bundles of CNTs are currently performed in our group. Indeed a correlation between the anisotropy of  $\lambda$  and the dimerization in the bondlengths has been found in a low-dimensional metal oxide<sup>34</sup>. For the coordinates  $\Delta r_1 < 0$  and  $\Delta r_2$  we expect that both  $\lambda_l$  and  $\lambda_t$  are reduced with increasing bond alternation. Its influence on the anisotropy  $\lambda_l/\lambda_t$  thus should be less pronounced.

## 5.6. References

- (1) Saito, R.; Dresselhaus, G.; Dresselhaus, M. S. *Physical Properties of Carbon Nanotubes*; Imperial College Press: London, 1998.
- (2) Harris, J. F. *Carbon Nanotubes and related Structures*; Cambridge University press: Cambridge, 1999.
- (3) Reich, S.; Thomsen, C.; Maultzsch, J. *Carbon Nanotubes, Basic Concepts and Physical Properties*; Wiley-VCH: Weinheim, 2004.
- (4) Charlier, J. C.; Blase, X.; Roche, S. *Reviews of Modern Physics* **2007**, *79*, 677.
- (5) Alaghemandi, M.; Leroy, F.; Algaer, E.; Böhm, M. C.; Müller-Plathe, F. *Nanotechnology* **2010**, *21*, 075704.
- (6) Alaghemandi, M.; Leroy, F.; Böhm, M. C.; Müller-Plathe, F. *Phys. Rev. B*, submitted.
- (7) Kim, P.; Shi, L.; Majumdar, A.; McEuen, P. L. *Physical Review Letters* **2001**, *vol.87, no.21*, 215502/1.
- (8) Fujii, M.; Zhang, X.; Xie, H. Q.; Ago, H.; Takahashi, K.; Ikuta, T.; Abe, H.; Shimizu, T. *Physical Review Letters* **2005**, *95*, 065502.
- (9) Choi, T. Y.; Poulidakos, D.; Tharian, J.; Sennhauser, U. *Nano Letters* **2006**, *6*, 1589.

- 
- (10) Yu, C. H.; Shi, L.; Yao, Z.; Li, D. Y.; Majumdar, A. *Nano Letters* **2005**, *5*, 1842.
  - (11) Hone, J.; Whitney, M.; Piskoti, C.; Zettl, A. *Physical Review B-Condensed Matter* **1999**, *59*, R2514.
  - (12) Pop, E.; Mann, D.; Wang, Q.; Goodson, K.; Dai, H. J. *Nano Letters* **2006**, *6*, 96.
  - (13) Lukes, J. R.; Zhong, H. L. *Journal of Heat Transfer-Transactions of the Asme* **2007**, *129*, 705.
  - (14) Che, J. W.; Cagin, T.; Goddard, W. A. *Nanotechnology* **2000**, *11*, 65.
  - (15) Yao, Z. H.; Wang, J. S.; Li, B. W.; Liu, G. R. *Physical Review B* **2005**, *71*, 085417.
  - (16) Berber, S.; Kwon, Y. K.; Tomanek, D. *Physical Review Letters* **2000**, *84*, 4613.
  - (17) Osman, M. A.; Srivastava, D. *Nanotechnology* **2001**, *12*, 21.
  - (18) Padgett, C. W.; Brenner, D. W. *Nano Letters* **2004**, *4*, 1051.
  - (19) Moreland, J. F.; Freund, J. B.; Chen, G. *Microscale Thermophysical Engineering* **2004**, *8*, 61.
  - (20) Maruyama, S. *Physica B-Condensed Matter* **2002**, *323*, 193.
  - (21) Alaghemandi, M.; Algaer, E.; Böhm, M. C.; Müller-Plathe, F. *Nanotechnology* **2009**, *20*, 115704.
  - (22) Chang, C. W.; Okawa, D.; Majumdar, A.; Zettl, A. *Science* **2006**, *314*, 1121.
  - (23) Yang, N.; Li, N.; Wang, L.; Li, B. *Physical Review B* **2007**, *76*, 020301.
  - (24) Wu, G.; Li, B. W. *Physical Review B* **2007**, *76*, 085424.
  - (25) Wu, G.; Li, B. W. *Journal of Physics-Condensed Matter* **2008**, *20*, 175211.
  - (26) Nuo, Y.; Gang, Z.; Baowen, L. *Applied Physics Letters* **2008**, *93*, 243111.
  - (27) Noya, E. G.; Srivastava, D.; Menon, M. *Physical Review B* **2009**, *79*, 115432.
  - (28) Yang, N.; Zhang, G.; Li, B. W. *Applied Physics Letters* **2009**, *95*, 033107.
  - (29) Bose, A.; Chatterjee, K.; Chakravorty, D. *Bulletin of Materials Science* **2009**, *32*, 227.
  - (30) Jobic, H.; Smirnov, K. S.; Bougeard, D. *Chemical Physics Letters* **2001**, *344*, 147.
  - (31) Torizuka, K.; Tajima, H.; Yamamoto, T. *Physical Review B* **2005**, *71*, 193101.
  - (32) Kwok, R. S.; Brown, S. E. *Physical Review Letters* **1989**, *63*, 895.
  - (33) Smontara, A.; Biljakovic, K.; Artemenko, S. N. *Physical Review B* **1993**, *48*, 4329.
  - (34) Bihar, Z.; Staresinic, D.; Biljakovic, K.; Sambongi, T. *Europhysics Letters* **1997**, *40*, 73.
  - (35) Smontara, A.; Bilusic, A.; Tutis, E.; Berger, H.; Levy, F. *Physica B* **1999**, *263*, 779.
  - (36) Kuo, Y. K.; Lue, C. S.; Hsu, F. H.; Li, H. H.; Yang, H. D. *Physical Review B* **2001**, *64*.
  - (37) Harigaya, K.; Fujita, M. *Physical Review B* **1993**, *47*, 16563.
  - (38) Özsoy, O.; Sünel, N. *Czechoslovak Journal of Physics* **2004**, *54*, 1495.
  - (39) Tanaka, K.; Ago, H.; Yamabe, T.; Okahara, K.; Okada, M. *International Journal of Quantum Chemistry* **1997**, *63*, 637.
  - (40) Budyka, M. F.; Zyubina, T. S.; Ryabenko, A. G.; Lin, S. H.; Mebel, A. M. *Chemical Physics Letters* **2005**, *407*, 266.
  - (41) Reich, S.; Thomsen, C.; Ordejon, P. *Physical Review B* **2001**, *64*, 195416.
  - (42) Reich, S.; Thomsen, C.; Ordejon, P. *Physical Review B* **2002**, *65*, 155411.

- 
- (43) Sun, G. Y.; Kürti, J.; Kertesz, M.; Baughman, R. H. *Journal of Physical Chemistry B* **2003**, *107*, 6924.
- (44) Moradian, R.; Behzad, S.; Azadi, S. *Physica E-Low-Dimensional Systems & Nanostructures* **2008**, *40*, 3055.
- (45) Peierls, R. *Quantum Theory of Solids*; Clarendon: Oxford, 1955.
- (46) Allen, F. H.; Bellard, S.; Brice, M. D.; Cartwright, B. A.; Doubleday, A.; Higgs, H.; Hummelink, T.; Hummelinkpeters, B. G.; Kennard, O.; Motherwell, W. D. S.; Rodgers, J. R.; Watson, D. G. *Acta Crystallographica* **1979**, *35*, 2331.
- (47) Dunitz, J. D.; Maverick, E. F.; Trueblood, K. N. *Angewandte Chemie-International Edition in English* **1988**, *27*, 880.
- (48) Dunitz, J. D. *X-Ray Analysis and the Structure of Organic Molecules*; Verlag Helvetica Chimica Acta: Zürich, 2007.
- (49) Longuet-Higgins, H. C.; Salem, L. *Proceedings of the Royal Society of London Series a-Mathematical and Physical Sciences* **1959**, *251*, 172.
- (50) Coulson, C. A.; Golebiewski, A. *Proceedings of the Physical Society of London* **1961**, *78*, 1310.
- (51) Pfirsch, F.; Böhm, M. C.; Fulde, P. *Zeitschrift Fur Physik B-Condensed Matter* **1985**, *60*, 171.
- (52) Schütt, J.; Böhm, M. C. *Journal of the American Chemical Society* **1992**, *114*, 7252.
- (53) Shaik, S. S.; Hiberty, P. C.; Lefour, J. M.; Ohanessian, G. *Journal of the American Chemical Society* **1987**, *109*, 363.
- (54) Jug, K. *International Journal of Quantum Chemistry* **1990**, *37*, 403.
- (55) Jug, K.; Hiberty, P. C.; Shaik, S. *Chemical Reviews* **2001**, *101*, 1477.
- (56) Müller-Plathe, F. *Journal of Chemical Physics* **1997**, *106*, 6082.
- (57) Müller-Plathe, F.; Bordat, P. *Novel Methods in Soft Matter Simulations* **2004**, *640*, 310.
- (58) Böhm, M. C. *Theoretica Chimica Acta* **1983**, *62*, 351.
- (59) Ramirez, R.; Böhm, M. C. *International Journal of Quantum Chemistry* **1988**, *34*, 47.
- (60) Koch, W.; Holthausen, M. C. *A Chemist's Guide to Density Functional Theory*; Wiley-VCH: Weinheim, 2001.
- (61) Böhm, M. C. *One-Dimensional Organometallic Materials: An Analysis of Electronic Structure Effects*; Springer: Berlin, Heidelberg, 1987; Vol. 45.
- (62) Böhm, M. C.; Schulte, J. *Molecular Physics* **1996**, *87*, 735.
- (63) Schedel-Niedrig, T.; Böhm, M. C.; Werner, H.; Schulte, J.; Schlögl, R. *Physical Review B* **1997**, *55*, 13542.
- (64) Böhm, M. C.; Schulte, J.; Schütt, J.; Schedel-Niedrig, T.; Werner, H.; Schlögl, R. *International Journal of Quantum Chemistry* **1997**, *65*, 333.
- (65) Böhm, M. C.; Schulte, J.; Schlögl, R. *Physica Status Solidi B-Basic Research* **1996**, *196*, 131.
- (66) Schulte, J.; Böhm, M. C. *Synthetic Metals* **1998**, *95*, 125.

- 
- (67) Zhang, M. M.; Lussetti, E.; de Souza, L. E. S.; Müller-Plathe, F. *Journal of Physical Chemistry B* **2005**, *109*, 15060.
- (68) Lussetti, E.; Terao, T.; Müller-Plathe, F. *Journal of Physical Chemistry B* **2007**, *111*, 11516.
- (69) Terao, T.; Lussetti, E.; Müller-Plathe, F. *Complex Systems* **2008**, *982*, 486.
- (70) Algaer, E. A.; Alaghemandi, M.; Böhm, M. C.; Müller-Plathe, F. *Journal of Physical Chemistry A* **2009**, *113*, 11487.
- (71) Algaer, E. A.; Alaghemandi, M.; Böhm, M. C.; Müller-Plathe, F. *Journal of Physical Chemistry B* **2009**, *113*, 14596.
- (72) Müller-Plathe, F. *Computer Physics Communications* **1993**, *78*, 77.
- (73) Tarmyshov, K. B.; Müller-Plathe, F. *Journal of Chemical Information and Modeling* **2005**, *45*, 1943.
- (74) Li, C. Y.; Chou, T. W. *International Journal of Solids and Structures* **2003**, *40*, 2487.
- (75) Lavrentiev, M. Y.; Köppel, H.; Böhm, M. C. *Chemical Physics* **1993**, *169*, 85.
- (76) Connetable, D.; Rignanese, G. M.; Charlier, J. C.; Blase, X. *Physical Review Letters* **2005**, *vol.94, no.1*, 015503/1.
- (77) Barnett, R.; Demler, E.; Kaxiras, E. *Physical Review B* **2005**, *71*, 035429.
- (78) Lieb, E. H.; Wu, F. Y. *Physical Review Letters* **1968**, *20*, 1445.
- (79) Salem, L. *Molecular orbital theory of conjugated systems*; Benjamin: Massachusetts, 1972.
- (80) Müller-Plathe, F. *Macromolecules* **1996**, *29*, 4782.
- (81) Wiberg, K. B. *Tetrahedron* **1968**, *24*, 1083.
- (82) Hockney, R. W.; Eastwood, J. W. *Computer Simulations Using Particles*; McGraw-Hill: New York, 1981.
- (83) Berendsen, H. J. C.; Postma, J. P. M.; Vangunsteren, W. F.; Dinola, A.; Haak, J. R. *Journal of Chemical Physics* **1984**, *81*, 3684.
- (84) Frey, J. T.; Doren, D. J. Tubegene program 3.2; Delaware, U. o., Ed. Newark DE, 2003.
- (85) Ramirez, R.; Böhm, M. C. *International Journal of Quantum Chemistry* **1988**, *34*, 571.
- (86) Sedeki, A.; Caron, L. G.; Bourbonnais, C. *Physical Review B* **2000**, *62*, 6975.
- (87) Bohnen, K. P.; Heid, R.; Liu, H. J.; Chan, C. T. *Physical Review Letters* **2004**, *93*, 259901.
- (88) Rossinsky, E.; Müller-Plathe, F. *Journal of Chemical Physics* **2009**, *130*, 134905.
- (89) Xu, Z. P.; Buehler, M. J. *Acs Nano* **2009**, *3*, 2767.

---

---

## 6. CONCLUSION AND OUTLOOK

---

In my PhD work I have surveyed computational modeling strategies to derive the thermal transport properties of carbon nanotubes. Now let me very briefly highlight some of the key results that have been obtained.

The calculated thermal conductivity for carbon nanotubes follows a  $L^\alpha$  law, with  $\alpha$  values between 0.54 and 0.77. The exponent  $\alpha$  is quite insensitive to the diameter and chiral index of the carbon nanotubes. These findings are in line with an analytical study of Wang et al. who found  $\alpha \approx 0.8$ .<sup>1</sup> Our calculated temperature dependence of the thermal conductivity (which shows a pick between 250 and 500 K that is shifted to higher temperatures with increasing diameter) qualitatively agrees with experimental data.<sup>2,3</sup> Again the chiral index is only a weak influence parameter. However, there is a crossover of the power law at lengths of  $\approx 50$  nm. Short nanotubes exhibit a weaker temperature dependence of  $\lambda$  than long nanotubes.

We have explained the microscopic origin for the thermal rectification in mass-graded nanosized systems.<sup>4,5</sup> For quasi-1D, 2D and 3D systems we have observed a more efficient heat current (i.e. higher thermal conductivity) in nanotubes when heat flows from the low-mass to the high-mass region. The opposite behavior has been found in mass-graded 1D chains. We have emphasized that the thermal conductivity in quasi 1D networks such as nanotubes and perfect 1D chains is controlled by different influence parameters. Only in nanotubes we can have a transfer of vibrational intensity to the longitudinal axis under the influence of anharmonic effects perpendicular to this direction. Such a transfer process is absent in single-file chains. At least in connection with thermal conductivities and rectification we have to conclude that nanotubes cannot serve as model structures to study the physical peculiarities of 1D systems. After reviewed the results of this work, it should be emphasized that the thermal rectification realized in the majority of systems studied has been caused by different efficiencies in the degrees of freedom. Their absolute number has been kept constant. Previous works in our group have shown that the heat transfer also scales with the number of the degrees of freedom.<sup>6,7</sup> This influence parameter might be decisive to explain thermal rectification in externally mass-loaded CNTs.<sup>8</sup> Here the heat transfer from the region with high loading (larger number in the degrees of freedom) to the region with low external loading (smaller number in the degrees of freedom) exceeds the opposite transfer route.

We have also investigated the thermal conductivity into the tube and perpendicular directions of crystalline nanotubes. The thermal conductivity in the perpendicular direction is by two to three orders smaller than in the parallel direction. These results are similar to our other findings in polystyrene materials.<sup>7,9</sup> In this context we can consider carbon nanotube bulks as an extreme example for high anisotropies. The origin of this anisotropy can be explained as follows. The heat conduction in the longitudinal direction of the tube driven by phonons is much more efficient than the collision mechanism between the tubes. An anisotropy in the thermal conductivity of carbon nanotubes has been verified experimentally after the application of pressure into the one direction of the sample.<sup>10</sup> In

---

this case the lattice thermal conductivity perpendicular to the pressure orientation is bigger than those parallel to the pressure direction.

In addition to the presented results, our preliminary findings for carbon nanotube-polymer nanocomposites show that the thermal conductivities calculated for nanocomposite are much smaller than the values expected on the basis of the thermal conductivities of the nanotube and the bare polymer. These results coincide with available experimental data.<sup>11,12</sup> In one case we have found that the thermal conductivity of polyamide-6,6 with 7% (mass fraction) of the carbon nanotube is only 20.7% higher than the value for the bare polyamide. These findings show us that a polymer matrix around the tube has an influence on the mechanism of the heat transport in the nanotube. However, more calculations and analyses are necessary to understand the heat transfer in nanocomposites.

- (1) Wang, J. A.; Wang, J. S. *Applied Physics Letters* **2006**, *88*, 111909.
- (2) Kim, P.; Shi, L.; Majumdar, A.; McEuen, P. L. *Physical Review Letters* **2001**, *87*, 215502.
- (3) Pop, E.; Mann, D.; Wang, Q.; Goodson, K.; Dai, H. J. *Nano Letters* **2006**, *6*, 96.
- (4) Alaghemandi, M.; Leroy, F.; Algaer, E.; Böhm, M. C.; Müller-Plathe, F. *Nanotechnology* **2010**, *21*, 075704.
- (5) Alaghemandi, M.; Leroy, F.; Böhm, M. C.; Müller-Plathe, F. *Phys. Rev. B*, submitted.
- (6) Lussetti, E.; Terao, T.; Müller-Plathe, F. *Journal of Physical Chemistry B* **2007**, *111*, 11516.
- (7) Rossinsky, E.; Müller-Plathe, F. *Journal of Chemical Physics* **2009**, *130*, 134905.
- (8) Chang, C. W.; Okawa, D.; Majumdar, A.; Zettl, A. *Science* **2006**, *314*, 1121.
- (9) Algaer, E. A.; Alaghemandi, M.; Böhm, M. C.; Müller-Plathe, F. *Journal of Physical Chemistry B* **2009**, *113*, 14596.
- (10) Qin, C.; Shi, X.; Bai, S. Q.; Chen, L. D.; Wang, L. J. *Materials Science and Engineering a-Structural Materials Properties Microstructure and Processing* **2006**, *420*, 208.
- (11) Haggemueller, R.; Guthy, C.; Lukes, J. R.; Fischer, J. E.; Winey, K. I. *Macromolecules* **2007**, *40*, 2417.
- (12) Shen, Z. Q.; Bateman, S.; Wu, D. Y.; McMahon, P.; Dell'Olio, M.; Gotama, J. *Composites Science and Technology* **2009**, *69*, 239.



---

---

## Publications

---

- 1- M. Alaghemandi, E. Algaer, M. C Böhm and F. Müller-Plathe, [The thermal conductivity and thermal rectification of carbon nanotubes studied using reverse non-equilibrium molecular dynamics simulations] *Nanotechnology* **20**, 115704 , 2009.
- 2- E. Algaer, M. Alaghemandi, M. C Böhm and F. Müller-Plathe, [Thermal conductivity of amorphous polystyrene in supercritical carbon dioxide studied by reverse non-equilibrium molecular dynamics simulations] *J. Phys. Chem. A*, **113** (43), 11487, 2009.
- 3- E. Algaer, M. Alaghemandi, M. C Böhm and F. Müller-Plathe, [Anisotropy of the Thermal Conductivity of Stretched Amorphous Polystyrene in Supercritical Carbon Dioxide Studied by Reverse Nonequilibrium Molecular Dynamics] Simulations] *J. Phys. Chem. B*, **113** (44), 14596, 2009.
- 4- M. Alaghemandi, F. Leroy, E. Algaer, M. C Böhm and F. Müller-Plathe, [Thermal ratification in mass-graded nanotubes: A model approach in the framework of reverse non-equilibrium molecular dynamics simulations] *Nanotechnology* **20**, 075704, 2010.
- 5- M. Alaghemandi, F. Leroy, F. Müller-Plathe and M. C Böhm, [Thermal rectification in nanosized systems studied by molecular dynamics simulations] *Phys. Rev. B*, submitted.
- 6- M. Alaghemandi, J. Schulte, F. Leroy, F. Müller-Plathe and M. C Böhm, [On the correlation between thermal conductivity and bondlength alternation in carbon nanotubes: A combined reverse non-equilibrium molecular dynamics – crystal orbital analysis] submitted.

---

---

## Curriculum Vitae

---

### Mohammad Alaghemandi

Martinstraße 41, 64285 Darmstadt

Date of birth: 07-12-1980

### Education:

#### *Darmstadt University of Technology (Darmstadt, Germany)*

*Eduard-Zintl-Institute for Inorganic and Physical Chemistry*

February 2007-March 2010

Ph.D., Theoretical Physical Chemistry (Molecular Dynamics simulations)

- Dissertation Topic: "Thermal conductivity and thermal rectification in carbon nanotubes studied by reverse non-equilibrium molecular dynamics simulations"
- Advisor: Prof. Dr. Florian Müller-Plathe

#### *Tarbiat Moallem University (Tehran, Iran)*

*Faculty of Chemistry*

September 2003- July 2006

M.S., Physical Chemistry (Quantum Chemistry)

- Topic of Master thesis: "The analytical solution of the diatomic nuclear Schrödinger equation with the Morse potential via Laplace transforms" and "The numerical solution of the diatomic nuclear Schrödinger equation with empirical and abinitio potentials via the Numerov method"
- Advisor: Prof. Dr. Reza Islampour

#### *Tehran University (Tehran-Iran)*

*Department of Chemistry*

February 2000- July 2003

B.S., Applied Chemistry

---

---

## **Eidesstattliche Erklärungen**

---

Mohammad Alaghemandi  
Martinstraße 41  
64285 Darmstadt

1.02.2010

### Eidesstattliche Erklärung

Ich erkläre hiermit bei Eides statt, dass ich meine Dissertation selbstständig und nur mit den angegebenen Hilfsmitteln angefertigt habe.

Mohammad Alaghemandi

---

Mohammad Alaghemandi  
Martinstraße 41  
64285 Darmstadt

1.02.2010

### Erklärung

Ich erkläre hiermit, noch keinen Promotionsversuch unternommen zu haben.

Mohammad Alaghemandi